Wireless Communications in Reverberant Environments

A Thesis

Submitted to the Faculty

of

Drexel University

by

Ryan Thomas Measel

in partial fulfillment of the

requirements for the degree

of

Doctor of Philosophy

January 2015

Dedications

For Mom, Dad, Michelle, Tyler, and Emily.

Acknowledgments

Moshe once told us that we would learn more from our lab mates than we would ever learn from our advisors and other faculty. The truth of that statement resonates throughout the entirety of my time at Drexel. The members of the Secure Wireless Agent Testbed (SWAT), the Protocol Engineering Advanced Networking (PROTEAN) Research Group, the Data Fusion Laboratory (DFL), and the Drexel Wireless Systems Laboratory (DWSL) have been instrumental in my studies, research, and growth as an academic. In particular, I would like to thank (in alphabetical order) Bradford Boyle, Donald J. Bucci, Raymond Canzanese Christopher S. Lester, Daniel P. Oakum, Jeffery Wildman, and Matt Wozniski for being willing teachers and my friends. It has been an honor.

Through both classes and research, I have had the privilege of working with an abundance of intelligent, thoughtful, and hardworking mentors. I would like to thank Dr. Kapil R. Dandekar for co-advising this work and also working with me in many other capacties. I would also like to give special thanks to (in alphabetical order) Dr. Pramod Abichandani, Dr. Thomas Chmielewski, Dr. Leon Hrebien, Dr. Timothy Kurzweg, Joseph Macker, Dr. Richard Primero, Dr. William Regli, and Dr. Leonardo Urbano.

With regards to this body of work, I would like to thank Gregory Tait and the other members of the Electromagnetic & Sensor Systems Department of the Naval Surface Warfare Center Dahlgren Division (NSWCDD) for providing access to the reverberation chambers and sharing their wealth of knowledge. I would also like to thank the Naval Inactive Ship Maintenance Facility (NISMF) in Philadelphia, PA for providing access to naval vessels. This work was supported in part by the Office of Naval Research (awards N00014-11-1-0327, N00014-13-1-0262, and N00014-13-1-0312) and the National Science Foundation (grants CNS-0923003 and CNS-0854946).

And finally, my advisor – Dr. Moshe Kam. He has guided me through three degrees and two theses. There is no amount of gratitude I could express that would be adequate.

Table of Contents

List of Tables

List of Figures

List of Acronyms

CCF Cavity Calibration Factor

CDF Cumulative Distribution Function

CDFs Cumulative Distribution Functions

COTS Commercial, Off-The-Shelf

CSI Channel State Information

EVM Error Vector Magnitude

IID Independent, Identically Distributed

ISI Inter-Symbol Interference

LOS Line Of Sight

MIMO Multiple Input Multiple Output

MRC Maximal Ratio Combining

NISMF Naval Inactive Ship Maintenance Facility

NLOS Non Line of Sight

NSWCDD Naval Surface Warfare Center Dahlgren Division

NSFD Naval Support Facility Dahlgren

OFDM Orthogonal Frequency-Division Multiplexing

PDP Power Delay Profile

PPSNR Post Processing Signal-to-Noise-Ratio

QAM Quadrature Amplitude Modulation

RMS Root Mean Squared

RLWA Reconfigurable Leaky Wave Antenna

SER Symbol Error Rate

SISO Single Input Single Output

SMUX Spatial Multiplexing

SDR Software Defined Radio

SDRs Software Defined Radios

SNR Signal-to-Noise-Ratio

STBC Space-Time Block Code

WLAN Wireless Local Area Network

WLANs Wireless LANs

VBLAST Vertical Bell Laboratories Layered Space-Time

List of Symbols

Δ	Time delay.
$u(t, \Delta)$	Impluse response.
$P_h(\Delta)$	Power delay Profile.
T_m	Normalized first-order moment of the power delay profile.
S_Δ	Root mean squared delay spread.
τ	Time constant.
S_{21}	Forward transmission coefficient.
V	Volume of a space.
$P_{\texttt{AvgRec}}$	Average received power.
$P_{\texttt{Input}}$	Input power.
$\eta_{\texttt{TX}}$	Transmit antenna efficiency.
$\eta_{\texttt{RX}}$	Receive antenna efficiency.
λ	Wavelength.
f	Center frequency.
Q	Dimensionless measure of the dampening of a resonator.
B_Q	Q bandwidth.
CCF	Cavity calibration factor.
I_L	Insertion loss.
C	System capacity.
$P_{\texttt{Tx}}$	Transmit power.
$\mathcal{N}_0$	Noise power.
K	Number of subcarriers in an OFDM transmission.
H_k	$m \times n$ channel matrix with m transmit antennas and n receive antennas.
h	Complex channel gain.
$h_{i,j}$	Complex channel gain from transmit antenna i to receive antenna j.
T	Throughput.
M	Modulation order.
S	Symbol rate.
B	Bandwidth.
$r_{\texttt{DSC}}$	Ratio of subcarriers in an OFDM transmission which hold payload data.

Abstract

Wireless Communications in Reverberant Environments
Ryan Thomas Measel
Moshe Kam, Ph.D., P.E., and Kapil R. Dandekar, Ph.D.

Implementation of WLANs in reverberant environments, such as industrial facilities, naval vessels, aircraft, and spacecraft, has proven challenging, because rich electromagnetic scattering can degrade link quality through multipath interference. As a result, the adoption of Wireless LANs in these environments has been slow. Previous studies concerning reverberant environments have focused on characterizing electromagnetic properties for the purpose of electromagnetic compatibility testing. Little attention has been given to the performance of wireless communications. In this effort, the effect of electromagnetic reverberance on wireless communications is investigated in order to assess the feasibility of WLAN deployment.

Work centered around two experimental measurement campaigns. The first campaign was performed in coupled reverberation chambers. The reverberation chambers provided a controllable environment which was configured to emulate the reverberance of below-deck spaces on a naval vessel. The process for quantifying and configuring the electromagnetic properties of a reverberation chamber is presented. The second campaign was performed on a naval vessel. Experimentation was conducted in a variety of locations on the ship. Locations were selected to represent a wide range of practical environments. Across both campaigns, several environment and node parameters were evaluated: level of reverberance, cavity coupling (effective aperture size), and LOS versus NLOS links. Additionally, advanced physical layer schemes and reconfigurable antennas are presented as methods to improve performance and mitigate multipath interference. To perform this work, a measurement platform and testing protocol were developed for systematic characterization of wireless communications in reverberant environments.

The primary contributions of this work are empirical characterization of wireless communications in reverberant environments, approaches to improving the performance of wireless communications

in presence of high levels of multipath interference, and a methodology for experimentation in reverberant environments.

Chapter 1: Introduction

1.1 Motivation

WLANs are ubiquitous in many common environments including residential, office, urban, and outdoor spaces. The migration from wired communications to WLANs has been much slower in some less "typical" environments, such as industrial facilities, military vessels, and spacecraft, though there has been increased interested in deploying WLANs to these environments [1, 2, 3, 4, 5, 6, 7, 2, 8, 6]. The slow adoption is due in part to regulation and standards but also because the environments have traditionally been viewed as challenging for wireless communication [1, 9, 10]. These environments are atypical because they characteristically exhibit high electromagnetic reflectivity resulting from physical obstructions and largely metallic construction. The notion that these highly reverberant environments are challenging is because the multipath interface produced from the high reflectivity is thought to degrade (and perhaps prevent) communication. Nevertheless, highly reverberant environments can benefit from the adoption of WLANs for all the same reasons that "typical" environments do: node mobility, ease of implementation, and reduction of infrastructure.

Often, highly reverberant environments are also physically complex and operationally demanding spaces which make WLANs particularly attractive to supplement or fully replace hardwire infrastructure. For example, consider the below deck spaces on a naval vessel: corridors, workshops, living quarters, storage compartments, machinery compartments, and engine rooms. The spaces range in shape, purpose, and design but share in that they are all highly reverberant. A selection of these spaces is shown in Figures 1.1-1.3 where the tight dimensions, physical obstructions, and metallic construction are evident.

A multitude of communications are needed throughout a naval vessel for telemetry, voice, and other purposes. Currently, these signals are routed via hardwire which presents many challenges and implementation constraints when installing new infrastructure, performing maintenance on existing infrastructure, and providing system redundancy:

Figure 1.1: Engine Room on the *Thomas S. Gates* (CG 51).

- *Installation* - Boundaries between decks and bulkheads must remain watertight, so it is not possible to drill a hole between compartments as you would to install a cable in a home or office. New hardwire infrastructure has to be routed through existing interfaces between the boundaries. While the compartments are watertight, they are not electromagnetically sealed. Electromagnetic leakage can occur from doors, hatches, windows, bulkhead penetrations, and floor joints, so a wireless signal can propagate between compartments without jeopardizing structural integrity.

- *Maintenance* - Performing maintenance on existing infrastructure is also simpler with WLANs. A faulty cable for a hardwire connection can be difficult to repair. If the cable can be fixed in place, the technician must first determine the point of failure (which is not always straightforward) and must be able to gain access to that point. If the cable has to be replaced, then it must be removed and a new cable routed in its place. This process can become time-consuming and cumbersome depending on the length and route of the cable. Comparatively, WLANs are distributed, so failures occur on a per-node basis. When a failure occurs, the faulty node can easily be determined through network diagnostics. The node can then be repaired or replaced at its point of installation and does not require the technician to work across multiple compart-

Figure 1.2: Corridor on the *Thomas S. Gates* (CG 51).

ments or decks. To promote signal propagation, wireless nodes are often placed in a location free from immediate physical obstruction, so it is likely the location will be easily accessible as well.

- *Redundancy* - Many highly reverberant environments, including naval vessels, have critical systems which require fail safes. To add redundancy with a hardwire connection, an additional cable must be installed. In situations where there is a threat of physical damage to an area (military and spacecraft), it would be advantageous to install redundant cables along different routes to prevent all redundant connections from being comprised in one physical event. Installing along different routes may not always be possible or practical though. For WLANs, redundancy can be added through network topology such that each node has multiple connections. If every node has at least two connections, then network routing will ensure that communications between end nodes continues even when a node fails. Multiple node failures could be tolerated if the number of interconnections between nodes is increased. Robustness will increase as more interconnections are added. Depending on the implementation of the system and the level of redundancy desired, little or no additional infrastructure will be

Figure 1.3: Work room on the *Thomas S. Gates* (CG 51).

required.

While there are many benefits that can be realized by deploying WLANs in highly reverberant environments, there are also potential trade-offs that must be addressed:

- *Power* - Wireless nodes require power which can be provided by either batteries or hardwire. Previously, it was discussed how routing cables throughout a naval vessel can be difficult, and it was a benefit of WLANs that they did not need to be routed. Yet, if power needs to be routed to the nodes, perhaps this benefit is negated. While routing power has its own challenges, it does not negate this benefit of WLANs, because naval vessels (and presumably many other highly reverberant environments requiring communication) must route power regardless of communications infrastructure. The power consumption of a wireless node is generally low compared to other equipment and machinery, but it may still be a consideration for some implementations (e.g., spacecraft).

- *Installation Location* - The coverage of a wireless node as well as the network design will dictate the position of a node. Furthermore, to prevent attenuation, it is advisable to position nodes

clear of immediate physical obstructions. These requirements may constrain deployment, but generally, it is not an issue as nodes can be installed on nearly any surface of the environment.

- *Data Rate* - Currently, twisted pair Ethernet cables can support a date rate of up to 1 Gbps. Fiber optic Ethernet cables can support up to 100 Gbps [11]. Meanwhile, IEEE 802.11 can support 867 Mbps [12]. Obviously, fiber optic cables are considerably faster than current wireless links, though the throughput of a connection is restricted to the data rate of the slowest link or interface (including the end user). Only sophisticated systems with extreme data rate requirements demand the use of fiber optic cables. Otherwise, the throughput provided by WLANs should be sufficient.

- *Cost* - The cost of wireless vs hardwire infrastructure is completely dependent on the requirements and scale of the implementation. The installation and maintenance costs should also be considered. In scenarios where the WLAN costs more upfront, it may still be cheaper to deploy a WLAN when installation and maintenance costs are factored in.

- *Lifetime* - Wireless nodes have many electronic components that will wear over time. Cables also wear over time but likely at a slower rate.

- *Security* - Wireless nodes communicate over the air which is disadvantageous for security concerns, since communications may be jammed or snooped. This is especially important for military applications [13].

Certainly, there are situations which would preclude the use of WLANs in highly reverberant environments, but there are many applications and advantages as well. While the examples presented were primarily in the context of a naval vessel, much of the discussion could easily be extended to other highly reverberant environments.

While the effect of multipath on wireless communications has been thoroughly studied for "typical" environments, such as indoor [14, 15] and urban [16, 17, 18] spaces, little focus has been given to communications in highly reverberant environments. Though, there has been work analyzing RF propagation [19, 20, 21, 22] in these environments.

1.2 Contributions

The primary objective of this work is to characterize the performance of wireless communications in reverberant environments and investigate methods to improve performance. Interpretation of the results and their application to practical wireless network implementations will also be provided. The principal contributions of this effort are:

1. An experimental methodology was developed for evaluating the performance of wireless communications including a measurement platform and testing protocol for SDRs.

2. A measurement campaign was performed in the coupled reverberation chambers of the NSWCDD at the NSFD where the performance of wireless communications was assessed with respect to node and environmental parameters.

3. A measurement campaign was performed in the below-deck spaces of a naval vessel on the *Thomas S. Gates*. (CG 51) at the NISMF in Philadelphia, PA, where the performance of wireless communications was assessed with respect to node and environmental parameters.

4. Empirical evaluation of a pre-existing RLWA was performed in the coupled reverberation chambers of the NSWCDD to evaluate its ability improve wireless communications performance in a highly reverberant environment.

1.2.1 Contribution 1: Experimental Methodology

Often, wireless communication performance is studied through modeling and simulation, but in this work, performance was evaluated through live experimentation. Experimentation is necessary to discover the practical implications of operating WLANs in highly reverberant environments which may not be apparent through modeling and simulation. In [23], ray tracing is performed for communications on board a ship. While the dimensions are realistic, the model is simplified to flat boundaries. Actual ships, as shown in Figures 1.1-1.3, have many protrusions and obstructions which vastly increase the surface area and the number of propagation paths. Though, advances in computer vision have provided solutions to three dimensional mapping of spaces [24, 25]. As

precision improves, this work could be used to develop highly accurate models of actual below-deck spaces, as well as other reverberant environments with complex physical geometry. Additionally, the simulation would need to account for electromagnetic leakage in the spaces.

The ability of modeling and simulation to predict the performance of communications in such environments is limited due to the high level of small-scale fading (i.e., multipath). The quantity, amplitude, and phase of the produced multipath components are dependent on the physical shape of the environment. Any change to the environment, including moving obstructions (e.g, machinery or people), moving the transmitter, moving the receiver, or changing boundary conditions (opening a door), will produce vastly different channels. This dependency on the physical environment diminishes the ability of stochastic modeling to accurately represent actual environments.

In order to thoroughly characterize the performance of wireless communications in reverberant environments, it is necessary to empirically evaluate through field experimentation. An experimental methodology was developed which includes a MIMO OFDM wireless measurement platform and a test protocol.

Comprehensive measurement and analysis of wireless communications with consumer-grade equipment is often hampered by lack of access to the physical layer. Specialized equipment tailored to collect comprehensive measurements, such as signal generators and signal analyzers, is expensive and incompatible with the constraints of field work and mobile applications. Software-defined radios can provide a similar level of measurement capability while being more cost-effective, lightweight, and mobile.

SDRs have been commonly used for research and commercial applications for several decades. Today, a variety of both hardware and software [26] solutions exist which can be tailored to meet the needs nearly any wireless application. Some notable current solutions include USRPs [27] and GNURadio [28]. For this effort, the WARPv3 Kit [29] was selected as the hardware platform (primarily due to availability). There are a few reference designs available for use with the WARPv3 Kit. Unfortunately, none of these designs could offer the full range of functionality which was desired with this project. Accordingly, a new MATLAB wireless measurement platform was developed

[30] that interfaces with the WARPv3 Kit. The platform implements IEEE 802.11g [31] wireless transmissions with four physical layer schemes: 1×1 SISO [32], 1×2 MRC [33], 2 × 2 Alamouti STBC [34], and 2 × 2 VBLAST SMUX [35]. Two different antenna types can be used with the system: a COTS omnidirectional antenna and a RLWA [36]. The platform provides a series of metrics, including channel capacity, EVM, PPSNR, and throughput to characterize link and network performance.

A test protocol was developed [30] which leverages the wireless platform for live experimentation. Since the platform operates with two antenna types and four physical layer schemes, it is vital to execute tests in a consistent and efficient manner. The test protocol encompasses calibrating the physical hardware, setting initial parameters, and executing the test. The protocol also considers the nuisances of testing in both a controlled (i.e., reverberation chamber) and a live (i.e., naval vessel) reverberant environment.

1.2.2 Contribution 2: Wireless Performance in Reverberation Chambers

A measurement campaign was performed in the coupled reverberation chambers of the NSWCDD at the NSFD. The reverberation chambers provide a controllable environment where the reflectivity of the wireless channel was configured to match the reflectivity of the below deck spaces on a naval vessel. The parameters used to quantify the reflectivity will be discussed along with the configuration of the reverberation chambers. Three (3) configurations were selected to emulate the full range of reflectivity exhibited in actual below-deck spaces [37]. Through wireless experimentation, a series of node and environments parameters were evaluated to provide insights on the expected performance in an actual reverberant environments.

1.2.3 Contribution 3: Wireless Performance in Below-Deck Spaces

A second measurement campaign [38, 39] was performed on the *Thomas S. Gates* (CG 51) at the NISMF in Philadelphia, PA. Tests were performed in a variety of locations which were selected based on their perceived likelihood of WLAN deployment. Experiments were conducted in a similar fashion to those done in the coupled reverberation chambers. Results and analysis will be provided

from each of the scenarios. Furthermore, both campaigns will be compared to demonstrate the validity of using reverberation chambers to emulate reverberant environments.

1.2.4 Contribution 4: Empirical Evaluation of Pre-Existing Reconfigurable Antennas

Electrically reconfigurable antennas can dynamically alter their radiation patterns through voltage control signals. They have been proposed for mitigating the multipath interference in "typical" environments [40]. Some work has been done concerning this proposition. The studies in [40, 41] analyze the ability of reconfigurable antennas to mitigate multipath interference but do so only through simulated results. The studies in [42, 43, 44] obtain communication performance measures using software-defined radios in typical lab or office environments. Little work has been done experimenting with reconfigurable antennas in highly reverberant environments. In this effort [45], a Reconfigurable Leaky Wave Antenna (RLWA) (developed by Piazza and Drexel Wireless Systems Laboratory [46, 47, 48]) was used to test the effectiveness of altering radiation patterns to improve the quality of communications in highly reverberant environments.

Chapter 2: Electromagnetic Characterization of Reverberant Environments

2.1 Introduction

Portions of this chapter have been included in a manuscript submitted to IEEE Transactions on Wireless Communications [49].

Reverberant environments are characterized by rich electromagnetic scattering which is a result of the low absorption of electromagnetic radiation by the surfaces within the environment. Energy not absorbed by the surfaces is reflected back into the space which produces a high field strength. Typically, reverberant environments have metallic surfaces with few openings through which energy can leak out.

The level of reflectivity in a reverberant environment is known as the *loading*. Loading is correlated to the absorption of the electromagnetic radiation and inversely correlated to the reflectivity (i.e, low loading equates to low absorption and high reflectivity). Loading changes based on the physical configuration of the environment. Any object (e.g., equipment, furniture, humans) added to or removed from the environment will affect how energy is absorbed, Opening or closing apertures (e.g, door, hatches, panels) alters how much energy leaks from the environment. For the remainder of this document, the terminology of low and high loading will be used relatively to compare different environmental configurations, but all the reverberant environments studied here will tend towards low loading (and high reflectivity).

Considering wireless signals, high reflectivity results in multipath which can cause destructive interference. Reverberant environments have high levels of multipath which is why they are being investigated. Before the wireless performance can be evaluated, it is necessary to first characterize the electromagnetic nature of the selected environments. The coupled reverberation chambers were tuned to match the reflectivity of actual highly multipath environments. Similar work has been done in [18] where the wireless propagation of outdoor urban environments was recreated in a

reverberation chamber.

2.2 Quantifying the Electromagnetic Nature of an Environment

For this effort, measures which can be derived from the Power Delay Profile (PDP) [50] of the wireless channel will be considered to characterize the electromagnetic nature of an environment. The PDP is the complex integral of the impulse response [51] where the impulse response is the output of a system given an instantaneous burst of energy as the input (i.e., an impulse) [52]. In the context of a wireless channel, an impulse response can be measured using the forward transmission coefficient, S_{21}, between a pair of antennas attached to a network analyzer [22].

2.2.1 Electromagnetic Properties

Power Delay Profile

The PDP is the amount of power received with a delay between $[\Delta, \Delta + d\Delta]$. It is expressed as the complex integral of the impulse response ($u(t, \Delta)$) [51],

$$P_u(\Delta) = \int_{-\infty}^{-\infty} |u(t, \Delta)|^2 dt. \tag{2.1}$$

While the PDP does provide detailed insight on the multipath channel to the receiver, it is often useful to consider generalized measures of this data. These measures are calculated through the moments of the PDP.

The normalized first-order moment is defined as,

$$T_m = \frac{\int_{-\infty}^{\infty} \Delta P_u(\Delta) d\Delta}{\int_{-\infty}^{\infty} P_u(\Delta) d\Delta.} \tag{2.2}$$

T_m is called the mean delay, which is the average delay of all multipath components reaching the receiver.

The normalized second-order, central moment of the PDP is calculated as,

$$S_\Delta = \sqrt{\frac{\int_{-\infty}^{\infty} P_u(\Delta)(\Delta - T_m)^2 d\Delta}{\int_{-\infty}^{\infty} P_u(\Delta) d\Delta}}. \quad (2.3)$$

The measure S_Δ is referred to as the Root Mean Squared (RMS) Delay Spread [32]. It is a measure of the richness of the scattering environment. It can be interpreted as difference in arrival times of the earliest and latest significant multipath components. The duration of symbols in wireless communication must be sufficiently greater than the RMS delay spread (approximately one order of magnitude) to prevent Inter-Symbol Interference (ISI).

Time Constant

The time constant, τ, is the rate at which energy is lost from the system when the input source turned off. It may be determined from the slope of the PDP.

Q Factor

Highly reverberant environments are characterized by rich electromagnetic scattering which is a result of low absorption of electromagnetic radiation by the metallic surfaces within the environment. Energy that is not absorbed is reflected back into the space. A reverberant environment is a damped resonator when excited by a wireless communication signal, so the loading can be quantified by the Q factor, a dimensionless measure of the dampening of a resonator [53]. The Q factor is the ratio of the energy stored to the energy lost per cycle in a resonator. A higher Q indicates less dampening, so oscillations die out more slowly. Q is related to the rate of decay of the impulse response and the volume of the space. It is calculated from the impulse response of the wireless channel which is found by calculating the inverse Fourier transform of the channel transfer function. The transfer function is measured using the forward transmission coefficient, S_{21}, between two antennas attached to a network analyzer [22].

The measure is expressed as a function of the volume of the space (V, m^3), average received power ($P_{\texttt{AvgRec}}$, W), input power ($P_{\texttt{Input}}$, W), transmit ($\eta_{\texttt{TX}}$) and receive ($\eta_{\texttt{RX}}$) antenna efficiency, and

the wavelength (λ) of the center frequency (f) of the input source,

$$Q = \frac{16\pi^2 * V^3 * \frac{P_{\text{AvgRec}}}{P_{\text{Input}}}}{\eta_{\text{TX}}\eta_{\text{RX}} * \lambda^3}. \tag{2.4}$$

The Q factor is also related to the time constant,

$$Q = 2\pi * f * \tau. \tag{2.5}$$

Q Bandwidth

The bandwidth of the resonance is equal to

$$B_Q = \frac{f}{Q}, \tag{2.6}$$

where f is the center frequency of the resonance. This relationship implies that a higher Q factor results in a smaller (and more stable) resonant frequency.

Cavity Calibration Factor

The Cavity Calibration Factor (CCF) is the normalized electric field [37] with units $V/m/\sqrt{w}$. It is defined[54] as

$$CCF = \frac{8\pi}{\lambda}\sqrt{\frac{5I_L}{\eta_{\text{RX}}}}, \tag{2.7}$$

where I_L is the insertion loss. This metric is commonly used in electromagnetic compatibility testing.

2.2.2 Measurement Protocol

Due to the non-uniformity of the electromagnetic field in a static environment, it is necessary to "stir" the environment and take multiple samples. An ensemble average of the time-resolved samples provides a stochastic representation of the impulse response [22]. The electromagnetic field can be stirred in several ways, including moving the transmitter, receiver, or obstructions. Each stirring

method is equally effective. When considering the 2.4 GHz ISM band, the wavelength is 12.5 cm, so even small variations impact the fading characteristics of the channel. With respect to wireless communication, stirring varies the magnitude, phase, and quantity of multipath components arriving at the receiver nodes.

For the experiment, stirring was performed by rotating two Z-fold mechanical tuners, each 2.7 meters in length, inside the main chamber (Figure 2.1). One tuner was positioned vertically in the southwest corner, while the other was located horizontally along the top of the north wall. The tuners rotate at aperiodic intervals to prevent periodicity in the produced channels.

Two dual-ridged, horn antennas (frequency range of 1-18 GHz) were connected to a network analyzer and placed inside the main chamber away from the walls. The network analyzer performed a frequency sweep of 200MHz with a center frequency of 2.462 GHz (IEEE 802.11, Channel 11 [31]), dwell time of 5 ms, and Intermediate Frequency (IF) bandwidth of 50 kHz. For each measurement, 25 sweeps were performed and averaged. The channel was stirred in between measurements. The impulse response was calculated as the ensemble average of 20 time-resolved measurements. This protocol is discussed in further detail in [22].

2.3 Below Decks Electromagnetic Characterization

The loading in below-deck spaces on naval vessels has been a primary focus of a number of studies [37, 19, 13, 22] on electromagnetic compatibility and emissions. The range of loading in below deck spaces was determined to be between 1100 and 5800. The reverberance in this highly reverberant environment can be compared to other measured environments through the use of RMS delay spread. The loading exhibited in below-deck spaces corresponds to a delay spread in the range of ˜200-1200 ns. Meanwhile, empirical studies [55, 56] of non-reverberant environments have measured a delay spread between ˜10-60 ns, which is approximately twenty (20) times less than the delay spread in the reverberant environments. The order of magnitude difference between non-reverberant and reverberant environments clearly demonstrates the stark contrast in their electromagnetic nature.

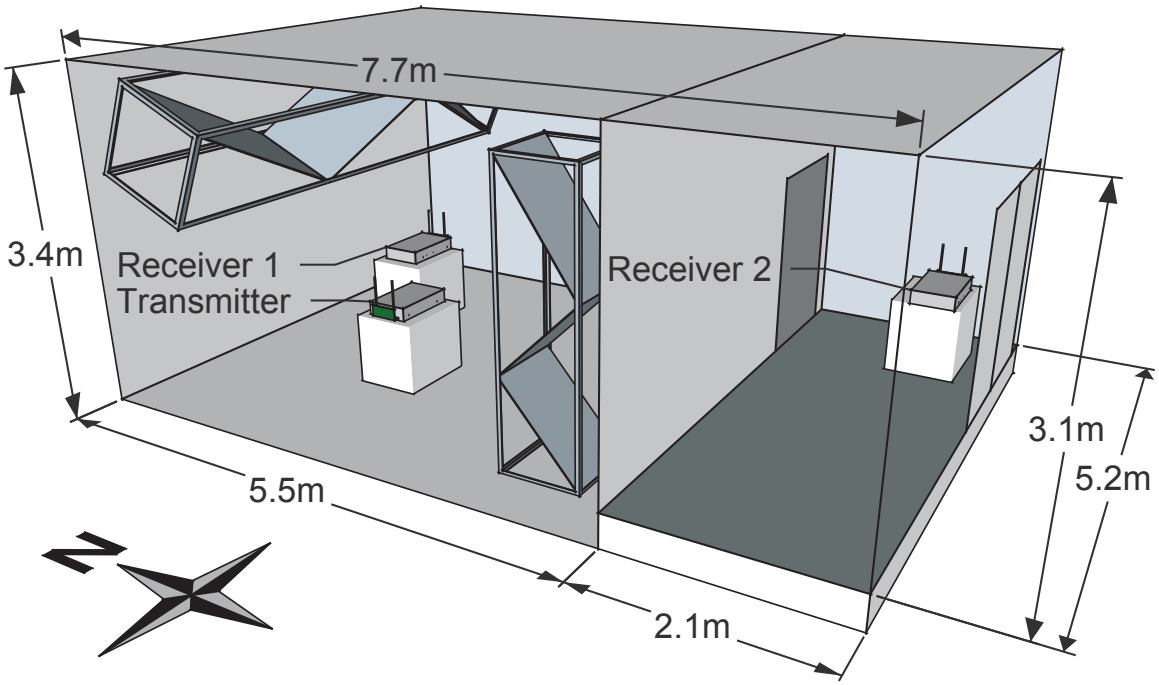

Figure 2.1: Cross section view of the main chamber and ante chamber in the coupled reverberation chambers of the NSWCDD.

2.4 Reverberation Chamber Electromagnetic Characterization

A reverberation chamber is metallic enclosure primarily intended for electromagnetic compatibility testing. Reverberation chambers have naturally low loading as they are designed to minimize electromagnetic absorption and maintain the electromagnetic field strength. The reflectivity of the chamber may be lowered by adding electromagnetically absorptive material inside the chamber. By varying the amount and location of the absorbing material, the chamber can be configured to mimic the Q factor of actual highly multipath environments.

For this work, the coupled reverberation chambers of the Naval Surface Warfare Center Dahlgren Division (NSWCDD) at the Naval Support Facility Dahlgren (NSFD) were used. The larger of the two chambers (the main chamber) has a volume of 97 m^3 (Figure 2.2), while the smaller of the two chambers (the ante chamber) has a volume of 34 m^3 (Figure 2.3). The chambers are adjoined by a 1×2 meter shielded door. A cross section of the environment is shown Figure 2.1.

The impulse responses of the three loading configurations are shown in Figure 2.4. The calculated

Figure 2.2: Main chamber of the coupled reverberation chambers of the NSWCDD. This picture was taken from the doorway connecting the main chamber to the ante chamber. The horizontal Z-fold mechanical tuner along the north wall is shown at the top of the image. One of the horn antennas used for the impulse measurements is on the tripod in the middle of the image. Two of the wireless nodes (described in Chapter 3) are shown on non-absorbing Styrofoam blocks.

Q factors were 5725 (High Q), 2031 (Medium Q), and 1142 (Low Q) which spans the range of loading exhibited by below deck spaces. For the remainder of this document, the loading configurations will be referred to as "High Q," "Medium Q," and "Low Q." The electromagnetic properties of the loading configurations are tabulated in Table 2.1.

2.5 Conclusions

The electromagnetic properties of highly reverberant environments need to be quantified in order to assess the performance of wireless communications and correlate that performance to the environment. A selection of measures, related to the PDP of the wireless channel, were described which

Figure 2.3: Ante chamber of the coupled reverberation chambers of the NSWCDD. This picture was taken from the south east corner of the ante chamber. One of the wireless nodes is shown on a non-absorbing Styrofoam block. The shielded door separating the main chamber and ante chamber is also shown.

serve this need. The protocol used to measure the PDP was presented as a means to develop a stochastic representation of the wireless channel. The range of loading in below deck spaces had been determined in previous studies and was used to calibrate three loading configurations in the coupled reverberation chambers. The impulse response and electromagnetic properties were calculated for each configuration. The experiments utilizing these configurations are analyzed in Chapter 4.

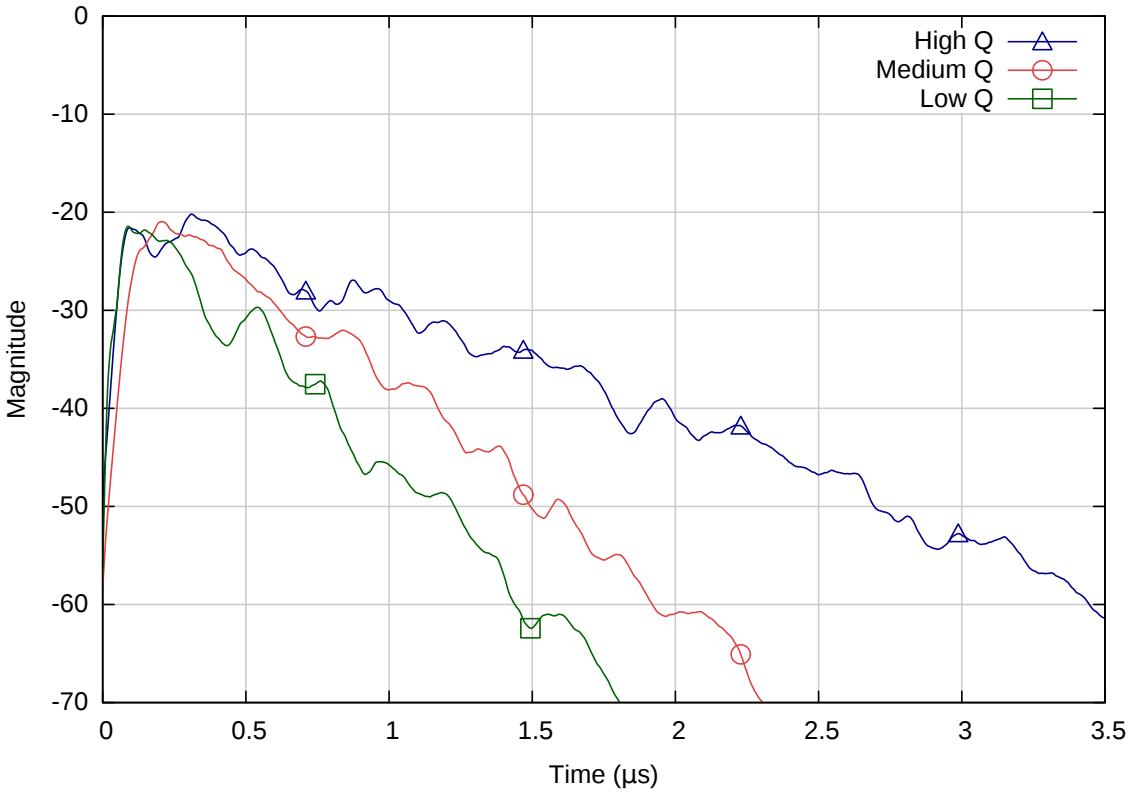

Figure 2.4: Coupled reverberation chambers. An ensemble average of the impulse response for each of the chamber configurations. The calculated Q factors were 5725, 2031, and 1142 for High Q, Medium Q, and Low Q, respectively.

Table 2.1: Coupled reverberation chambers. Electromagnetic properties at the low, medium, and high loading configurations.

	Q		
Property	Low	Medium	High
τ (ns)	75	133	374
Q	1142	2031	5725
B_Q (MHz)	2.134	1.200	0.426
CCF (V/m/$\sqrt{W}$)	11.47	15.29	25.67

Chapter 3: Experimental Methodology

3.1 Introduction

Portions of this chapter were published in the IEEE Antennas and Wireless Propagation Letters [38] and the Proceedings of the 2014 IEEE International Communications Quality and Reliability Workshop [30].

In order to characterize the performance of wireless communications in these highly reverberant environments, channel and link level metrics are needed which are not routinely available on consumer-grade hardware. Specialized, professional equipment is often used in such circumstances requiring considerable investment in hardware and logistics. Measurement platforms that incorporate Software Defined Radios (SDRs) are a viable option to fill this gap. SDRs have a small, lightweight form factor, and they can be used in physically constrained locations and in conjunction with mobile applications. They are also relatively inexpensive.

SDRs have been commonly used for research and commercial applications for several decades. Today, a variety of both hardware and software [26] solutions exist which can be tailored to meet the needs nearly any wireless application. Some notable current solutions include USRPs [27] and GNURadio [28]. For this effort, the WARPv3 Kit [29] was selected as the hardware platform (primarily due to availability). There are several reference designs available for the WAPRv3 kit such as Mango 802.11 Reference Design [57], the WARPLab Reference Design [29], and the ODFM Reference Design [29]. Unfortunately, none of these designs could offer the full range of functionality which was required for this work including the ability to interface with mechanical components in the coupled reverberation chambers and support for reconfigurable antennas. Thus, a new software implementation was developed to accommodate these requirements.

A MATLAB-based SDR measurement platform is presented here for the direct characterization of Multiple Input Multiple Output (MIMO) Orthogonal Frequency-Division Multiplexing (OFDM) communications. The platform has a modular subsystem design that implements a MIMO OFDM

wireless network with one of four physical layer schemes similar to IEEE 802.11g: 1×1 Single Input Single Output (SISO), 1×2 Maximal Ratio Combining (MRC), 2×2 Alamouti Space-Time Block Code (STBC), and 2×2 Vertical Bell Laboratories Layered Space-Time (VBLAST) Spatial Multiplexing (SMUX). The current version of the platform uses the *Wireless Open-Access Research Platform (WARP)* v3 SDR [58], although its modular nature would allow it to employ any SDR with appropriate buffer access. Data is OFDM-encoded and decoded based on the specified physical layer scheme entirely within software. The raw receive data can be used to derive a variety of desired channel and link-level metrics, including channel capacity, Error Vector Magnitude (EVM), Post Processing Signal-to-Noise-Ratio (PPSNR), and throughput.

There are many benefits to implementing the PHY and MAC layers in software instead of the SDR. The SDR only handles the transmission and reception of the RF waveforms, so no knowledge of embedded systems is required. Furthermore, a common hardware framework can be used across all four of the PHY layer schemes. It is not necessary to change physical connections or update the firmware on the SDR, even when extending the platform to incorporate additional MIMO physical layer schemes.

3.2 Measurement Platform Implementation

3.2.1 Packet Structure

This implementation of the OFDM packet structure is similar to IEEE 802.11g [31]. A packet contains 30 OFDM words and each word contains 64 subcarriers. Four of the subcarriers are reserved for pilot tones, which are used in frequency offset correction of channel estimates [31, Expression 18–25]. Twelve of the subcarriers are set to null as in [31, Figure 18–3], and the remaining 48 subcarriers contain data.

A packet is comprised of three types of blocks: *preamble*, *training symbols*, and *data*. The preamble block has two IEEE 802.11 long OFDM training symbols [31, Section 18.3.3], which are used for timing synchronization and packet detection. The training symbols block has four OFDM words. Two of the four OFDM words are arbitrary BPSK streams used to estimate Channel State Information (CSI). The remaining two OFDM words are null, to prevent beamforming when estimating

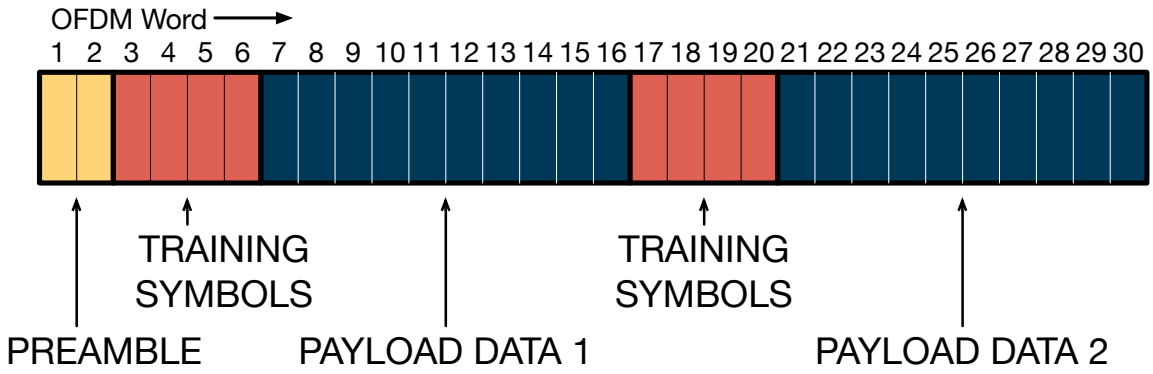

Figure 3.1: Packet structure. The first 2 OFDM words contain the preamble. The remaining 28 words alternate between 4 OFDM words for training data and 10 words for the data payload.

the channel coefficients for MIMO physical layer schemes. The data block contains 10 OFDM words filled with randomly generated data.

Due to the time varying nature of the channel, a trade-off exists between the length of a data block and the validity of the Channel State Information (CSI). Long data blocks can have stale CSI that causes carrier frequency offset, while short data blocks incur more overhead and require more packet transmissions. Since all the processing on this platform is done in software, there is a large delay (on the order of hundreds of milliseconds) between packet transmissions. While a slow rate of transmission does not affect the results, it does increase the length of the test.

A method was developed to decrease the testing time of the platform. The training symbols and data payload are duplicated and concatenated into a single packet as shown in Figure 3.1. A total of 20 OFDM words (960 symbols) of data is sent per transmission. The overhead is slightly increased with the inclusion of the second set of training symbols, but the higher data payload transmission rate vastly reduces the testing time without sacrificing the integrity of the data.

3.2.2 Transmitter Subsystem

Figure 3.2 shows the OFDM transmission subsystem for a single transmission stream. First, the data is Quadrature Amplitude Modulation (QAM) modulated before being reshaped into the 48 OFDM data subcarriers. The subcarriers are then encoded if required by the specified physical layer (e.g., Alamouti STBC). Pilot tones are inserted according to [31, Section 18.3.5.9]. In the MIMO

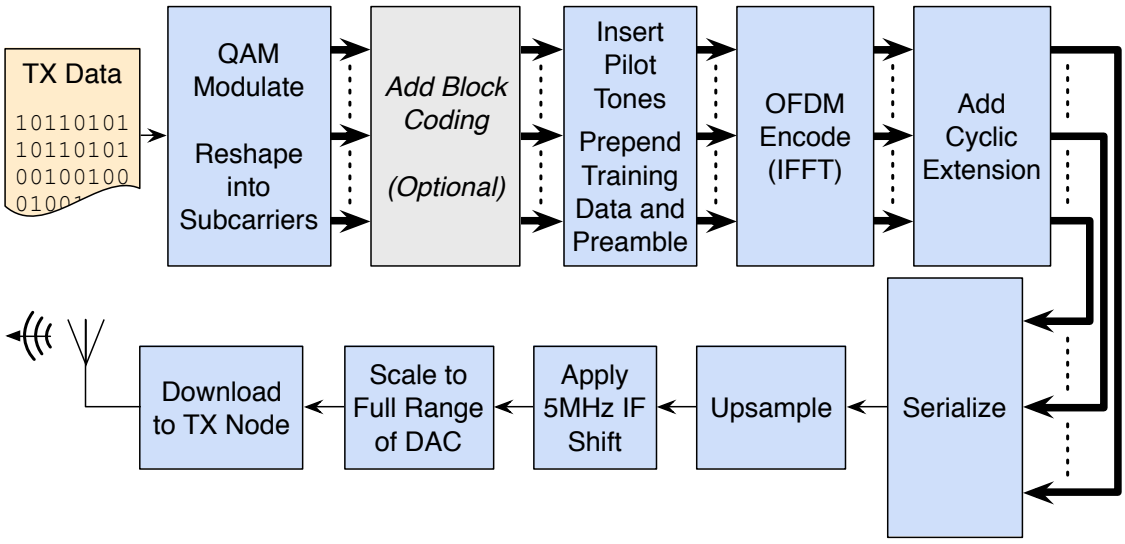

Figure 3.2: Block diagram of the OFDM transmitter subsystem.

cases, the pilot tones are interleaved in space and time (i.e., across subcarriers and OFDM words) to prevent deconstructive combining [59, Section 3.6]. The training symbols and preamble OFDM words are prepended to the data/pilot tone OFDM words. The entire packet is then OFDM-encoded via a 64 point IFFT, producing the OFDM waveforms for each word. For the second set of training symbols and data payload, the first set is repeated and appended to the packet. A guard interval consisting of a 16 sample cyclic prefix is added to each OFDM waveform, increasing the size of the OFDM word to 80 samples. After serializing the OFDM waveforms, the entire packet is upsampled by a factor of 4 to reduce the bandwidth to 10 MHz. The packet is upconverted to an IF of 5 MHz to prevent attenuation near DC. Finally, the preamble, training data, and data payload waveforms are individually scaled to the dynamic range of the WARP D/A and A/D converters to ensure maximum resolution in quantization while preventing clipping.

3.2.3 Receiver Subsystem

Figure 3.3 shows the general OFDM receiver subsystem. For each reception, the raw received data plus an additional 300 samples are downloaded from the SDR. The additional 300 samples act as a synchronization buffer to ensure that sufficient samples are downloaded to synchronize the transmission. Packet detection and synchronization occur via cross correlating the known preamble

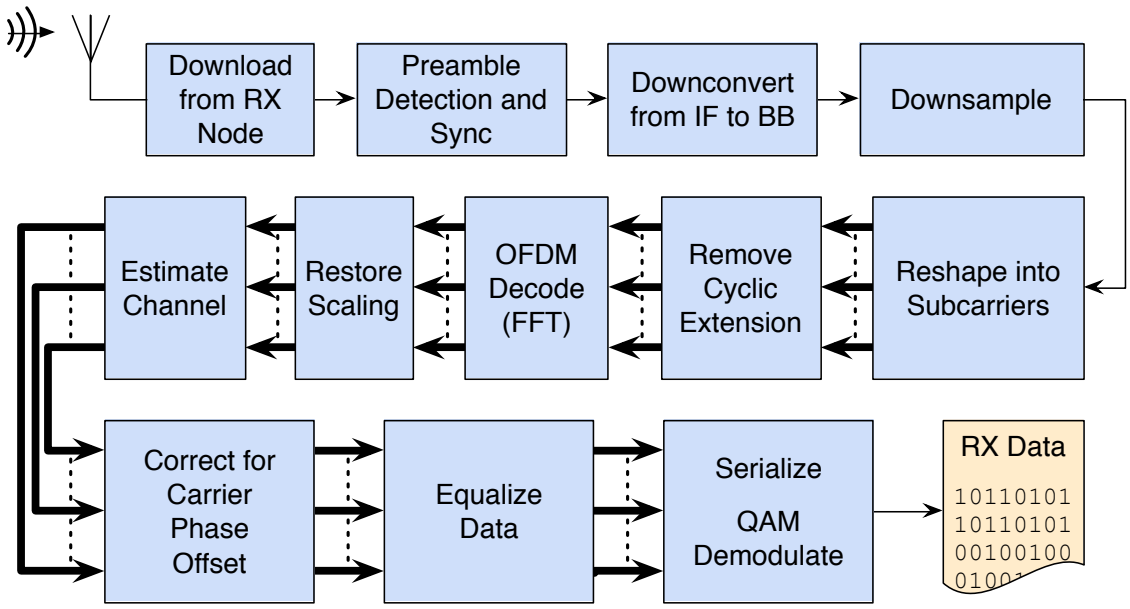

Figure 3.3: Block diagram of the OFDM receiver subsystem.

sequence (a single IEEE 802.11 long training symbol) with the received data. A packet is considered detected if the largest cross correlation magnitude is greater than a prespecified threshold.

After synchronization, the stream is downconverted to baseband and downsampled by a factor of 4. The entire packet is reshaped into subcarriers, and the cyclic extension guard interval is removed. The OFDM words are then recovered from the waveforms by performing a 64 point FFT. The channel coefficients are estimated from the training symbols. The carrier phase offset for each OFDM word is estimated using the dedicated pilot tones as in [33, Equation 8.17] and corrected by applying an inverse phase shift. The data payload is equalized using the channel estimates according to the specified physical layer, after which the received QAM symbols are serialized and demodulated.

3.2.4 Physical Layer Schemes

The platform currently implements four physical layer schemes: 1×1 SISO, 1×2 MRC, 2×2 Alamouti STBC, and 2×2 VBLAST SMUX. In the SISO scheme, the channel coefficients of each OFDM subcarrier are used to equalize the subcarriers of the OFDM packet. In 1×2 MRC [32], the signals from each receive antenna are weighted according to their individual Signal-to-Noise-

Ratio (SNR) and then summed. The weights are formed in terms of the channel coefficients for each subcarrier, as in [60, Chapter 7]. In the 2×2 Alamouti STBC, the data is split into two separate streams at the transmitter node and redundancy is added in the form of orthogonal representations of the data [61]. Finally, a 2×2 SMUX scheme is implemented via the VBLAST algorithm [62] which splits the transmitted data across two streams. At the receiver, the streams are decoded using a combination of linear nulls and symbol cancellation on each OFDM subcarrier.

3.2.5 WARP v3 Software Defined Radio (SDR)

The WARP v3 Kit is a SDR platform developed by Rice University and Mango Communications [58]. It is built on a Xilinx Virtex-6 LX240T FPGA with two programmable RF interfaces operating at 2.4 and 5 GHz with a 40 MHz bandwidth. The WARP v3 Kit was selected for use with the platform due to its accessibility and ease of interface with MATLAB. The WARPLab 7.1 reference design is a buffer-based design with no physical or MAC layer which allows for implementation in software. The generated transmit waveforms are sent directly to the transmit buffers and the received waveforms are extracted directly from the receive buffer. Modulation, coding, and equalization are performed in MATLAB.

3.3 Performance Metrics

The received data is converted first into raw IQ, decoded IQ, and finally demodulated IQ. The CSI is estimated using the received training symbols. Several channel and link level metrics can be derived from the data in each of these states.

1. **System Capacity** is the upper bound on the rate of information that can be sent through a transceiver system (transmitter, channel, receiver) with an arbitrarily small level of error. For this implementation, capacity is calculated (in bits per Hertz) on a per packet basis from the normalized channel gain estimates recovered in each 802.11 packet. MIMO OFDM Channel capacity is defined as a function of CSI and SNR. The physical interpretation of the SNR is dependent on the channel normalization employed [63].

   For a flat fading channel, the capacity is defined as

$$C = \log_2\left(1 + \frac{P_{\mathtt{Tx}}|h|^2}{\mathcal{N}_0}\right), \tag{3.1}$$

where $P_{\mathtt{Tx}}$ is transmit power, $|h|$ is the complex channel gain, and $\mathcal{N}_0$ is the noise power in the channel.

For an OFDM link with K subcarriers, there are K narrowband flat fading channels. The channel capacity becomes the summation of the capacities of each subcarrier

$$C = \sum_{k=1}^{K} \log_2\left(1 + \frac{P_{\mathtt{Tx},k}|h_k|^2}{\mathcal{N}_{0,k}}\right). \tag{3.2}$$

This expression can be further expanded for the MIMO scenario as

$$C = \sum_{k=1}^{K} \log_2\left[\det\left(\mathbf{I}_{m\times n} + \frac{P_{\mathtt{Tx},k}}{m\mathcal{N}_{0,k}}\mathbf{H_k}\mathbf{H_k^\dagger}\right)\right]. \tag{3.3}$$

where $\mathbf{H_k}$ is an $m \times n$ channel matrix with m transmit antennas and n receive antennas. The entries $h_{i,j}$, represent the complex channel gain from Tx antenna i to Rx antenna j. To compare system capacity fairly from experiments using separate physical layers, the channel gains are normalized such that, $||\mathbf{H}||_{\text{Frobenius}} = mn$ [63]. While there are different methods of normalization, the Frobenius norm was selected to coincide with the literature and common practices [64, 65].

2. *Error Vector Magnitude* is the magnitude of the vector between a transmitted (expected) symbol and the received (actual) symbol. The distribution of the EVM is used to assess the quality of communications and has been proven to be a reliable predictor of signal integrity at the physical layer [66].

3. *Post-Processing Signal-to-Noise-Ratio* is defined as the ratio of signal power to signal error,

$$\text{PP-SNR}(dB) = \mathbb{E}\left[\frac{\|x\|^2}{\|\hat{x} - x\|^2}\right]. \tag{3.4}$$

In addition to channel noise, PP-SNR includes noise resulting from the specific hardware and processing implementation (e.g., non-linear distortion in the radio transceiver, error in channel estimation, and noise enhancement from equalization) [38].

4. *Throughput* is the amount of data successfully transmitted to a receiver per unit time (bits per second). Since the measurement platform implements the packet structure but not the timing protocol of IEEE 802.11g, it is not possible to directly measure the link throughput, but the achievable throughput can be estimated using the observed PPSNR and a Symbol Error Rate (SER) constraint [66]. For a given M-ary modulation scheme, the theoretical SER can be determined from the SNR [32]. Conversely, when SER is constrained, the minimum SNR needed to achieve that constraint can be determined. Any SNR above this threshold will support the chosen modulation scheme at the constrained SER or better. Thus, for a measured link with an observed SNR and a selected SER constraint, any modulation scheme with an SNR threshold less than the measured SNR will be supported. This process is demonstrated in Figure 3.4.

The throughput (T) can be estimated using the modulation order (M, number of symbols in the constellation) and the symbol rate (S, Baud per second),

$$T = S * \log_2 M. \tag{3.5}$$

The symbol rate of an OFDM word is calculated as

$$S = B * r_{\texttt{DSC}}, \tag{3.6}$$

where B is the bandwidth and $r_{\texttt{DSC}}$ is the ratio of subcarriers which hold payload data.

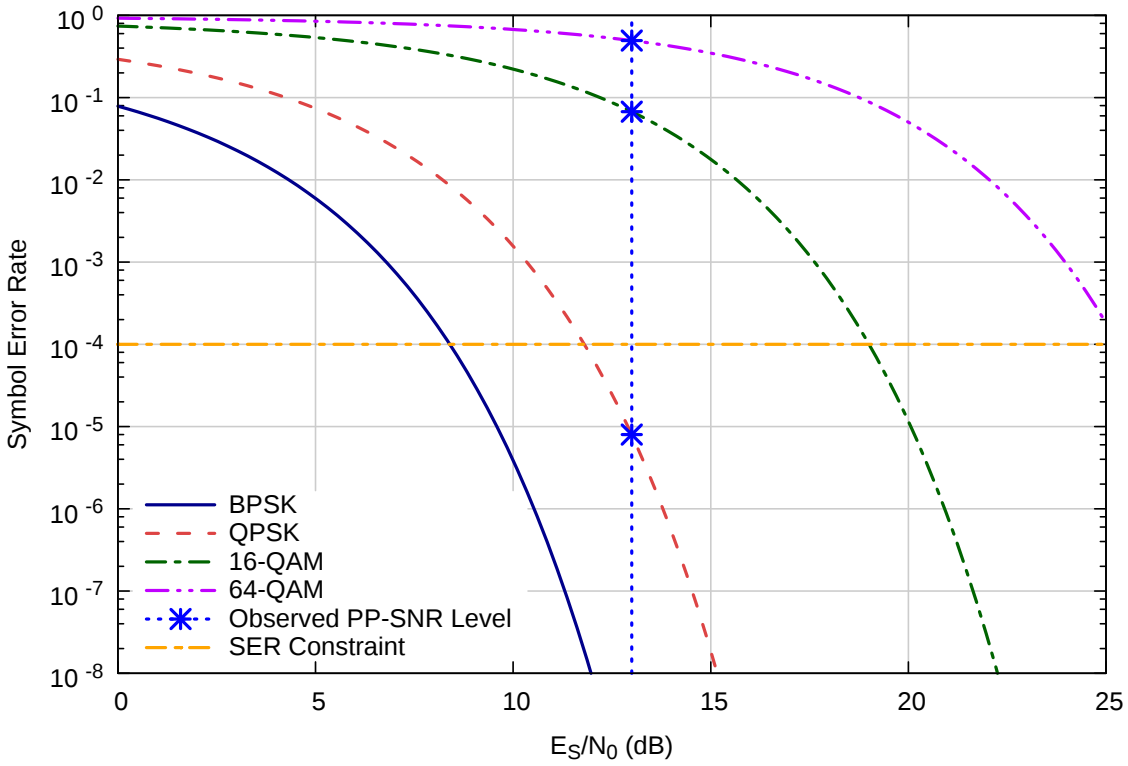

Figure 3.4: Theoretical SER curves for common, rectangular modulation schemes [32]. A vertical line is extended at the observed PPSNR of a link. A horizontal line is extended at the selected SER constraint of 1×10^{-4}. Each modulation scheme whose SER curve intersects the vertical PPSNR line below the horizontal SER constraint line is supported. In this example, an observed PP-SNR of 13 dB was selected with an SER constraint of 1×10^{-4}. This link supports both BPSK and QPSK with an achievable throughput of 6 and 12 Mbps, respectively. It is also possible to use this graph to estimate the SER for a specified modulation scheme. Using the same observed PP-SNR of 13 dB, the link would incur an SER of 3.4×10^{-2} if it were to use the 16-QAM modulation scheme.

In this effort, the frames were constructed with 64 subcarriers (including 48 data subcarriers) and a 16 sample cyclic extension with a bandwidth of 10 Mhz. Therefore, the symbol rate is

$$S \quad = \quad 10\text{MHz} * \frac{48}{64+16} = 6\text{MBdps}. \tag{3.7}$$

No coding schemes are considered, so the modulation schemes of BPSK, QPSK, 16-QAM, 64-QAM correspond to an achievable throughput of 6, 12, 18, and 24 Mbps, respectively.

3.4 Experimental Protocol

When the doors on the reverberation chamber are sealed, the electromagnetic field becomes static and the wireless channel exhibits only small variations. Such conditions are disadvantageous to communication measurements, because a single channel does not represent well the range of channels possible in actual environments. Typical wireless environments are more dynamic.

A dynamic wireless environment was created inside the reverberation chamber by altering, or "stirring," the reflective surfaces in the chamber. This stirring had the effect of changing the boundary conditions of the system, varying the electromagnetic field and also the magnitude, phase, and quantity of multipath components arriving at the receiver nodes.

Stirring was accomplished by rotating two Z-fold mechanical tuners, each 2.7 meters in length, inside the main chamber (seen in Figure 2.1). One tuner was positioned vertically in the southwest corner, while the other was located horizontally along the top of the north wall. The two tuners rotated at aperiodic intervals to prevent periodicity in the changing boundary conditions.

For meaningful comparison of different antenna types, antenna pattern configurations, and physical layer schemes, it is necessary to have identical channel conditions across the different configurations as experimental control. Modal stirring was used to ensure high channel correlation within a single trial. Stirring only occurred between trials so that the environment would be static across all test parameters.

A test protocol which uses the SDR platform is outlined below. Prior to the start of the test, the gains on each transmitting port are normalized to allow for unbiased comparisons between single-input and multiple-input transmission schemes. An Agilent U2001H USB Power sensor was used to measure the output power. The transmit gains were adjusted accordingly to match output power. When multiple physical layer schemes are being compared, the transmissions of the different schemes are interleaved to improve the correlation between channels and reduce the effect of time variance. The test protocol is as follows:

1. Configure the node topology.

2. Calibrate the transmitter.

   (a) Select a gain and send a SISO transmission.

   (b) Repeat (2.a) until the PP-SNR is maximized without exhibiting gain saturation [67].

   (c) Measure the transmit power of the transmitting port with a power sensor.

   (d) Adjust the gain on the additional transmitting port to match the calibrated output power. If saturation occurs, repeat 2.a with a lower initial gain.

3. Execute the test.

   (a) Send a SISO transmission (SISO/MRC).

   (b) Receive the SISO transmission on both antennas.

   (c) Send a MIMO transmission (Alamouti code/SMUX).

   (d) Receive the MIMO transmission on both antennas.

   (e) Repeat (3.a-b) for the desired number of trials.

Both SISO and MRC can be decoded from a SISO transmission (Step 3.a), since a copy of the transmitted signal is received on both receiver antennas. SISO decoding only uses a single RX stream, while MRC decoding uses both streams. Similarly, both Alamouti code and SMUX can be decoded from a MIMO transmission (Step 3.b) when the Alamouti encoding has been applied to both transmitted streams. For SMUX decoding, the two streams are interpreted as independent data streams, ignoring that they contain an Alamouti block code. By decoding all four physical layer schemes using only two transmissions, the total number of transmissions (and length of the test) is halved.

3.5 Conclusions

Consumer-grade equipment is incapable of performing detailed analysis of wireless communications in certain challenging environments. Specialized equipment for these environments is often cost prohibitive and not suited for mobile applications and field testing. A MATLAB-based SDR platform

was presented as a cost-effective, lightweight alternative. The platform implements four MIMO OFDM transmission schemes based on the IEEE 802.11g protocol and allows full user access to transmit and receive buffers. The raw data extracted from the platform can be used to derive a host of metrics necessary for evaluation of channel and link properties.

Chapter 4: Characterization of Wireless Communication Performance

4.1 Introduction

Portions of this chapter were published in the IEEE Antennas and Wireless Propagation Letters [38] and the Proceedings of the 2014 IEEE International Communications Quality and Reliability Workshop [30]. Portions of this chapter have been included in a manuscript submitted to IEEE Transactions on Communications [49].

To characterize the performance of wireless communications in highly reverberant environments, two experimental measurement campaigns were undertaken. The first campaign was in the controlled environment of the coupled reverberation chambers at the Naval Surface Warfare Center Dahlgren Division (NSWCDD). Using previously measured ranges for the loading in below deck spaces, the loading in the chambers was selected to match. A series of node and environments parameters were evaluated to provide insights on the expected performance in an actual multipath environment. The second campaign was conducted on board the *Thomas S. Gates* (CG 51) at the Naval Inactive Ship Maintenance Facility (NISMF) in Philadelphia, PA. A series of locations were selected in the vessel to test based on their perceived utility as locations for wireless network installations. During both campaigns, the measurement platform described in Chapter 3 was used for all experiments.

Discussion of the results begins with the first campaign in the coupled reverberation chambers. The following section describes the second campaign in the below deck spaces. The chapter concludes with a comparison of the results from both campaigns.

4.2 Coupled Reverberation Chambers

The objective of this effort is to investigate the effect of electromagnetic reverberance on WLAN communications through experimentation in a controlled environment. Experiments were conducted in coupled reverberation chambers of the NSWCDD at the Naval Support Facility Dahlgren (NSFD). The level of electromagnetic reverberance (loading) in the chambers was tuned to mimic the rever-

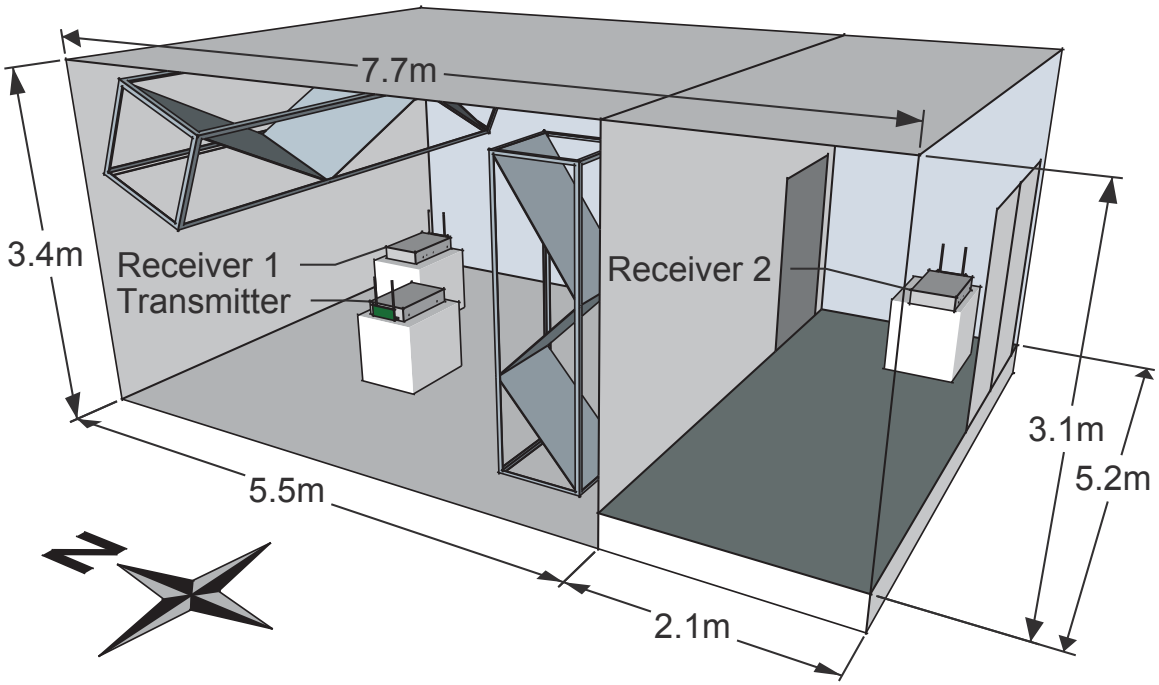

Figure 4.1: Cross section view of the main chamber and ante chamber in the coupled reverberation chambers of the NSWCDD.

berance in the below deck spaces of a naval vessel. The range was determined from measurements taken on actual naval vessels [37]. A similar methodology was followed in [18] where the wireless propagation of outdoor urban environments was recreated in a reverberation chamber. The influence of several parameters was considered in relation to the loading: signal propagation (line-of-sight vs non-line-of-sight), receiver diversity (Single Input Single Output (SISO) vs Maximal Ratio Combining (MRC)), and cavity coupling between the chambers (small vs large effective aperture).

4.2.1 Experimental Setup

To mimic practical, highly reverberant environments, the main chamber was tuned to the Q of actual below-deck environments on a naval vessel in the range of $Q = 1100$ to $Q = 5800$ [37, 19, 13]. Reverberation chambers have naturally low loading as they are designed to minimize electromagnetic absorption and maintain field strength. The loading of the chamber may be increased by adding electromagnetically absorptive material inside the chamber.

Three (3) nodes were used in the experiments, one (1) transmitter and two (2) receivers. Receiver

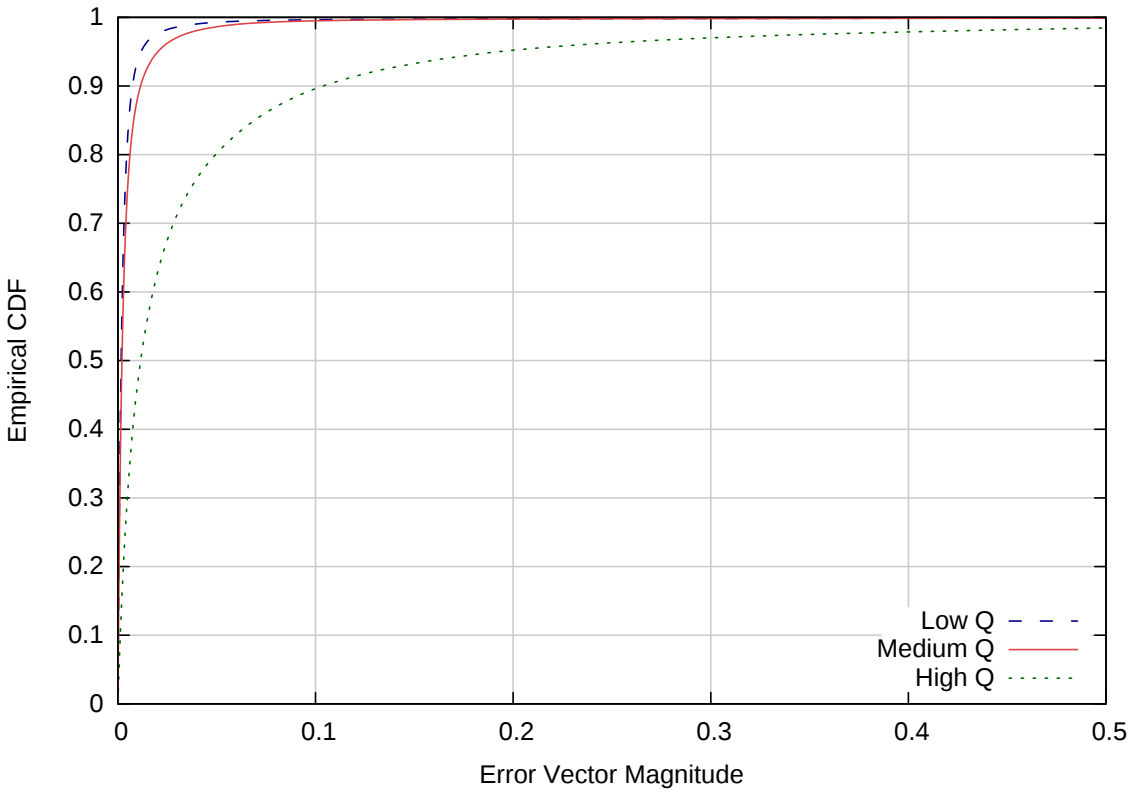

Figure 4.2: Coupled reverberation chambers. CDF of the EVM of the LOS Receiver.

1 (Line Of Sight (LOS) receiver) was deployed in the main chamber with the transmitter. Receiver (Non Line of Sight (NLOS) receiver) was deployed in the ante chamber behind the adjoining, shielded door such that it did not have line of sight into the main chamber. The precise locations are shown in Figure 4.1. All nodes were elevated off the ground by non-absorbing, Styrofoam blocks.

The loading in the reverberation chamber was tuned by adding electromagnetic absorbing foam into the chamber until the desired Q was achieved. At the start of each experiment, the transmit gain was calibrated using an Agilent U2001H USB Power sensor to ensure equal gains across tests. An experiment consisted of 500 transmissions where each transmission contained 960 symbols for a total of 480,000 samples per experiment. The channel was stirred every 10 transmissions by rotating the two Z-fold mechanical tuners.

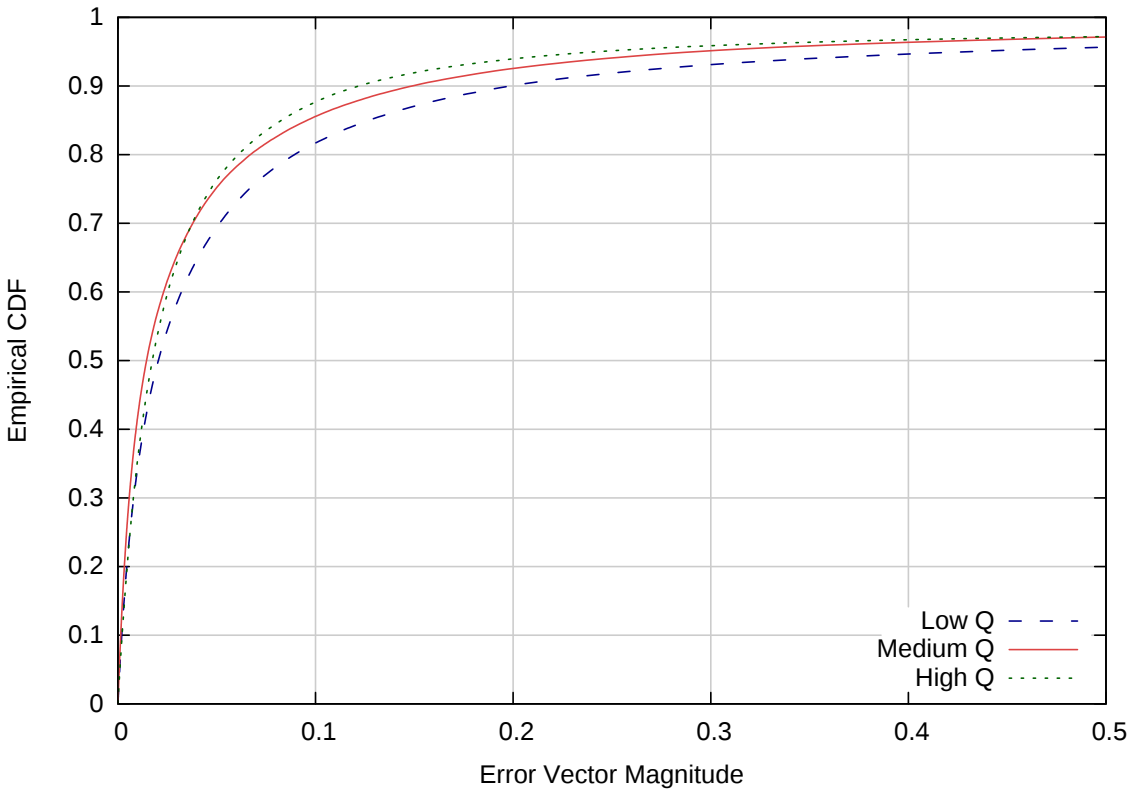

Figure 4.3: Coupled reverberation chambers. CDF of the EVM of the NLOS Receiver.

4.2.2 Results

Receivers (LOS v NLOS)

.

The two receivers were positioned such that one had a Line-Of-Sight (LOS) signal component with the transmitter, while the other did not. The LOS receiver was positioned in the main chamber with the transmitter while the NLOS receiver was positioned behind the door in the ante chamber (Figure 4.1). The Cumulative Distribution Function (CDF) of the Error Vector Magnitude (EVM) for the LOS receiver and the NLOS receiver are shown in Figures 4.2 and 4.3, respectively. Since lower EVM is preferred, better performance is indicated by the distribution being closer to the top left corner of the plot. For the LOS receiver in Figure 4.2, Low Q has slightly better signal quality than Medium Q, while both are significantly better than High Q. As expected, when the loading decreases, the performance of the LOS receiver degrades due to an increase in multipath interference.

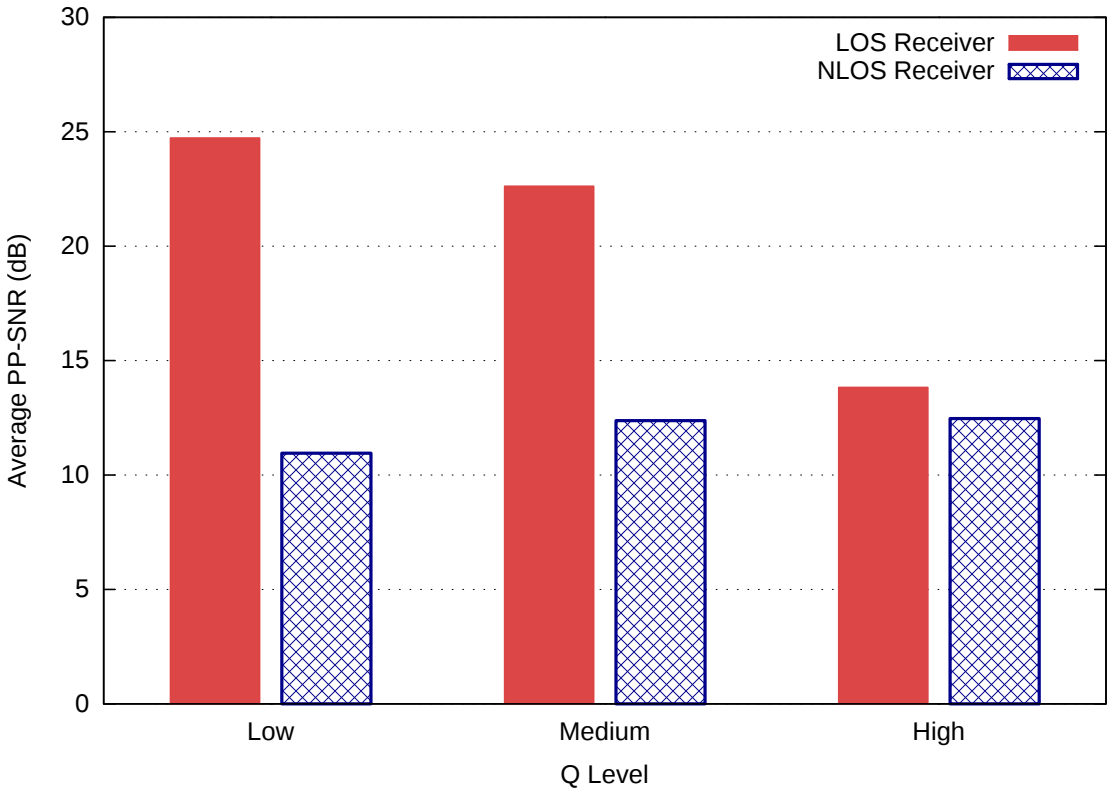

Figure 4.4: Coupled reverberation chambers. PPSNR for the LOS receiver and NLOS receiver across all loading configurations

This notion is further exemplified in Figure 4.4, where the PP-SNR drops by nearly 11 dB from Low Q to High Q. The loss in PP-SNR decreases the achievable throughput from 18 Mbps to 12 Mbps (Table 4.1).

Interestingly, the trend is reversed for the NLOS receiver (Figures 4.3 and 4.4). When loading decreases, the performance *improves*. Since less signal energy is absorbed by the environment, more energy propagates into the coupled chamber resulting in greater received energy at the NLOS receiver. The largest improvement is between Low Q and Medium Q where the gain in PP-SNR is enough to increase the throughput by 6 Mbps.

The NLOS receiver had lower signal quality than the LOS receiver in each case. The power of the received signal at the NLOS receiver is lower due to path loss and partial absorption of reflected multipath components that comprise its received signal. The gap in performance between the LOS receiver and NLOS receiver narrows as the loading decreases. This observation is evident in both

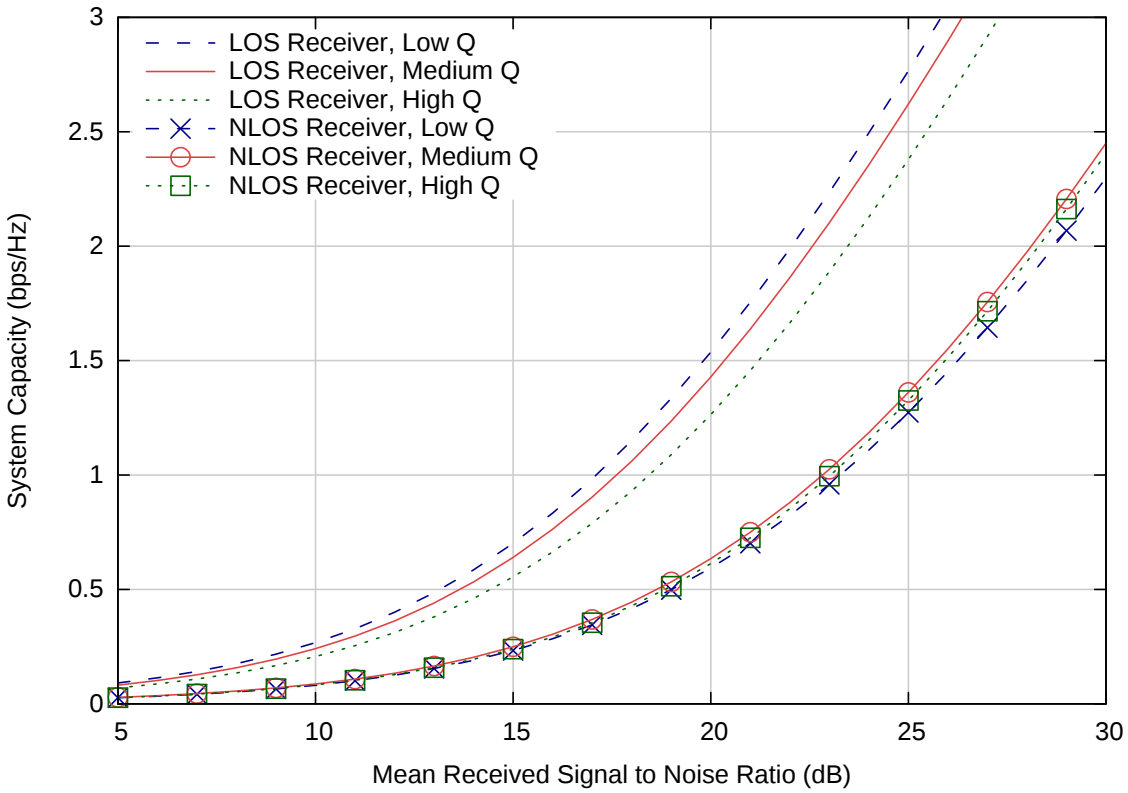

Figure 4.5: Coupled reverberation chambers. Observed system capacity for the LOS receiver and NLOS receiver across all loading configurations.

Figure 4.4 and Table 4.1. For Low Q, the LOS receiver has a PP-SNR 13.8 dB higher than the NLOS receiver. For High Q, the LOS receiver only has a PP-SNR 1.4 dB higher than the NLOS receiver, and both receivers have a throughput of 12 Mbps.

It is likely that the trends for line-of-sight would extend to non-reverberant environments, albeit at much smaller scales. The LOS receiver degrades significantly (˜11db) as multipath interface increases in to High Q. In a non-reverberant environment, multipath interface will also decrease signal quality, but not nearly at that magnitude [14, 15, 16, 17, 18]. It is more difficult to predict the performance of a NLOS receiver in non-reverberant environments as the propagation paths can vary widely. The trend for the NLOS receiver was observed in the coupled reverberation chamber which is a highly controlled environment. As will be shown in the results from the below-decks measurement campaign (4.3), the performance of NLOS receivers can change on a link-by-link basis that it is depend on the physical geometry of the space. Similarly, there are most likely situations in

Table 4.1: Coupled Reverberation Chambers. Achievable throughput (Mbps) with symbol error rate constrained to 1×10^{-4} for the LOS Receiver and NLOS Receiver across all loading configurations.

	Q		
Receiver	Low	Medium	High
LOS	18	18	12
NLOS	6	12	12

non-reverberant environments in which multipath both can improve and degrade the performance of NLOS receivers.

The capacity for the LOS Receiver and NLOS Receiver are shown across all loading configurations in Figure 4.5. The LOS receiver improves in capacity considerably as the loading increases and also approximately double the capacity of the NLOS receiver. In following with the previous results for the NLOS receiver, the capacity is greater for lower loading.

Receiver Diversity

Two physical layer schemes were used by the receivers: 1×1 SISO and 1×2 MRC [32]. SISO is a simple point to point (1×1) scheme where the received signal from only one of the receiver's two antennas is used. MRC computes the weighted average of both received streams, so it is expected to outperform SISO.

Line-of-Sight For the LOS receiver, the CDF of the EVM is shown in Figure 4.6, and the PP-SNR is shown in Figure 4.7. In both figures, the performance of SISO and MRC are compared across all three Q configurations where the results show MRC has a notable gain in signal quality over SISO. The gap in performance widens as the loading decreases. The difference in PP-SNR goes from 3.0 dB at Low Q to 5.3 dB at High Q. MRC is able to mitigate increased multipath interference better than SISO, so its performance does not degrade as much when the loading decreases.

At High Q, the individual received signals have lower correlation which is advantageous for MRC since it computes the weighted average of the signals. This phenomenon is exemplified by the CDFs of the EVM for SISO and MRC at High Q. In this case, SISO has a higher median EVM and a

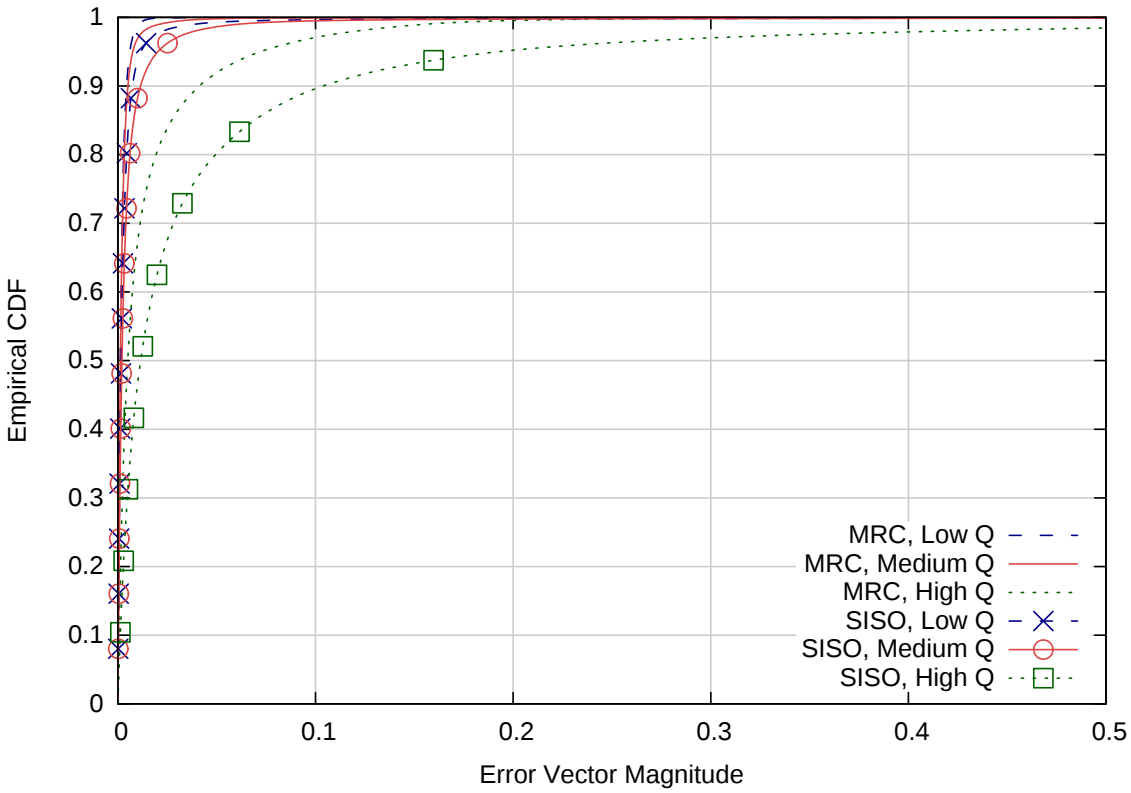

Figure 4.6: Coupled reverberation chambers. CDF for the EVM of the LOS Receiver across both physical layer schemes.

heavier tail than MRC. When one received signal has a high level of error, MRC can heavily weight the better stream to reduce symbol error (i.e., the heavy tail). The low correlation between received streams is leveraged to improve signal quality. The effectiveness of receiver diversity is diminished when the received streams are highly correlated. This implies that the use of receiver diversity is particularly well suited for reverberant environments. Benefit would still be provided in non-reverberant environments, which have higher received stream correlation (due to lower multipath), but not at the magnitude provided in reverberant environments.

The throughput for the LOS receiver with both physical layer schemes is shown in Table 4.2. Even though the transmit rate of SISO and MRC are equal, MRC outperforms SISO in throughput by 6 Mbps due to its improved PP-SNR. While the gap in PP-SNR increases as the loading decreases, the difference in throughput remains constant across all configurations.

The capacity for the LOS Receiver shown across all loading configurations and SISO and MRC

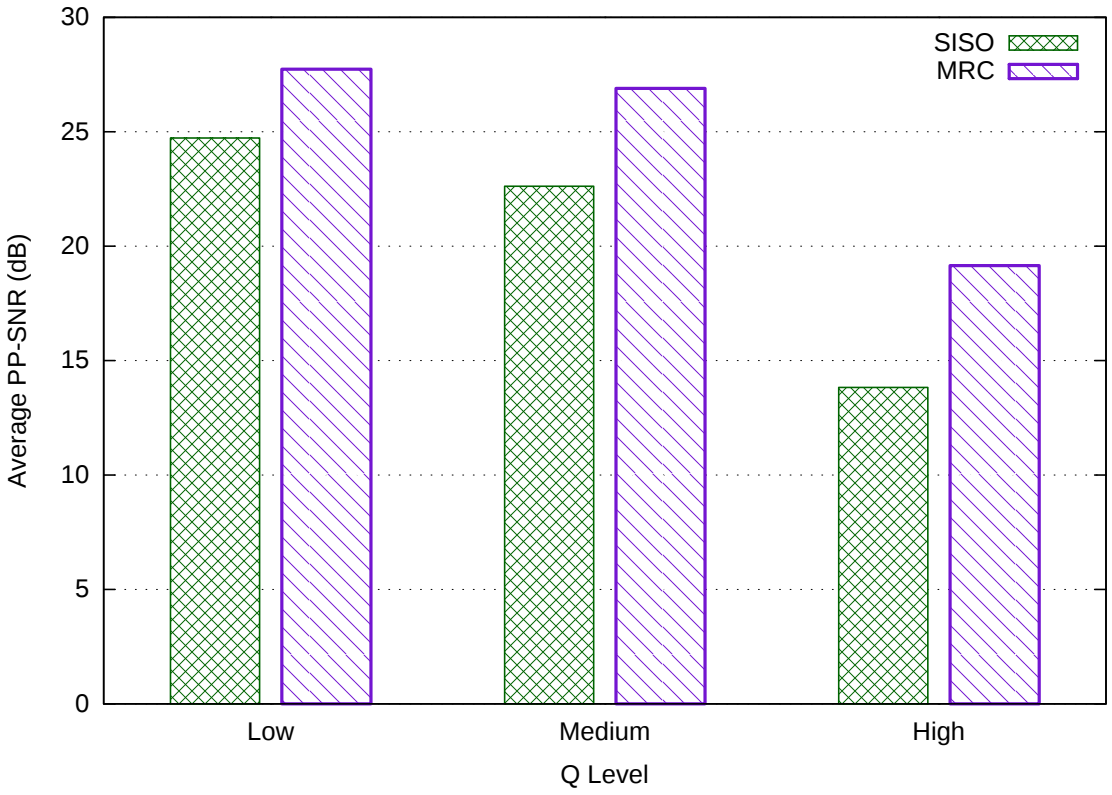

Figure 4.7: Coupled reverberation chambers. PPSNR for the LOS Receiver across both physical layer schemes.

is shown in Figure 4.8. MRC proves to have approximately double the system capacity of SISO while each physical layer scheme individually improves substantially as the loading decreases. This coincides with the earlier observations regarding the effect of multipath interference on the LOS receiver.

Non-Line-of-Sight For the NLOS receiver, the CDF of the EVM is shown in Figure 4.9, and the PP-SNR is shown in Figure 4.10. Again, the results show that MRC outperforms SISO. MRC follows the same overall trend as SISO by increasing when the loading decreases. The difference in PP-SNR is 4.6 dB at Low Q and 4.7 dB at High Q, so, unlike the LOS case, there is no significant change in the performance gap between SISO and MRC.

The throughput for the NLOS receiver with both physical layer schemes is shown in Table 4.3. There is not a significant difference in the throughput of SISO and MRC for the NLOS receiver.

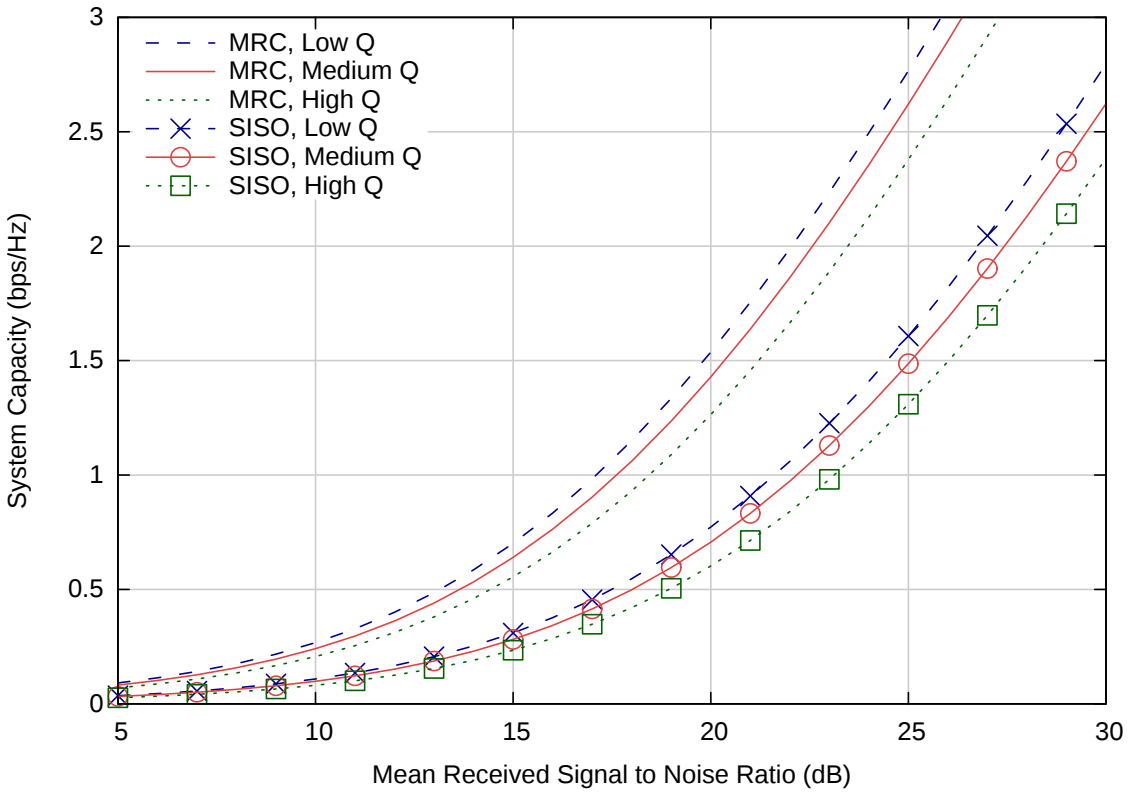

Figure 4.8: Coupled reverberation chambers. Observed system capacity for the LOS Receiver across all loading configurations and both physical layer schemes.

MRC only has a higher throughput in the Low Q configuration. Despite the notable gains in PP-SNR for MRC, the quantization which occurs when placing a threshold on the Symbol Error Rate (SER) does not result in increased throughput in this case. Even so, the gains achieved by MRC would often result in increased throughput for NLOS links.

The capacity for the LOS Receiver shown across all loading configurations and SISO and MRC is shown in Figure 4.11. As in the LOS case, MRC approximately doubles the capacity of SISO. Interestingly, there is not clear trend and minor differences in the capacity between the different loading configurations. This result differs from the EVM and PPSNR which distinctly increase as the loading decreases. The lack of improvement in the capacity likely indicates that the frequency selectivity of the channel is not diminishing, rather the path loss is improving. The NLOS receiver receives only reflected components, so there is no dominant line of sight component which it is being disrupted. The decreased loading is improving the wave guiding effect such that more energy is

Table 4.2: Coupled reverberation chambers. Achievable throughput (Mbps) for the LOS Receiver across all loading configurations and both physical layer schemes with SER constrained to 1×10^{-4}.

	Q		
Physical Layer Scheme	Low	Medium	High
SISO	18	18	12
MRC	24	24	18

Table 4.3: Coupled reverberation chambers. Achievable throughput (Mbps) for the NLOS Receiver across all loading configurations and both physical layer schemes with SER constrained to 1×10^{-4}.

	Q		
Physical Layer Scheme	Low	Medium	High
SISO	6	12	12
MRC	12	12	12

coupled into the ante chamber.

Cavity Coupling

"Cavity coupling" refers to the size of the effective aperture that exists between connected cavities. The effective aperture size is the combined electromagnetic leakage from doors, hatches, windows, cables, bulkhead penetrations, floor joints, etc. Since the reverberation chambers are constructed to prevent electromagnetic leakage, the effective aperture size can be controlled by the position of the door between the main chamber and ante chamber. To test the effect of the cavity coupling on the performance of wireless communications, the loading was held constant at the Medium Q configuration while the door between the cavities was varied across three settings: nearly closed, halfway closed, and fully open. For the remainder of the document, these configurations will be referred to respectively as "Low Coupling," "Medium Coupling," and "High Coupling."

The Cumulative Distribution Functions (CDFs) of the EVM are shown for the LOS receiver and NLOS receiver in Figures 4.15 and 4.16, respectively. The PPSNR of both receivers are shown in Figure 4.17. Performance improves for both receivers as the level of coupling increases. Both receivers improve in PPSNR by approximately 3 dB when moving from Low Coupling to High

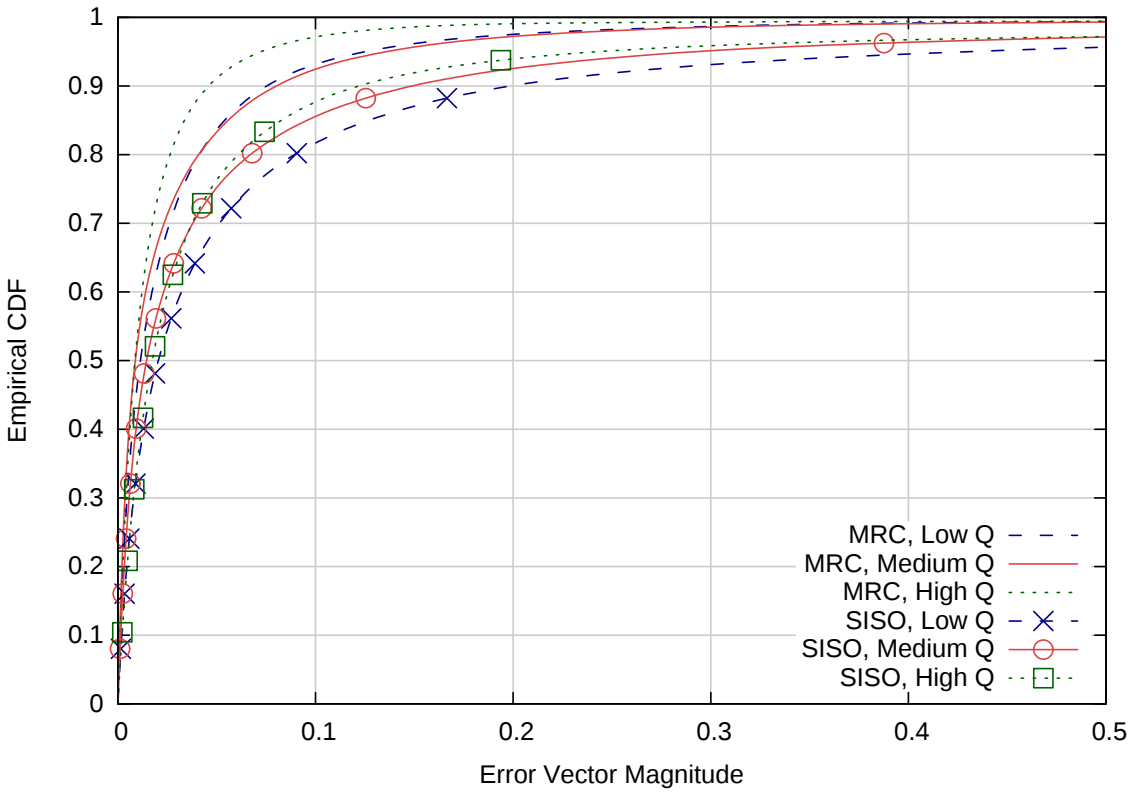

Figure 4.9: Coupled reverberation chambers. CDF for the EVM of the NLOS Receiver across both physical layer schemes.

Coupling. At high coupling, more energy propagates into the ante (coupled) chamber. The LOS receiver likely experiences less multipath interference as a result. Meanwhile, the NLOS receiver receives greater signal power, thereby improving performance for that receiver as well.

The effect of coupling would likely be difficult to observe in non-reverberant environments, but it results from a restricted propagation path. Non-reverberant environments are not electromagnetically sealed and therefore exhibits electromagnetic leakage through physical barriers. Signal propagation does not depend as much on "open apertures" to reach NLOS receivers. Furthermore, LOS links will likely not be impacted by the coupling increasing since the change in multipath would be minimal.

The throughput for both receivers across all levels of coupling is shown in Table 4.4. The improved PPSNR is not enough to increase the throughput for the LOS Receiver which remains at 18 Mbps throughput for all coupling configurations.

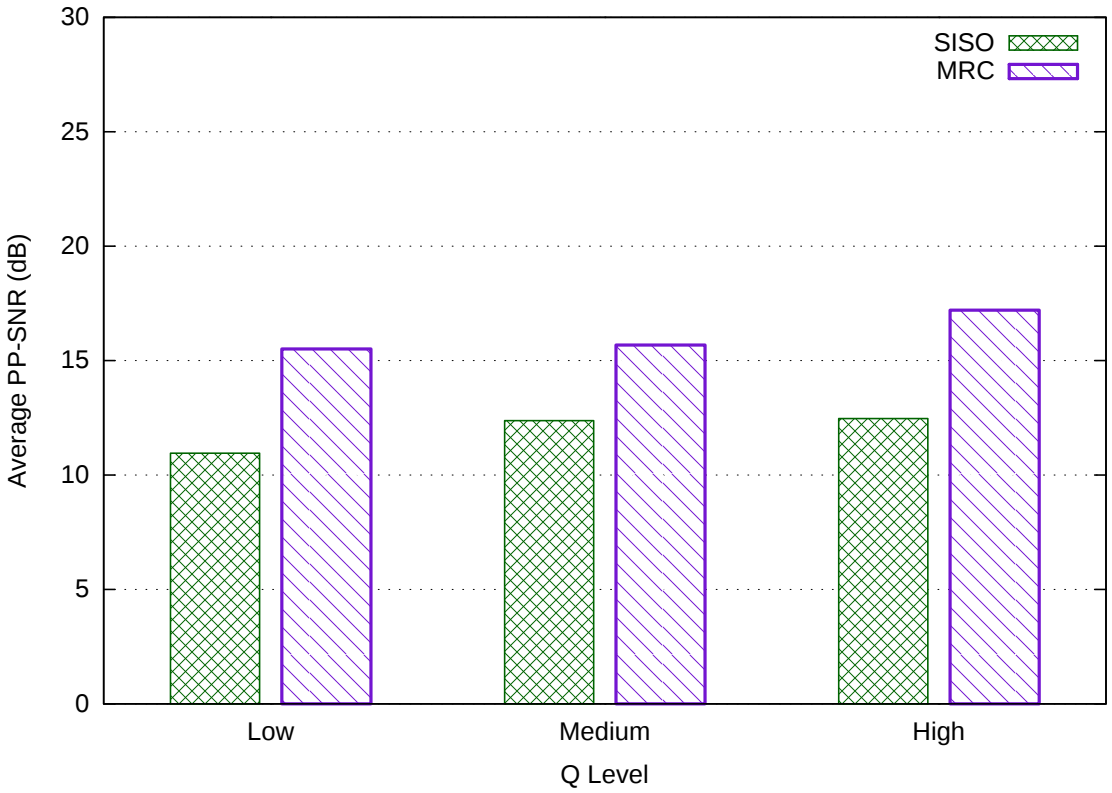

Figure 4.10: Coupled reverberation chambers. PPSNR for the NLOS Receiver across both physical layer schemes.

The capacity for the LOS Receiver and NLOS Receiver are shown across all coupling configurations with both physical layer schemes in Figures 4.18 and 4.19, respectively. There is a negligible difference in capacity for the LOS receiver while the capacity does improve at higher capacity for the NLOS receiver. This result implies the coupling has little influence on the frequency selectivity of the channel. The reverberance is not changing, only the distribution of the energy in the cavities. As the coupling increases, a greater quantity of the signal propagates into the ante chamber, thereby improving the capacity for the NLOS receiver.

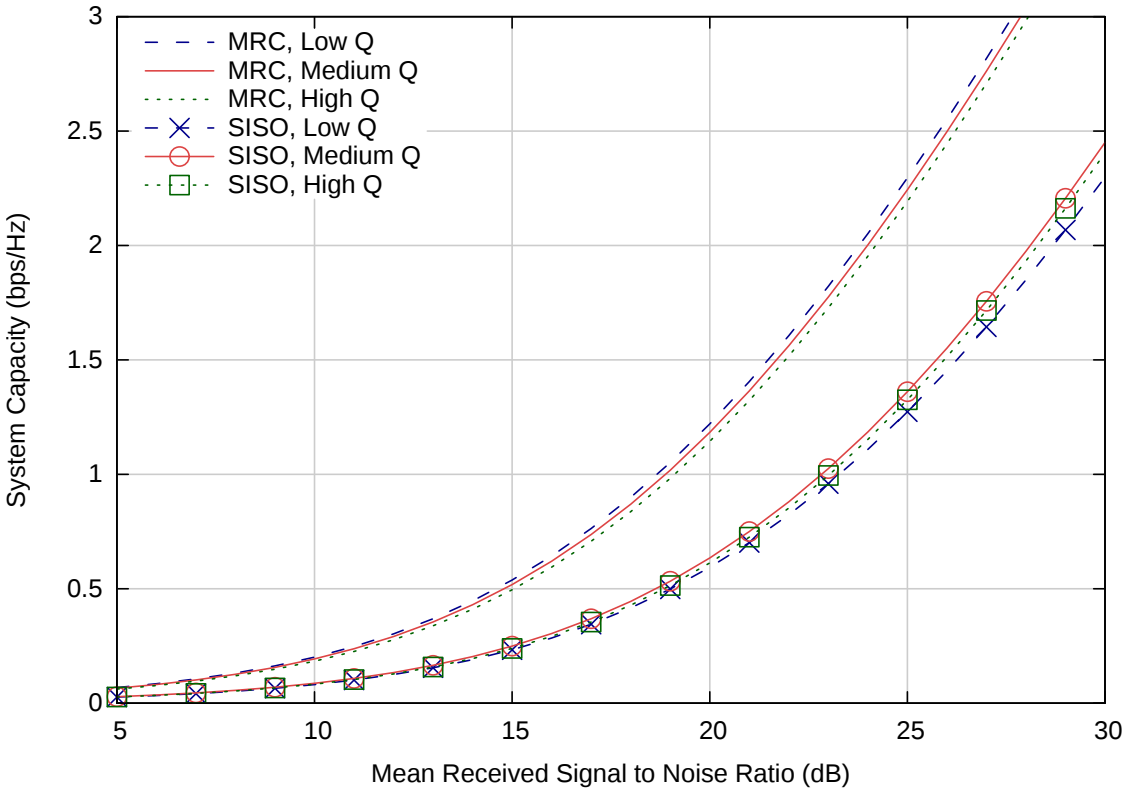

Figure 4.11: Coupled reverberation chambers. Observed system capacity for the NLOS Receiver across all loading configurations and both physical layer schemes.

Figure 4.12: Position of the shielded door between the main chamber and the ante chamber for Low Coupling configuration.

Figure 4.13: Position of the shielded door between the main chamber and the ante chamber for Medium Coupling configuration.

Figure 4.14: Position of the shielded door between the main chamber and the ante chamber for High Coupling configuration.

Table 4.4: Coupled reverberation chambers. Achievable throughput (Mbps) for the LOS Receiver and NLOS Receiver across all coupling configurations with SER constrained to 1×10^{-4}.

	Coupling		
Receiver	Low	Medium	High
LOS	18	18	18
NLOS	6	12	12

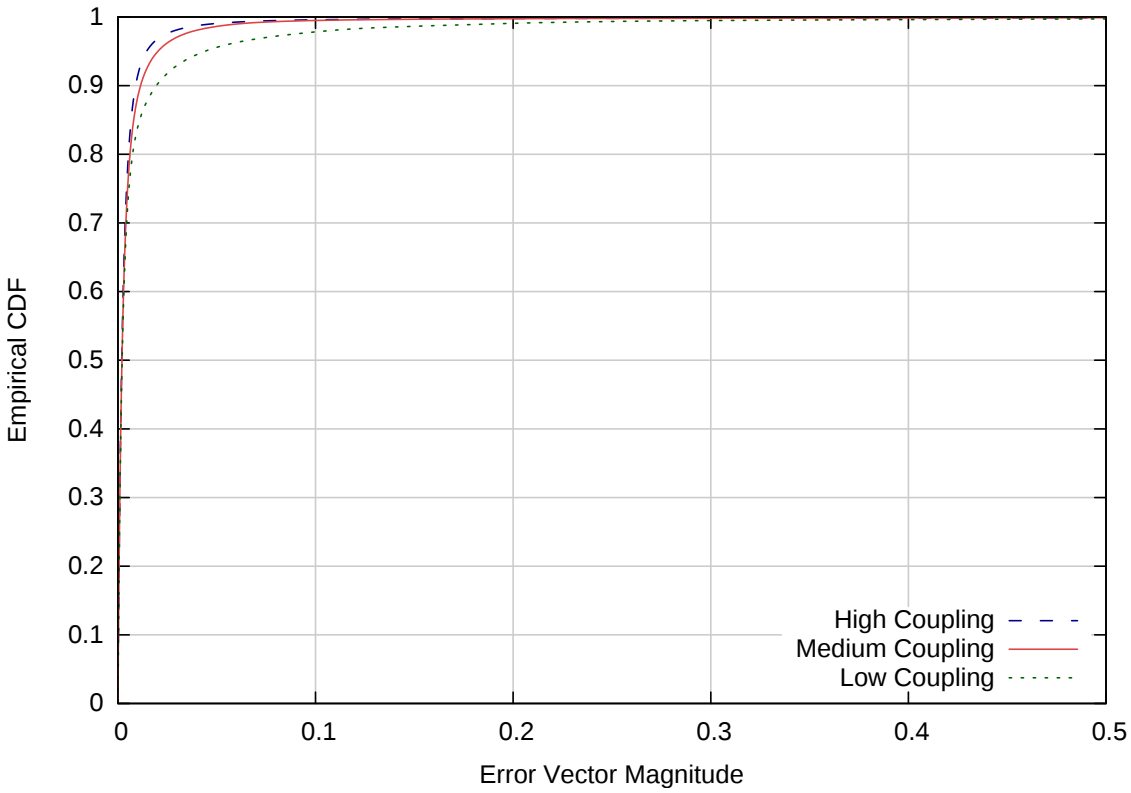

Figure 4.15: Coupled reverberation chambers. CDF for the EVM of the LOS Receiver across all coupling configurations.

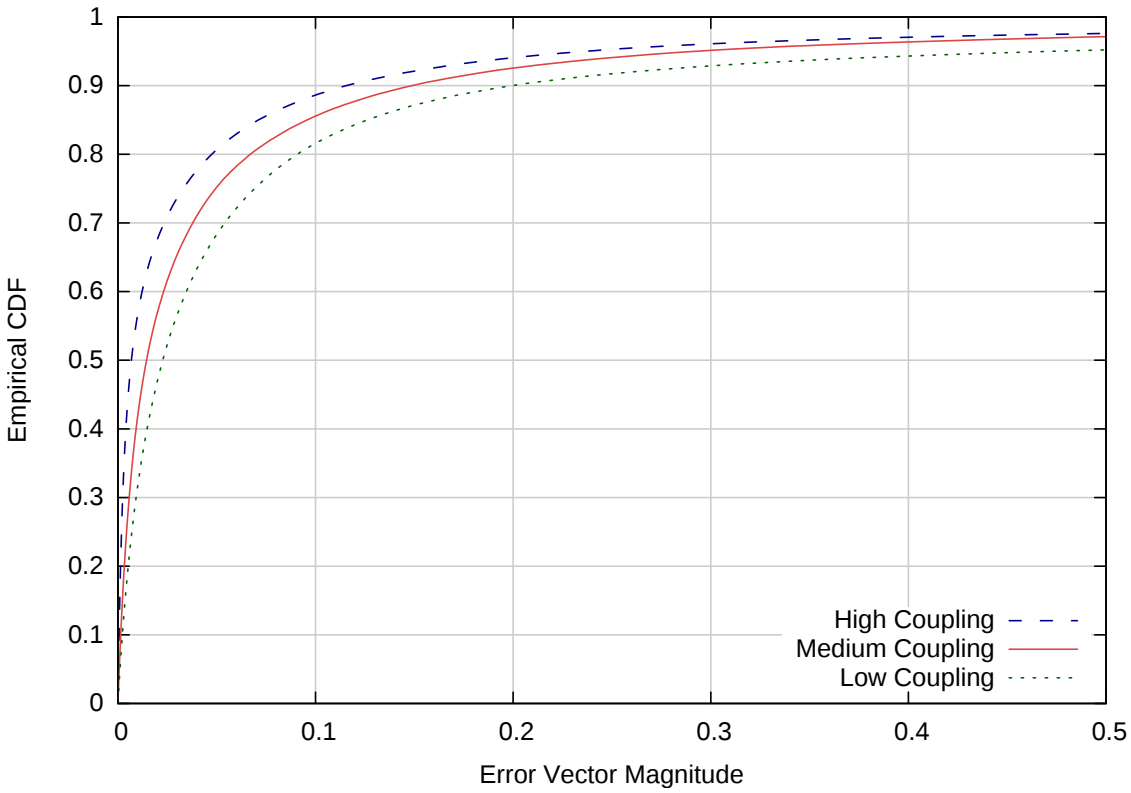

Figure 4.16: Coupled reverberation chambers. CDF for the EVM of the LOS Receiver across all coupling configurations.

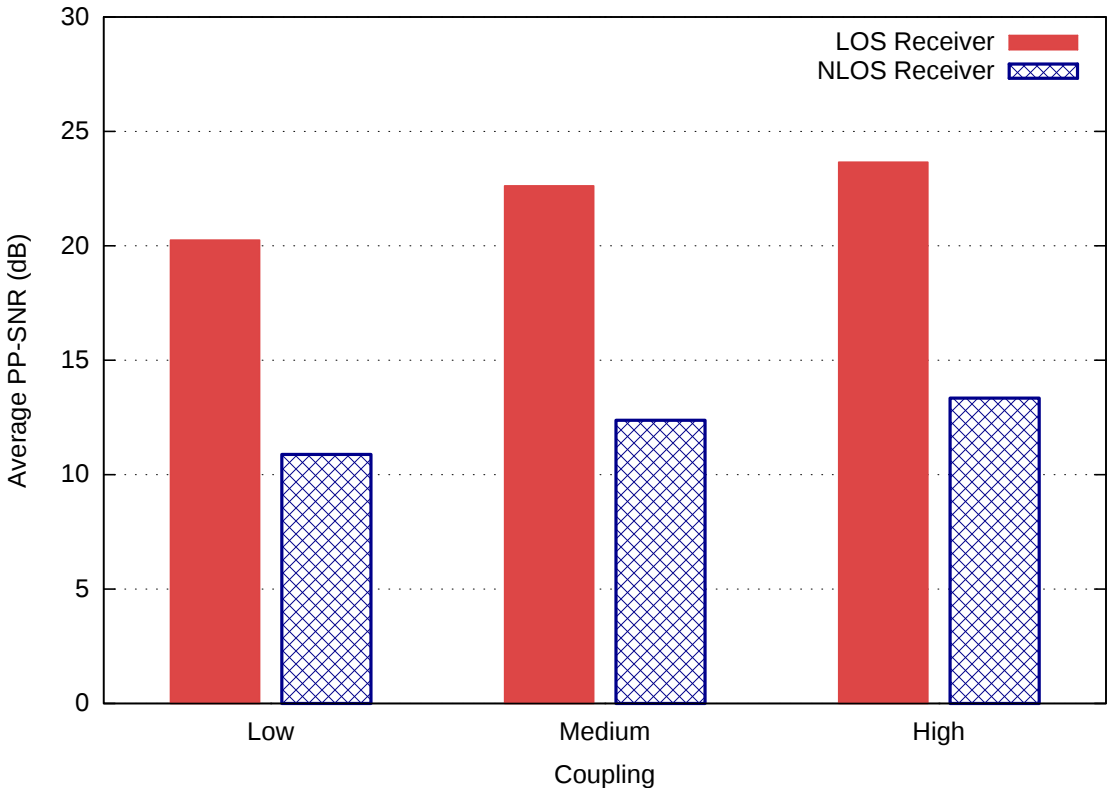

Figure 4.17: Coupled reverberation chambers. PPSNR for the LOS Receiver and the NLOS Receiver across both physical layer schemes.

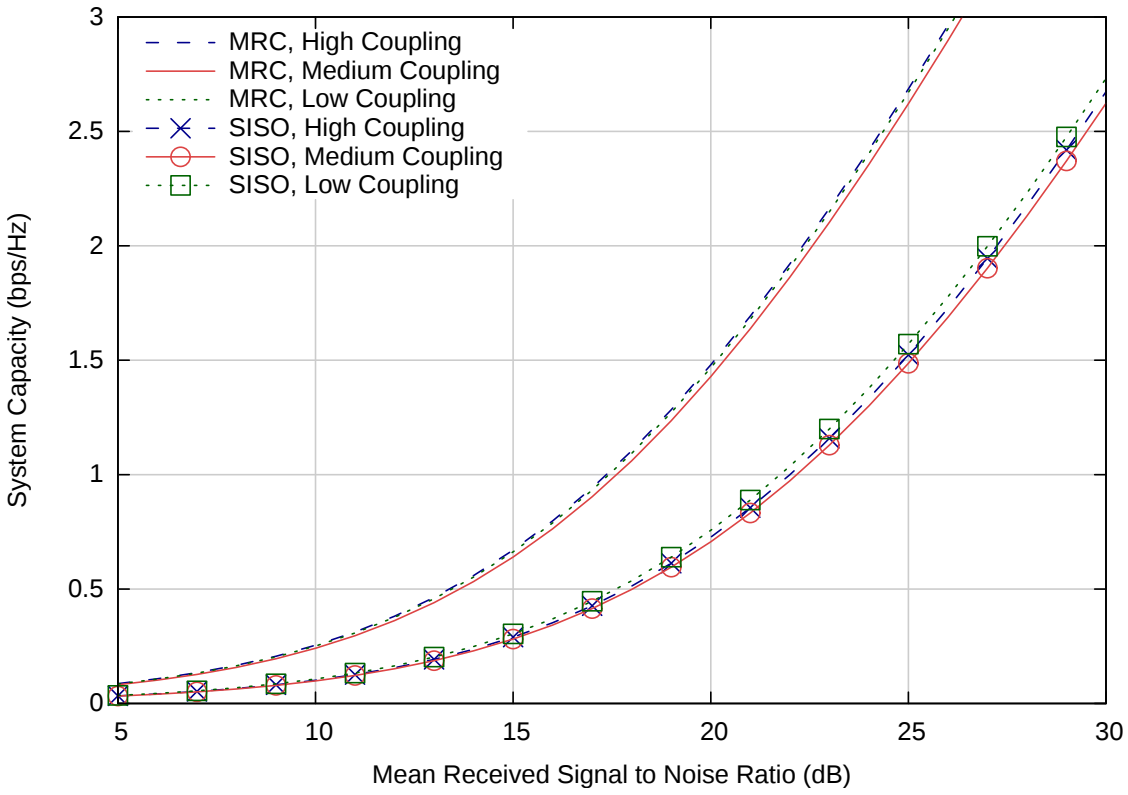

Figure 4.18: Coupled reverberation chambers. Observed system capacity for the LOS Receiver across all coupling configurations.

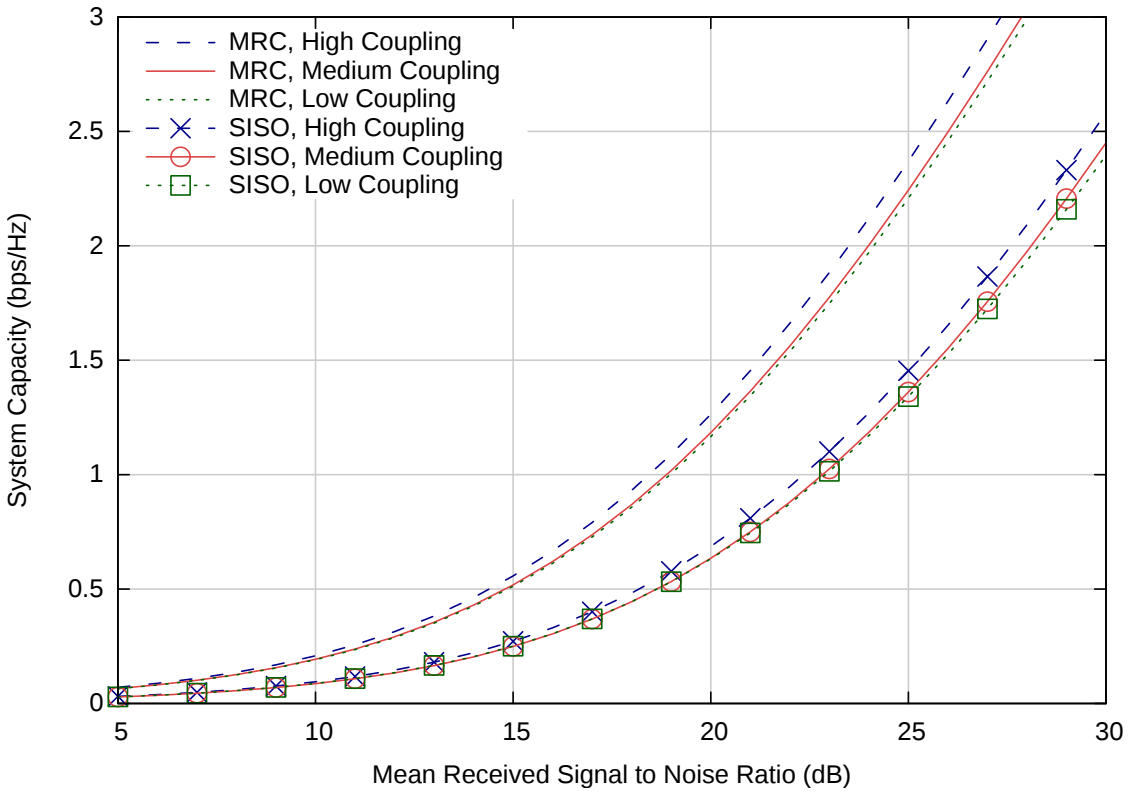

Figure 4.19: Coupled reverberation chambers. Observed system capacity for the NLOS Receiver across all coupling configurations.

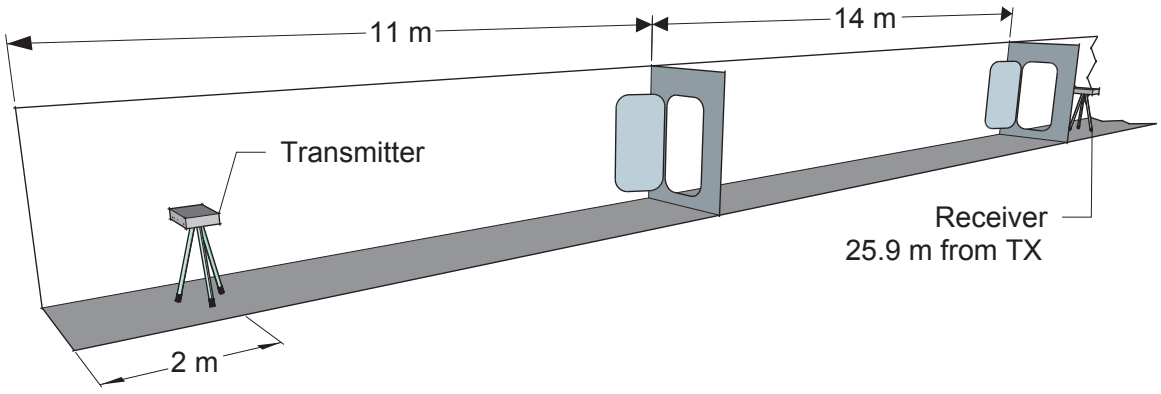

Figure 4.20: Cross section of the port-side passageway test scenario on the *Thomas S. Gates* (CG 51).

4.3 Below-Deck Spaces

The scenarios that were tested on the decommissioned cruisers were selected to provide a range of spaces that might be considered for deployment of wireless networks on a ship. Each scenario represents a typical below decks configuration that might be encountered aboard any class of ship (or even some aircraft). The chosen scenarios include the aft engine room; three clustered compartments on the same deck near the stern; and the main port-side passageway. A description of each scenario is described below along with the corresponding experiment results.

The experiment protocol was the same on the naval vessel as it was on the reverberation chamber with one exception. Stirring was accomplished by moving the transmitter around a 1 meter radius at periodic intervals. Since this method alters the wireless channel, it is equivalent to having rotating tuners, as in the reverberation chambers.

4.3.1 Port-side Passageway

Experiment Description

A long passageway (Figure 4.20) was selected as a prime location for the installation of core network infrastructure. Watertight doors located at each structural frame would normally be open, likely allowing wireless communication over a significant distance due to the wave guide effect of the passage. By testing with the doors both open and closed, performance was assessed both for normal operating conditions and for adverse conditions when the doors would be closed.

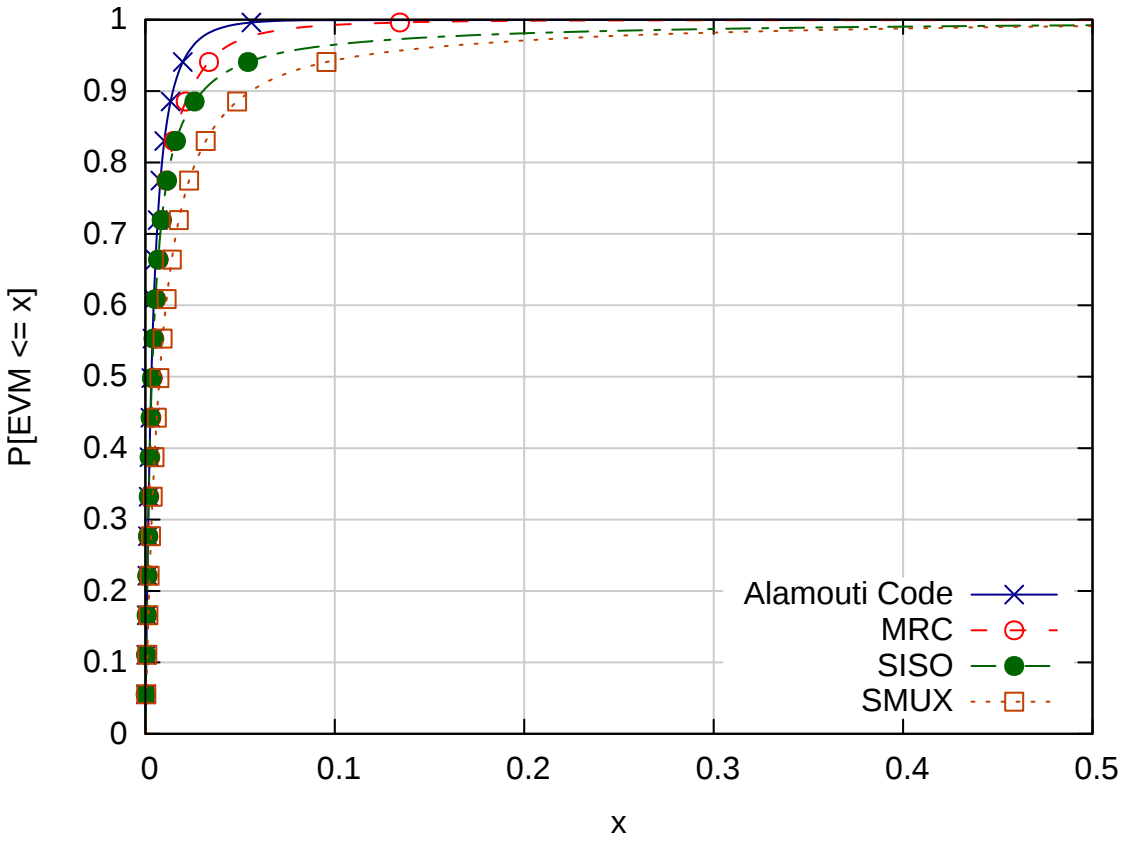

Figure 4.21: Port-side passageway. CDF of the EVM of across all physical layer schemes with the door open.

A two node topology was deployed in the passage with a transmitter at the end of the corridor and a receiver 25.9 meters down the corridor beyond two watertight doors as shown in Figure 4.20. Both nodes were outfitted with two omnidirectional antennas. One test was conducted with both doors open, and another was conducted with just the first door closed.

Results

The CDFs of the EVM with the door open and closed are shown Figures 4.21 and 4.25) respectively. The amount of link degradation is indicated by increased variance and heavy tails of the EVM distributions when the door is closed. Since the signal cannot penetrate the bulkhead, it must propagate through apertures in and around the watertight door, including a rubber gasket and a glass porthole.

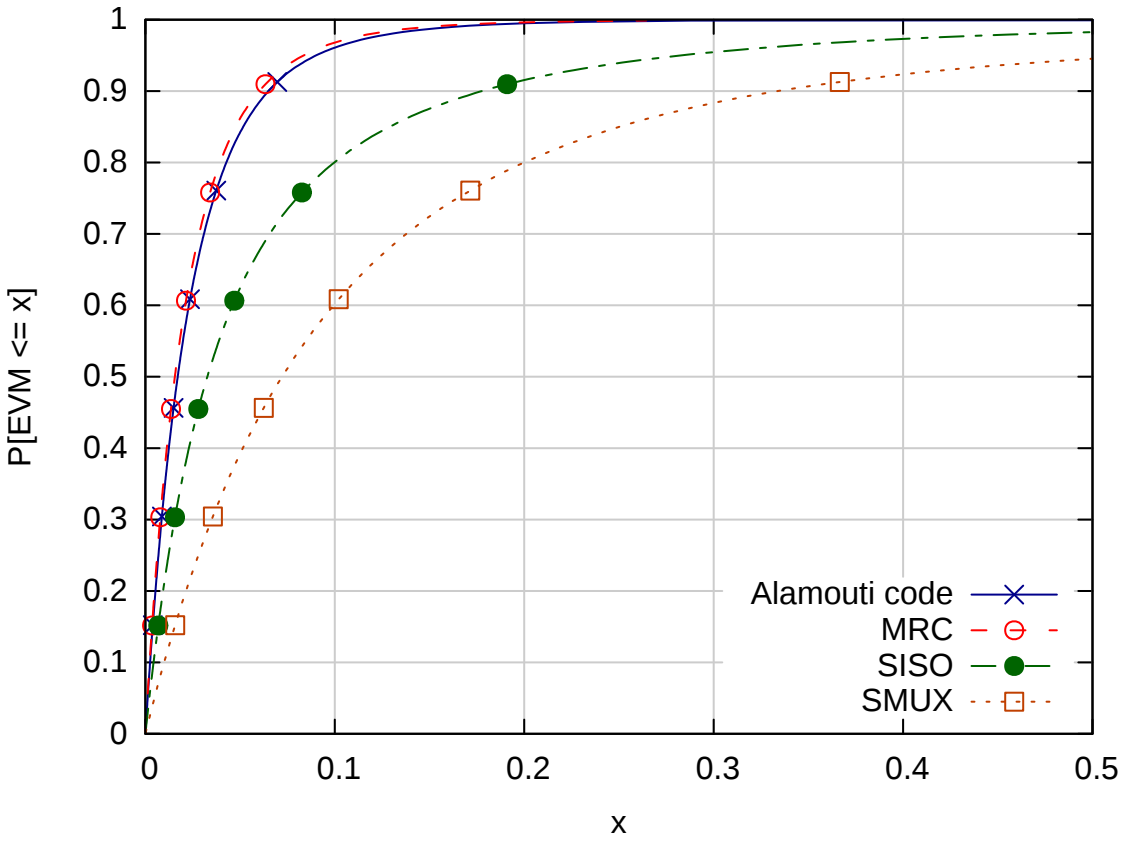

Figure 4.22: Port-side passageway. CDF of the EVM of across all physical layer schemes with the door closed.

The signal integrity for all physical layer schemes with the door open and closed is displayed in Figure 4.23. The two diversity schemes, MRC and Alamouti code, outperform SISO and Spatial Multiplexing (SMUX) in both cases as expected. Since Alamouti code and MRC have similar PPSNR when the door is closed, it is probably that one of the Alamouti code transmit streams is severely degraded (likely by the door) which negates the benefits of the transmitter diversity. Closing the door resulted in approximately 5 dB of loss for SISO, MRC, and Alamouti Space-Time Block Code (STBC) and about 8 dB for SMUX.

The channel capacity of the physical layer schemes is shown in Figs. 4.24–4.25. The observed Channel State Information (CSI) is normalized such that the horizontal axis shows the mean received Signal-to-Noise-Ratio (SNR) per receiver from all transmitters [63]. The capacity for an Independent, Identically Distributed (IID) channel is presented for comparison. The IID capacity represents the

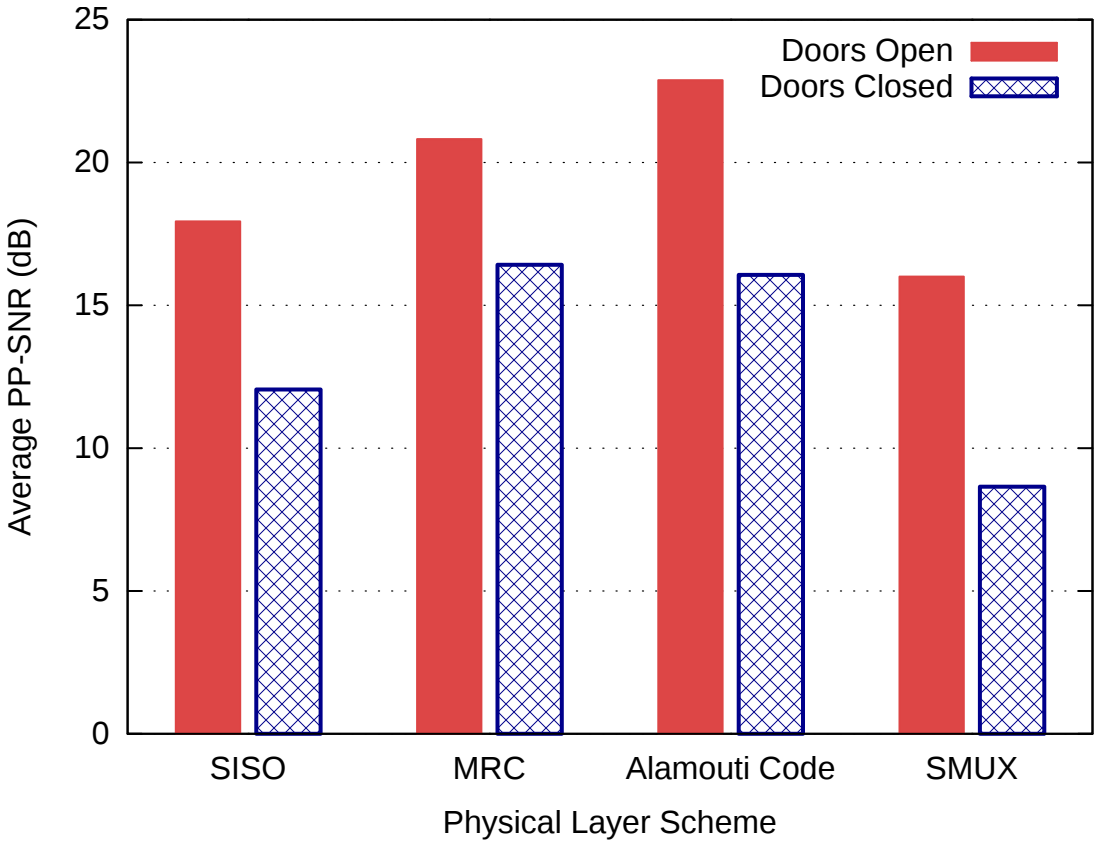

Figure 4.23: Port-side passageway. PPSNR across all physical layer schemes with the door open and closed.

upper bound of the capacity in a MIMO link of equal channel gain. SMUX has the highest capacity of all the physical layer schemes. Since the CSI is normalized, SMUX should have the highest capacity, because it is transmitting at twice the rate of the other schemes. Alamouti code and MRC both outperform SISO by a minimum of 24% due to the added transmit and receiver diversity. Somewhat surprisingly, the capacity increases for all four schemes when the door is closed. In this case, less energy couples into the cavity with the receiver, which decreases the multipath interference characteristic of a highly reverberant environment. This trend indicates that the channel may become less frequency selective when the door is closed.

With respect to the Multiple Input Multiple Output (MIMO) physical layer schemes, it should be considered whether a "keyhole" channel is being created when the door is closed (i.e., the effective aperture is decreased). In a keyhole channel, the capacity of MIMO schemes is low (i.e., significantly

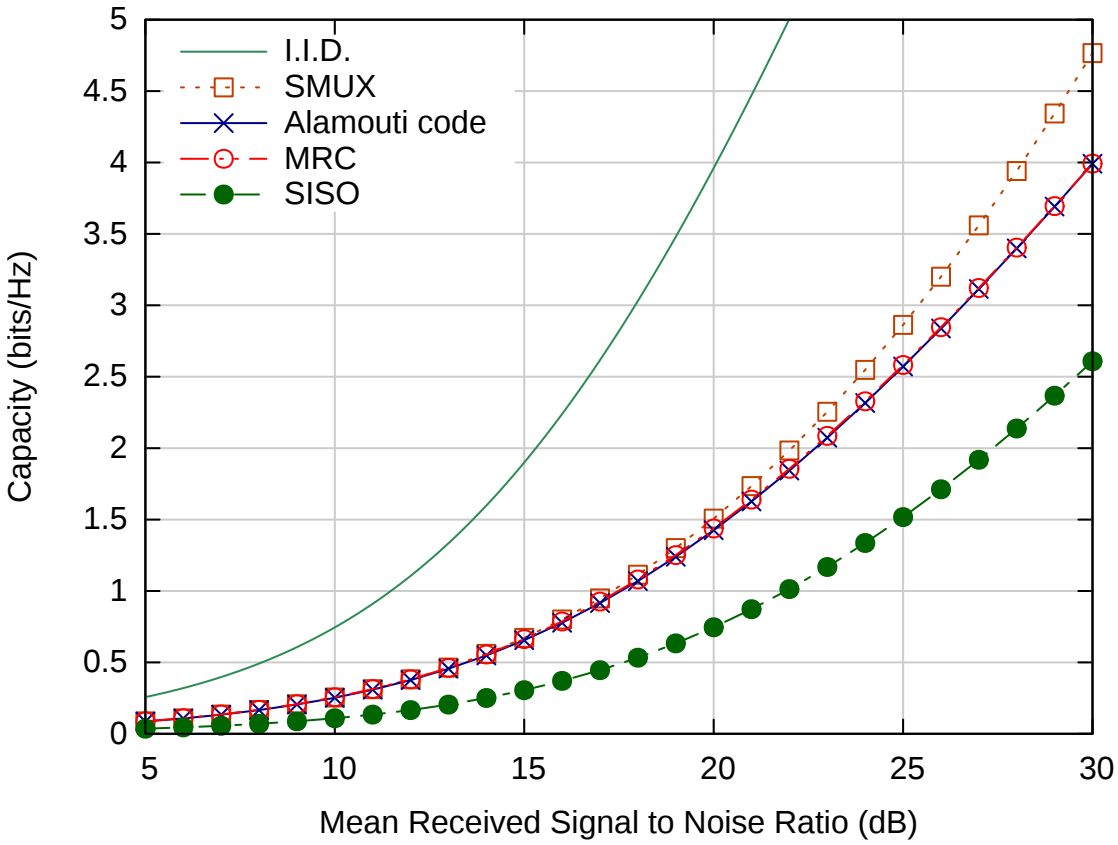

Figure 4.24: Port-side passageway. Observed system capacity across all physical layer schemes with the door open.

less than the theoretical maximum of N times the single channel capacity where N is the lesser number of transmit and receive antennas) despite uncorrelated channels [68, 69]. The low capacity is due to a rank reduction in the transfer function matrix [70]. The keyhole channel was demonstrated in [70] by placing a transmitting array in a shielded room and a receiving array in an adjacent room. The propagation between them was restricted to a small hole, the "keyhole," which had a waveguide attached to it. This test scenario is very similar to the scenario in the corridor with the door closed. It would appear the corridor is not a keyhole channel, because the capacity increases instead of decreases. Additionally, the SISO link (which cannot succumb to the keyhole effect) also follows the same trend as the MIMO schemes.

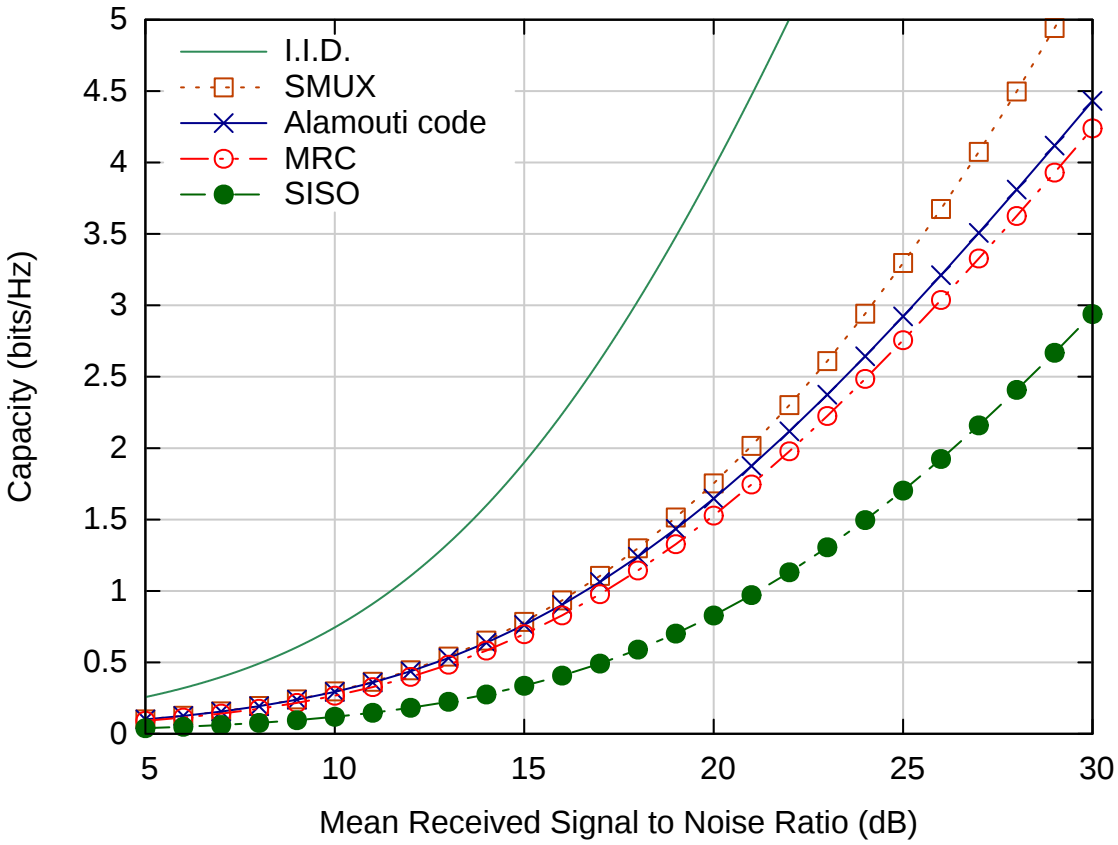

Figure 4.25: Port-side passageway. Observed system capacity across all physical layer schemes with the door closed.

4.3.2 Engine Room

Environment Description

Wireless measurements were taken in the aft engine room for the purpose of studying a contiguous space with largely metal construction. The engine room spans four decks and includes large and geometrically complex objects. This space was seen as a prime candidate for implementing a wireless sensor network to monitor the status of the ship engines and other vital ship machinery. A cross section of the environment is shown in Figure 4.26.

Nodes were located on three out of the four decks. The large void between Receivers 2 and 3 was occupied by the engine and exhaust stack, which spanned all decks. Receiver 1 was located so that it had a line of sight with the Transmitter, whereas Receivers 2 and 3 were located on separate decks with no line of sight to the transmitter. These locations were chosen to gain an understanding

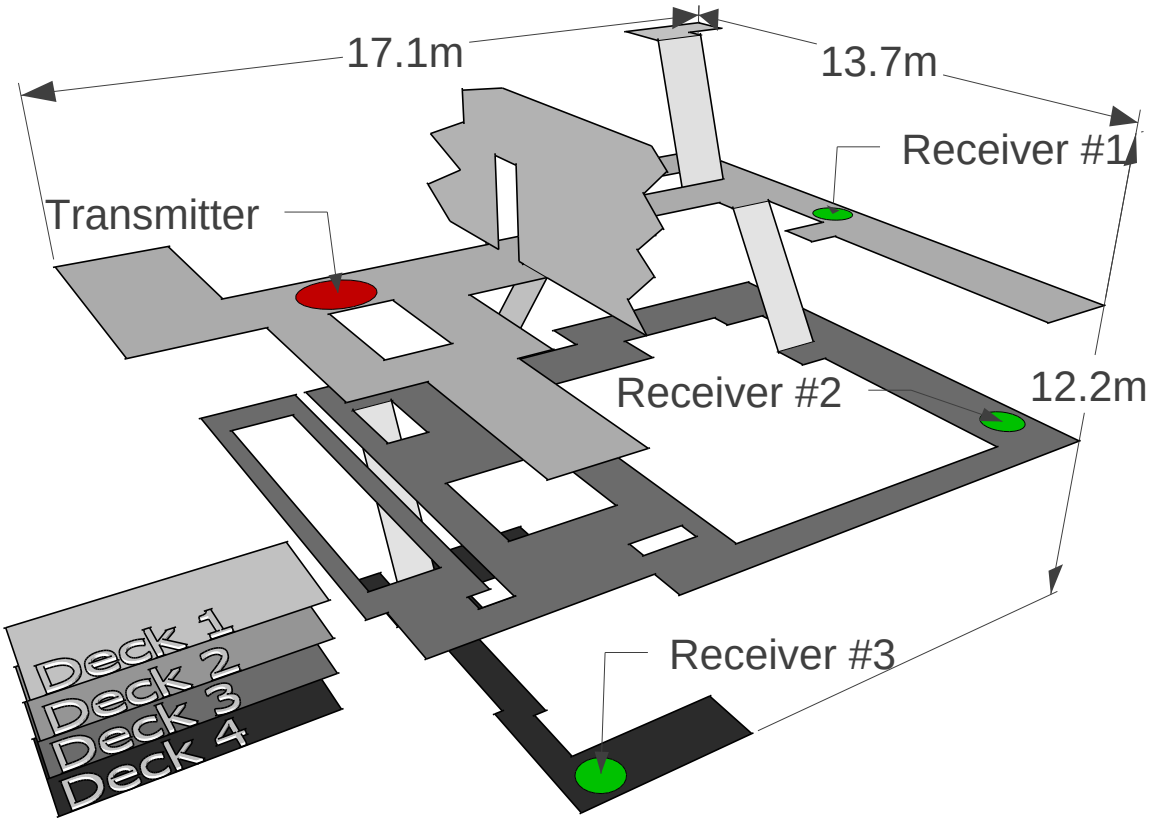

Figure 4.26: Cross section of the engine room test scenario on the *Thomas S. Gates* (CG 51).

of the network coverage possible in a contiguous space spanning multiple decks.

Results

Figure 4.27 shows the system capacity versus the received signal to noise ratio, averaged over all wireless links for each physical layer tested. The water-filling curve represents the upper bound of capacity for the links when the CSI is known [71, 32], while the IID curve represents the highest theoretical gain achievable in a MIMO link of equal channel gain. Since the channels are normalized with respect to gain per receiver, the effect of spatial correlation is isolated in the MIMO SMUX curve [63]. As demonstrated in Figure 4.27, the channel is spatially decorrelated enough to support the use of MIMO techniques to improve performance of SISO techniques. The capacity is approximately doubled by using SMUX over SISO.

PPSNR values for each physical layer and receiver location are shown in Table 4.5. The link between the Transmitter and Receiver 1 is the closest to a LOS condition. As a result, it has the

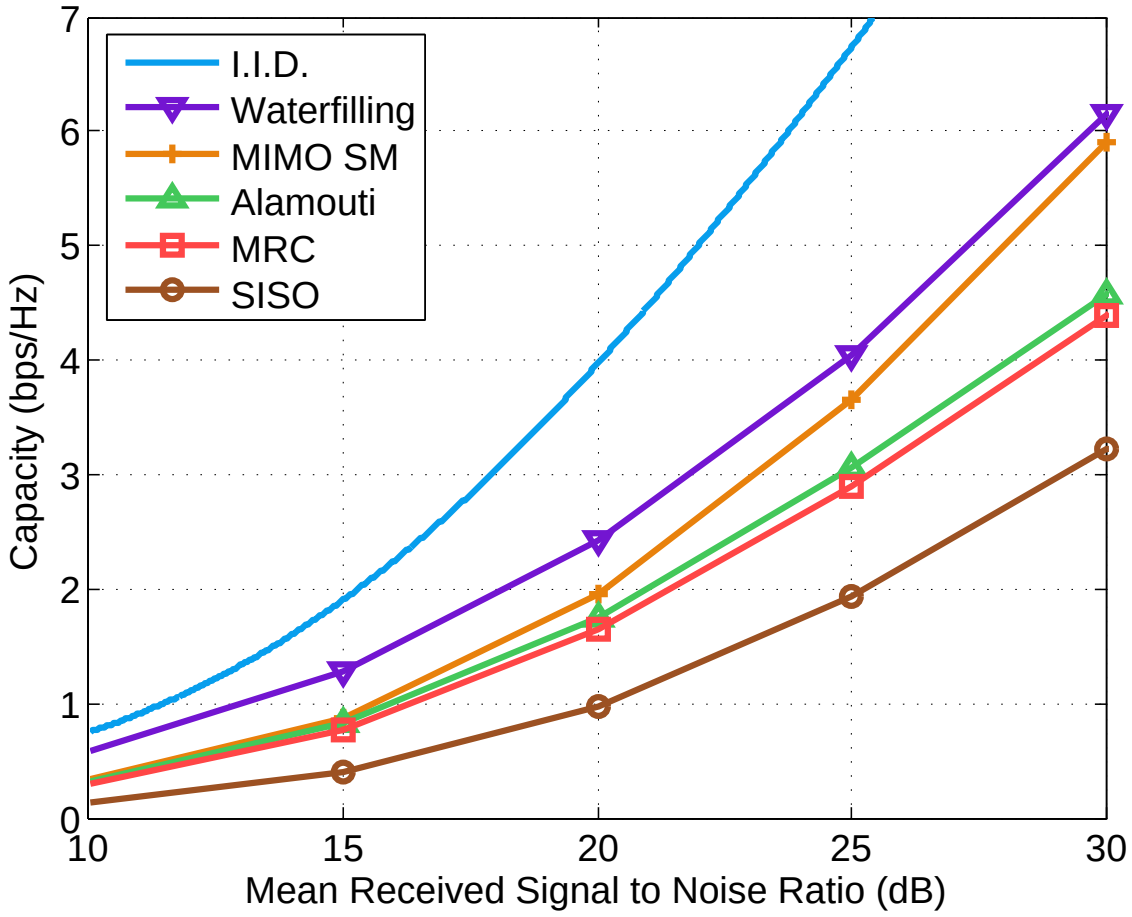

Figure 4.27: Engine room. Observed system capacity averaged across all nodes for all physical layer schemes.

highest PPSNR. In most scenarios, the PPSNR is highest when using Alamouti STBC. This result is expected due to added diversity gain from space time coding at the transmitter. Comparable PPSNR performance is achieved by MRC. While SMUX has the lowest PPSNR, it is transmitting at twice the data rate of the other physical layers.

The minimum and maximum achievable throughput are shown in Table 4.5. The minimum achievable throughput for each scheme represents the throughput of the worst performing link in this scenario, while the maximum throughput represents the best performing link.

For the poorest quality links, the SISO physical layer was only able to obtain a throughput of 6 Mbps in the engine room, while MIMO techniques were able to provide double the throughput. At maximum, Vertical Bell Laboratories Layered Space-Time (VBLAST)-SMUX throughput reached

Table 4.5: Engine room. PPSNR (dB) across all receivers and physical layer schemes.

Receiver	SISO	MRC	Alamouti	MIMO-SMUX
1	21.4	23.1	22.8	16.8
2	11.5	17.6	18.5	11.6
3	10.4	13.9	14.6	7.4

Table 4.6: Engine room. Minimum and Maximum achievable throughput (Mbps) with SER constrained to 1×10^{-3}.

SISO		MRC		Alamouti		SMUX	
Min	Max	Min	Max	Min	Max	Min	Max
6	18	12	18	12	18	12	36

36 Mbps.

4.3.3 Coupled Compartments

Experiment Description

A cluster of adjacent compartments on an interior deck of the ship were used to analyze the coupling between adjacent and near-adjacent compartments, similar to the coupled reverberation chamber. The primary objective of this scenario was to measure RF leakage through ship bulkheads and determine the effect of closing watertight doors on signal integrity. Characterizing communications integrity between compartments is necessary to assess the connectivity of a wireless network that spans several compartments and/or decks in the ship environment. A cross section of the environment is shown in Figure 4.28.

The Transmitter was located in the towed array room, and the two receiver nodes were located in the NIXIE compartment and the multi-purpose workshop. While the doors and hatches were watertight, there exist ventilation ducts, piping, and other protrusions which created an effective aperture for electromagnetic signals to propagate between the compartments. An emergency escape scuttle was located in the bulkhead between the towed array room and the NIXIE compartment. This scuttle was closed for the duration of the testing. An exhaust duct with vents connects the towed array room and the multi-purpose workshop.

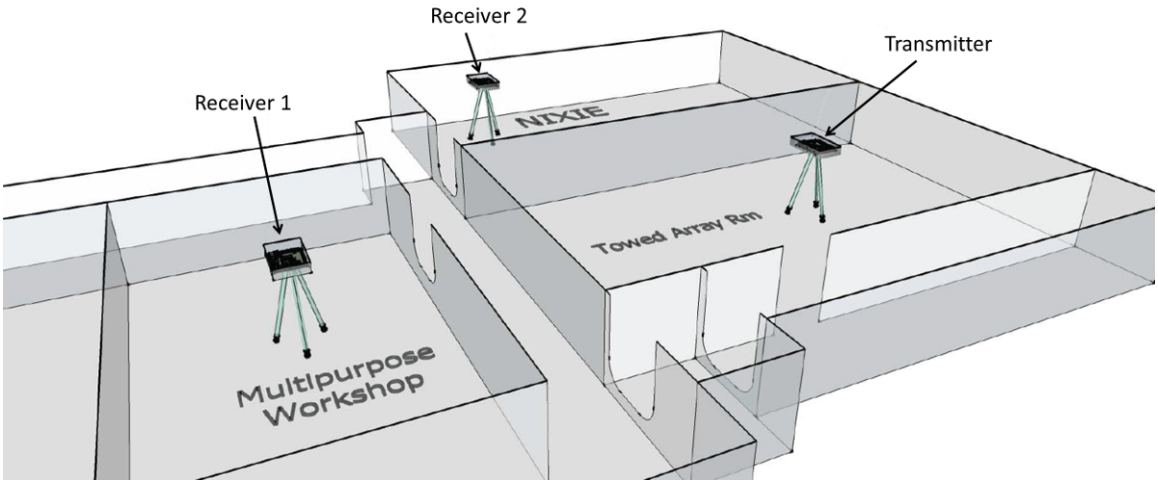

Figure 4.28: Cross section of the coupled compartments test scenario on the *Thomas S. Gates* (CG 51).

Results

The results in the coupled compartments show two distinct behaviors emerging from differences in physical layout. As shown in Figure 4.28, the Transmitter is separated from Receiver 1 by two bulkheads and a hallway. The primary pathway for the signal is through this hallway when the doors are open, but it must propagate through apertures in the bulkheads (such as the ventilation ducts) when they are closed. However, the Transmitter is separated from Receiver 2 by a single bulkhead. When the doors are open, there is a single long pathway for the signal to propagate to the receiver via the hallway.

The capacity for the channel between the Transmitter and Receiver 1 (Figure 4.29) improves for SISO communications when the doors are closed. Since the path loss from the channel is normalized, this improvement indicates the channel has a flatter response (less frequency selectivity). This is consistent with a decrease in multi-path signals arriving at Receiver 1 and an increase in the dominance of the signals arriving via ductwork connecting the two spaces. Since MIMO techniques mitigate frequency selectivity through antenna diversity, the negligible change in the capacity of these schemes would indicate that the channel correlation (a major factor in capacity) does not change in a significant way when the doors are opened or closed.

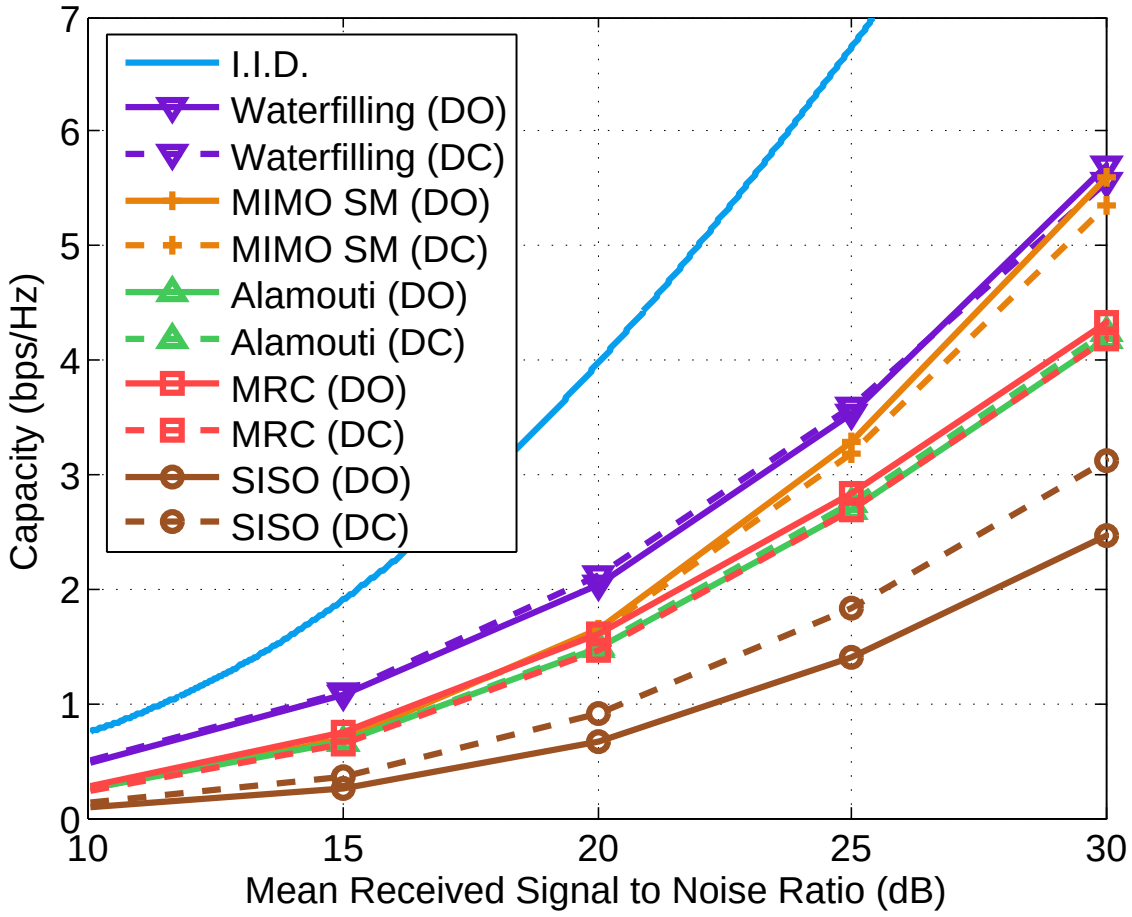

Figure 4.29: Coupled compartments. Observed system capacity for Receiver 1 across all physical layer schemes with doors open and closed.

The capacity for the channel between the Transmitter and Receiver 2 (Figure 4.30) improves for both SISO and MIMO schemes when the doors are closed. The improvement for SISO indicates that frequency selectivity decreases, similar to the effect seen at Receiver 1. The improvement for MIMO indicates that the channel correlation also decreases, in contrast to the effect seen at Receiver 1.

The PPSNR of both receivers is shown in Table 4.7 for open and closed doors. The signal integrity decreases for Receiver 1 when the doors are closed. Despite the decrease in frequency selectivity, the attenuation of the signal when the doors are closed still results in an overall decrease in integrity.

PPSNR increases for Receiver 2 when the doors are closed, consistent with the dominant signal component coming through apertures in the bulkhead and the multi-path signal from the hallway deconstructively interfering when the doors are open.

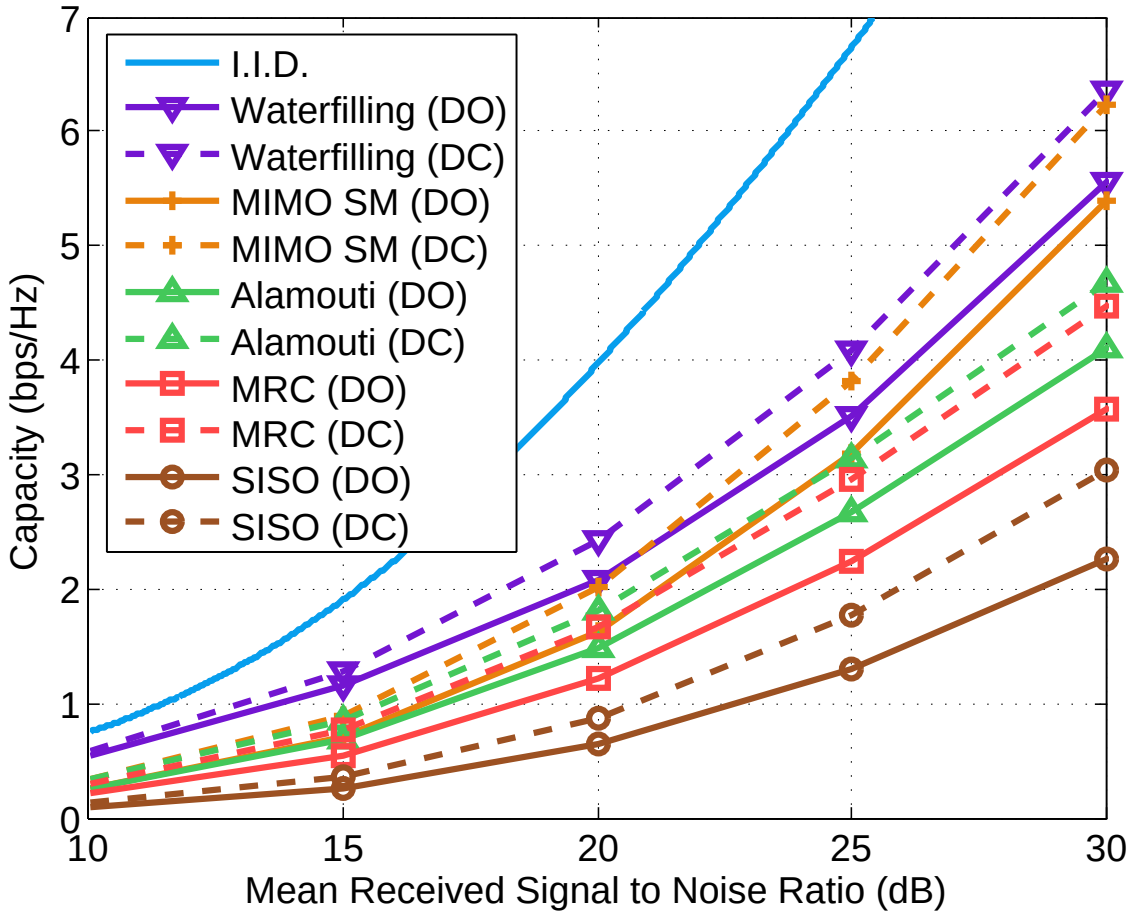

Figure 4.30: Coupled compartments. Observed system capacity for Receiver 1 across all physical layer schemes with doors open and closed.

Both the minimum and maximum achievable throughput for each scenario are shown in Table 4.8. All of the physical layers except for SISO have a higher minimum achievable throughput when the doors are open. For SISO, the maximum achievable throughput is higher than doors open by 6 dB for doors closed. The other physical layers have the same maximum achievable throughput regardless.

4.4 Conclusion

The results and analysis of two measurement campaigns were presented. The purpose of the campaigns was to assess the performance of wireless communications in highly reverberant environments, both controlled and live, using the measurement platform and test protocol developed for this work.

The first campaign was in the coupled reverberation chambers of the NSWCDD which provided

Table 4.7: Coupled compartments. PPSNR (dB) across all receivers and physical layer schemes for doors open (DO) and doors closed (DC).

RX Location	SISO		1x2 MRC		Alamouti		MIMO-SM	
	DO	DC	DO	DC	DO	DC	DO	DC
1	11.4	11.0	21.5	15.3	18.5	15.0	14.2	8.6
2	15.0	21.1	19.8	22.3	18.2	19.8	12.6	15.5

(DO) = doors opened, (DC) = doors closed

Table 4.8: Coupled compartments. Minimum and Maximum achievable throughput (Mbps) for doors open and doors closed with SER constrained to 1×10^{-3}.

Doors	SISO		MRC		Alamouti		MIMO-SM	
	Min	Max	Min	Max	Min	Max	Min	Max
Open	12	12	18	18	18	18	24	24
Closed	12	18	12	18	12	18	12	24

(DO) = doors opened, (DC) = doors closed

a controllable test environment. The loading of the chambers was varied to match the loading of below deck spaces on a naval vessel. The multipath in reverberant environments is often thought to be challenging for wireless communications [1, 9, 10]. The performance of the LOS Receiver was consistent with this notion as lower loading did result in a degradation of PPSNR and throughput. Surprisingly, the reverse was true for the NLOS Receiver as it had improved performance for lower loading. Two physical layer transmission schemes were compared in which the receiver diversity scheme produced substantial gains in PPSNR. The gains were increased for lower loading likely due to the decreased correlation of the received signals. Cavity coupling was also investigated where the effective aperture size between the two connected cavities was varied. The largest effective aperture proved to be the best for both receivers. The LOS Receiver benefited from reduced multipath while the NLOS benefited from the higher signal power.

The second campaign was in the below deck spaces of a naval vessel. Several scenarios on board the vessel were selected to represent the locations which would likely benefit for the inclusion of a Wireless Local Area Network (WLAN). Across all of the scenarios, improvements in PPSNR, capacity, and throughput were demonstrated by leveraging receiver diversity schemes. In the passageway and coupled compartment scenarios, it was shown that communication was possible with hatches closed as signals were still able to propagate between coupled cavities through the effective aper-

ture formed by electromagnetic leakage. Link specific effects were observed in several cases which emphasizes the unintuitive nature of these environments and the necessity for experimentation.

The two measurement campaigns were designed to have as many experimental controls as possible. Wireless nodes, antennas, gain calibration, and testing protocol were all constant across both campaigns. Furthermore, the coupled reverberation chambers were configured to emulate the reverberance of the below deck spaces of a naval vessel. Yet, there were are a few key differences in the experiments which dictate caution when comparing the results. The physical geometry and node topologies are not consistent between the reverberation chamber and the below deck spaces as well as among the individual below decks scenarios. As a consequence, path loss cannot be considered on a per-link basis which precludes the direct comparison of PPSNR and throughput. Even so, it is still possible to compare the change in PPSNR (and resulting trends) when varying node or environmental parameters. The system capacity can be compared as well since the normalization of the metric removes the effect of path loss.

In the coupled reverberation chambers, the receivers exhibit a range in PPSNR of approximately 13 dB. The configurations encompassed across that range include LOS and NLOS propagation paths, low to high loading, and low to high coupling. This range is similar to the range of configurations tested throughout the different scenarios and receivers in the below decks campaign. It is reassuring to note that the range in PPSNR for the below decks campaign is approximately 14 dB. Incidentally, the PPSNR range is ˜10-23dB for the coupled reverberation chambers campaign and ˜9-23 dB in the below decks campaign. As it has been stated, the actual values of the PPSNR cannot be directly compared, but the similarity is ranges does provide validation towards the selected loading configurations and the use of the coupled reverberation chambers as an emulated test environment.

The improvement in PPSNR by using MRC over SISO is similar throughout both campaigns. In the coupled reverberation chambers, the PPSNR increase from using MRC is between 3-5 dB for all configurations. In the below deck spaces, the PPSNR increase for MRC is between 2-5 dB with the exception of Receiver 1 in the coupled compartments scenario with the doors open where the PPSNR improves by 10 dB. Since the range of loading was the same in both campaigns, both

environments have a similar amount of multipath which is a driving factor in The system capacity curves are also closely aligned between the two campaigns for the SISO and MRC links.

Overall, the results of the two campaigns closely coincided. From these encouraging results, it appears that the coupled reverberation chambers serve well to emulate actual reverberant environments.

Additionally, it was discussed how the trends exhibited in reverberant environments apply to non-reverberant environments. The multipath interference that impacts LOS links heavily in reverberant environments would still impact LOS links in non-reverberant environments, but not to the same extent. NLOS links vary greatly within reverberant environments since they are specific to the physical geometry and topology. NLOS links in non-reverberant environments will also have link specific effects, though the performance gap will be less than the range exhibited by links in reverberant environments. Finally, the high levels of electromagnetic leakage in non-reverberant environments severely diminish the impact of coupling.

Chapter 5: Empirical Evaluation of Reconfigurable Antennas

5.1 Introduction

Portions of this work were published in the proceedings of the 2014 IEEE Antennas and Propagation Symposium [45], the proceedings of the 2014 American Society of Naval Engineers Electric Machines Technology Symposium [39], and the IEEE Antennas and Wireless Propagation Letters [72].

Reconfigurable antennas have been proposed for mitigating the multipath interference in highly multipath environments [40]. However, only little work has been done on the communications performance of electrically reconfigurable antennas in such extreme multipath environments. For example, the studies in [40, 41] attempt to observe performance gains of employing reconfigurable antennas in terms of mitigating multipath interference, but do so only through simulated results. The studies in [42, 43, 44] obtain communication performance measures using software-defined radios, but the experiments were conducted in typical lab or office environments.

This study seeks to measure the communications performance benefits of using electronically reconfigurable antennas in a highly multipath environment. A pre-existing reconfigurable antenna was chosen for use in this experiment – a Reconfigurable Leaky Wave Antenna (RLWA) developed by Piazza and the Drexel Wireless Systems Laboratory [36, 46, 47, 48]). For testing, a Wireless Local Area Network (WLAN) was constructed in the coupled reverberation chambers of the Naval Surface Warfare Center Dahlgren Division (NSWCDD). The WLAN used Software Defined Radios (SDRs) and the Reconfigurable Leaky Wave Antenna (RLWA) described in [48].

Error Vector Magnitude (EVM), Post Processing Signal-to-Noise-Ratio (PPSNR), and system capacity were obtained from wireless measurements taken in the coupled reverberation chambers under low loading. The reconfigurable antennas were found to improve signal integrity over Commercial, Off-The-Shelf (COTS) omnidirectional antennas for a Single Input Single Output (SISO) system, and by a lesser amount when employing Maximal Ratio Combining (MRC). Similar trends were observed for system capacity estimates. These findings indicate that reconfigurable antennas

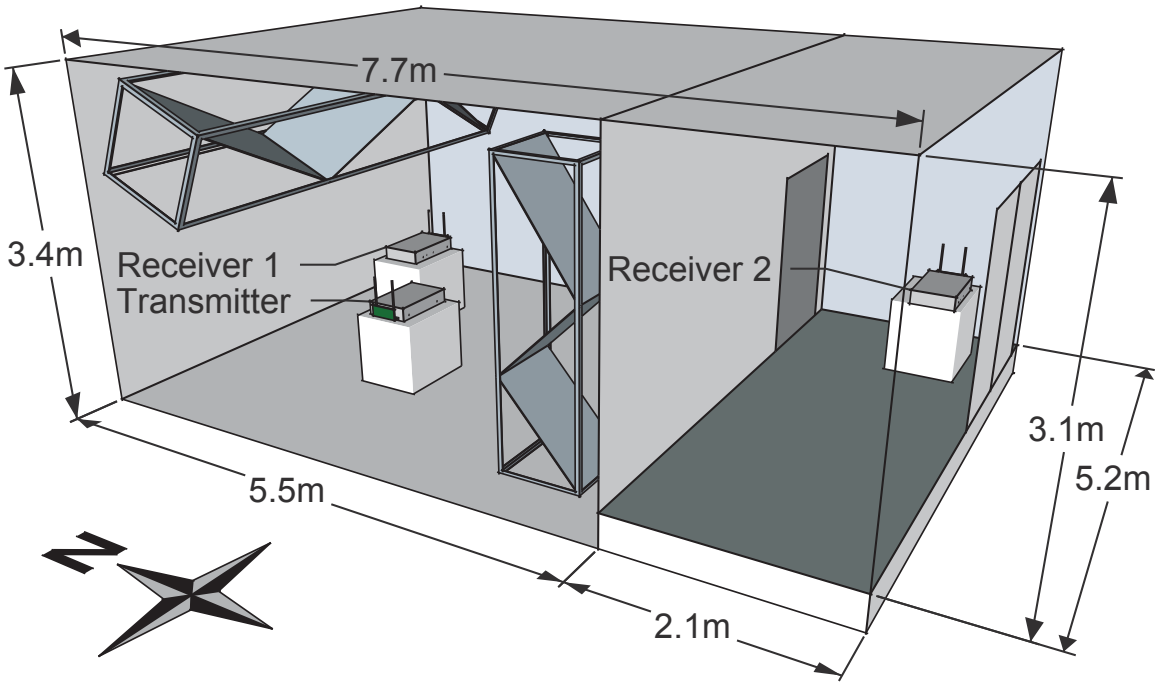

Figure 5.1: Cross section view of the main chamber and ante chamber in the coupled reverberation chambers at the NSWCDD.

may be well suited for use with a stationary network infrastructure to facilitate the design and mobility of receivers in high multipath environments.

5.2 Experimental Setup

In total, three wireless nodes were deployed, one transmitter and two receivers. The Transmitter and Receiver 1 were located in the main chamber. Receiver 1 had a Line Of Sight (LOS) to the Transmitter. Receiver 2 was positioned in the ante chamber behind the separating door such that it did not have LOS into the main chamber. All nodes were elevated off the ground by non-absorbing, Styrofoam blocks.

One of the objectives of this effort was to compare a reconfigurable antenna to a COTS antenna. The selected COTS antenna was a standard, dual-band (2.4/5.8 GHz) omnidirectional antenna (model HG2458RD-SM, manufactured by L-com). The reconfigurable antenna used was a RLWA designed by Piazza, et al. [36, 46, 47, 48]. It is a two-port antenna comprised of a series of 12 DC-bias networks. The gain pattern of each port can be altered dynamically via the voltage fed to

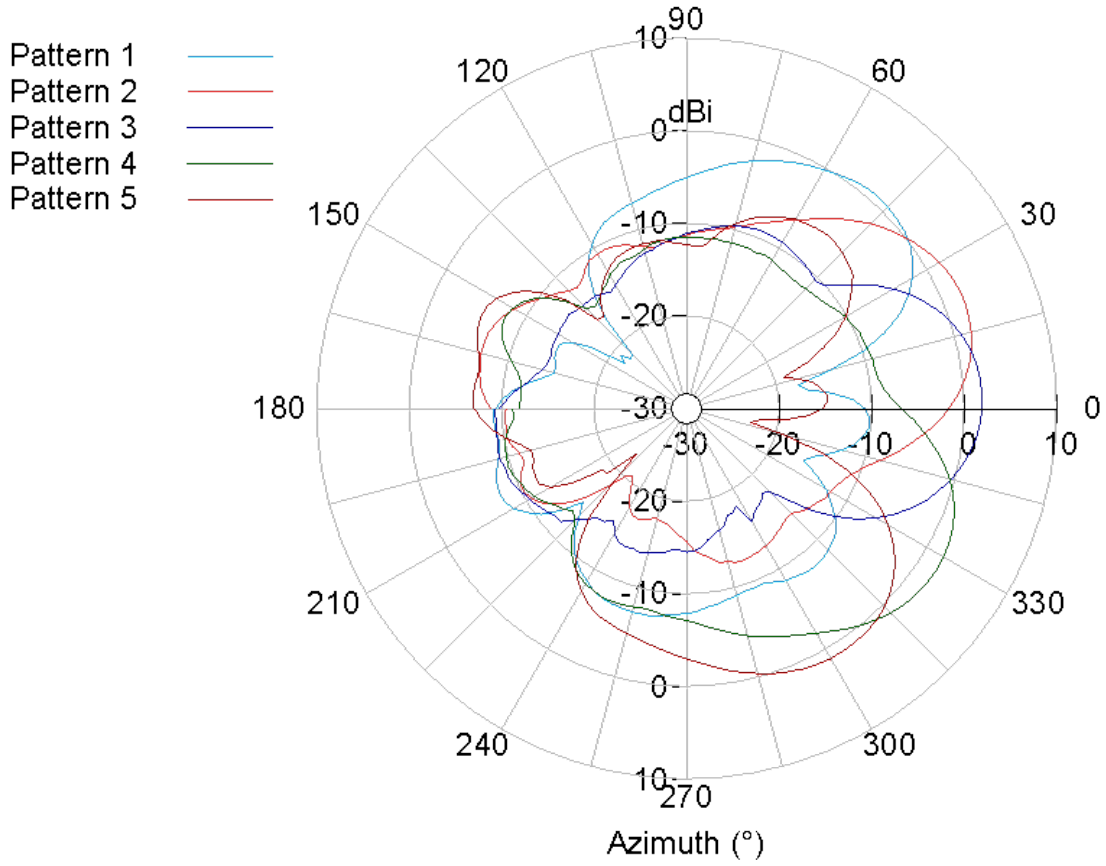

Figure 5.2: Selected radiation patterns of the reconfigurable leaky wave antenna.

the DC-bias networks.

Five distinct radiation pattern configurations were selected for the reconfigurable antenna, shown in Figure 5.2. The number of configurations was chosen based on the work done by Grau in [73], where it was demonstrated that the ergodic capacity of reconfigurable antennas has a diminishing return for more than five configurations.

The MATLAB-based measurement platform described in Chapter 3 was across all experiments. In total, 1,600 trials were performed total for each experiment.

5.3 Experimental Results

While five configurations of the reconfigurable antenna were tested, the optimally performing configuration was selected for evaluation in order to simplify analysis and represent an upper bound on the best-case scenario performance for the antenna. The optimal configuration is selected based on

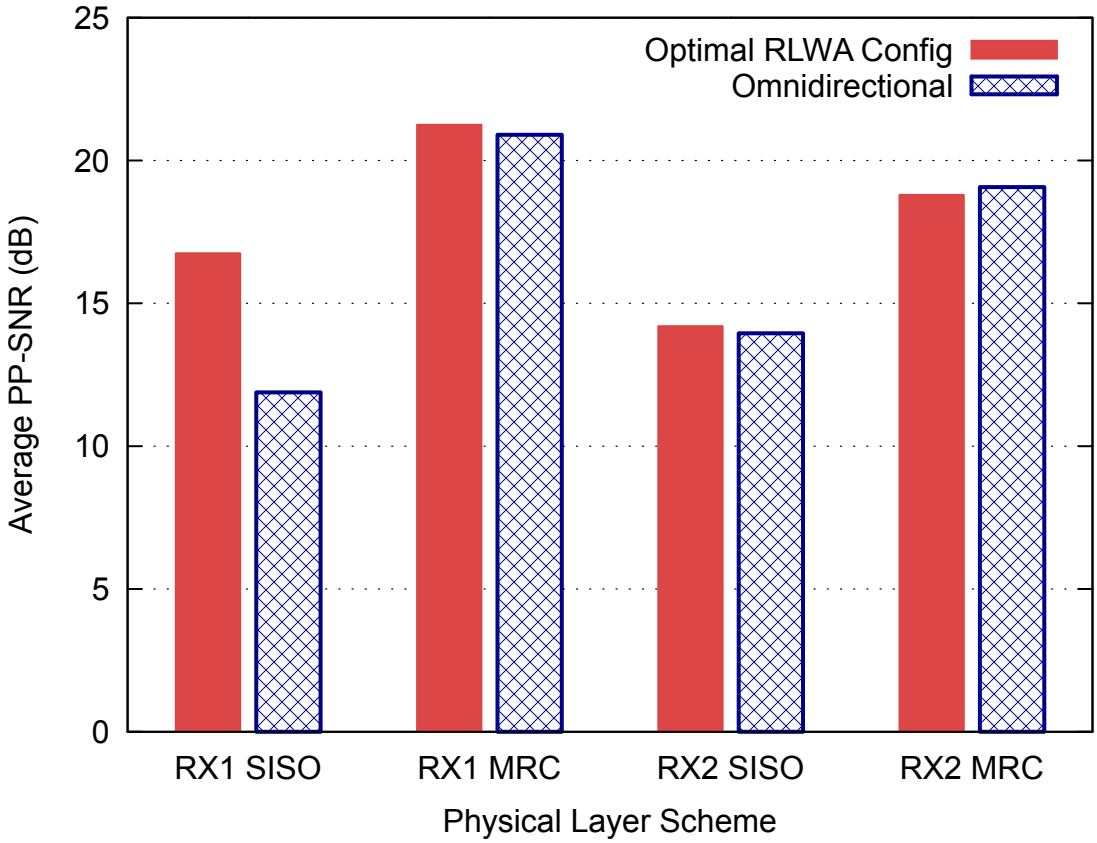

Figure 5.3: Coupled reverberation chambers. PPSNR for both receivers, both antennas, and both physical layer schemes.

the minimal EVM as determined on a per-transmission basis. It is assumed that specific implementations of the selected reconfigurable antenna will determine which of the configuration options are optimal.

PPSNR for all receivers, antenna types, and physical layer schemes is shown in Figure 5.3. The empirical CDF of the EVM are shown for Receiver 1 and Receiver 2 in Figs. 5.4 and 5.5, respectively.

The most readily apparent observation is that reconfigurable SISO outperforms omnidirectional SISO by 4.9 dB in PPSNR for Receiver 1. This improvement is explained by the distribution of the corresponding EVM in Figure 5.4. The omnidirectional SISO EVM shows a heavy tail. 18% of the EVMs are greater than 0.1 and 7% are greater than 0.5. In contrast, only 5% of the reconfigurable SISO EVMs are greater than 0.1% and a negligible amount are greater than 0.5. Since Receiver 1 has LOS to the transmitter, the heavy EVM tail for omnidirectional SISO is likely the result of

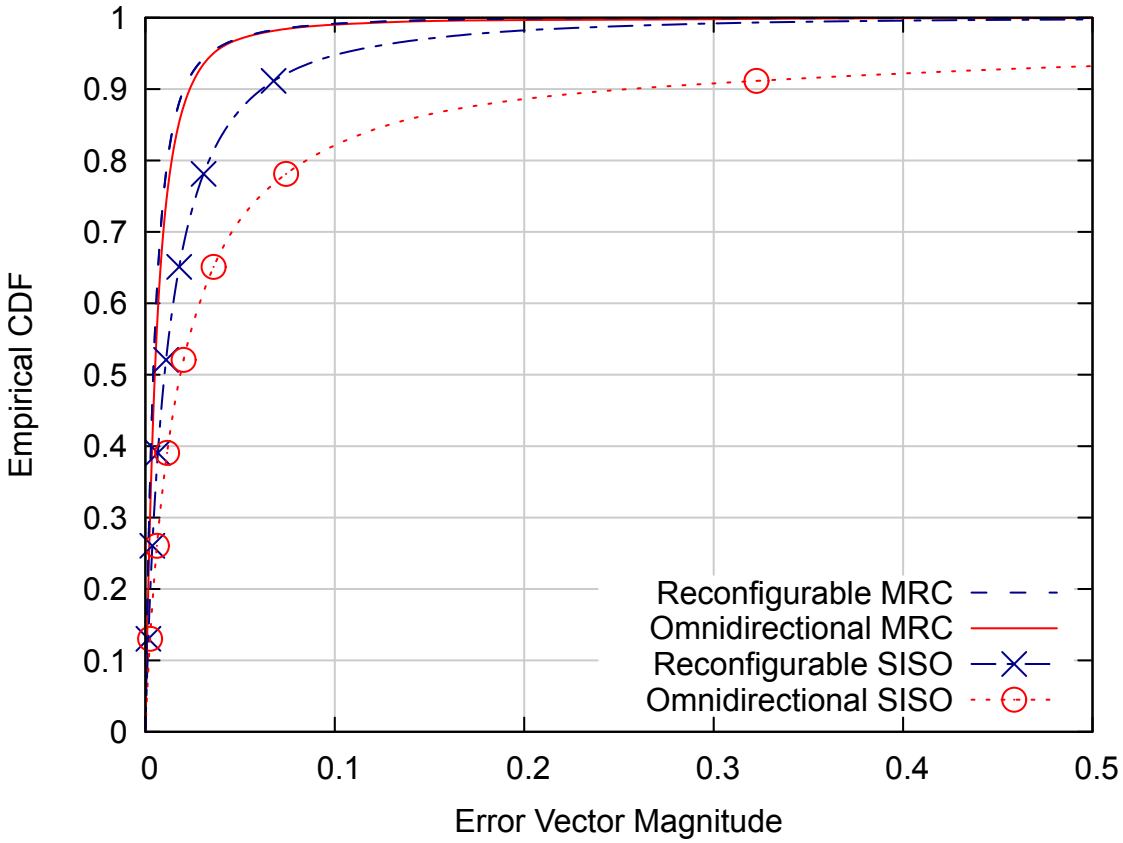

Figure 5.4: Coupled reverberation chambers. CDF of the EVM for Receiver 1 across both antennas and both physical layer schemes.

destructive multipath interference. The reconfigurable antenna does not succumb to this level of interference as choosing the optimal configuration minimizes it.

These trends differ for Receiver 2, where the PPSNR of both reconfigurable and omnidirectional SISO are nearly the same. This observation is reasonable since the received components must enter through the doorway aperture to reach Receiver 2. Due to the highly reverberant nature of the main chamber, nearly the same quantity of energy is coupled into the ante chamber regardless of the transmit antenna pattern or type. Since both antennas are transmitting at the same power level and coupling into the ante chamber through the same aperture, it should be expected that both have similar performance. Figure 5.5 confirms the hypothesis as both antennas follow the same EVM distribution.

The tail of the omnidirectional EVM distribution is not as heavy for Receiver 2 as it was for

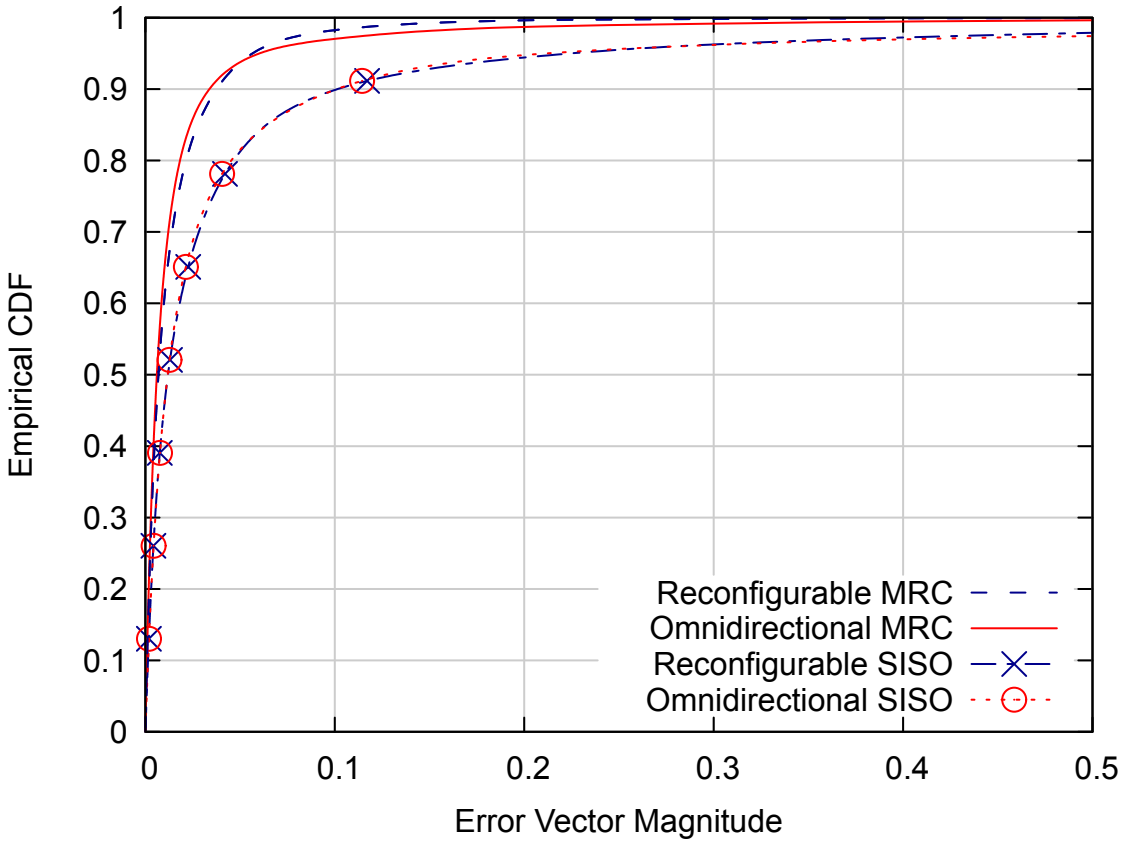

Figure 5.5: Coupled reverberation chambers. CDF of the EVM for Receiver 2 across both antennas and both physical layer schemes.

Receiver 1 due to less severe multipath in the ante chamber despite the lower energy levels and lack of a LOS component. In fact, the PP-SNR of omnidirectional SISO improves 2 dB from Receiver 1 to Receiver 2.

For MRC, the reconfigurable antenna provides only minor advantage over the omnidirectional antenna. It is not surprising that the reconfigurable antenna has greater performance in this regard. MRC implements receiver antenna diversity, which provides a greater improvement than altering the radiation pattern of a single transmit antenna. Both reconfigurable and omnidirectional MRC outperform their SISO counterparts in terms of PP-SNR and EVM. MRC is expected to always outperform SISO since it uses the weighted combination of two SISO signals.

The channel capacities for Receiver 1 and Receiver 2 are shown in Figs. 5.6 and 5.7, respectively. Reconfigurable SISO has greater than a 16% increase over omnidirectional SISO, further strength-

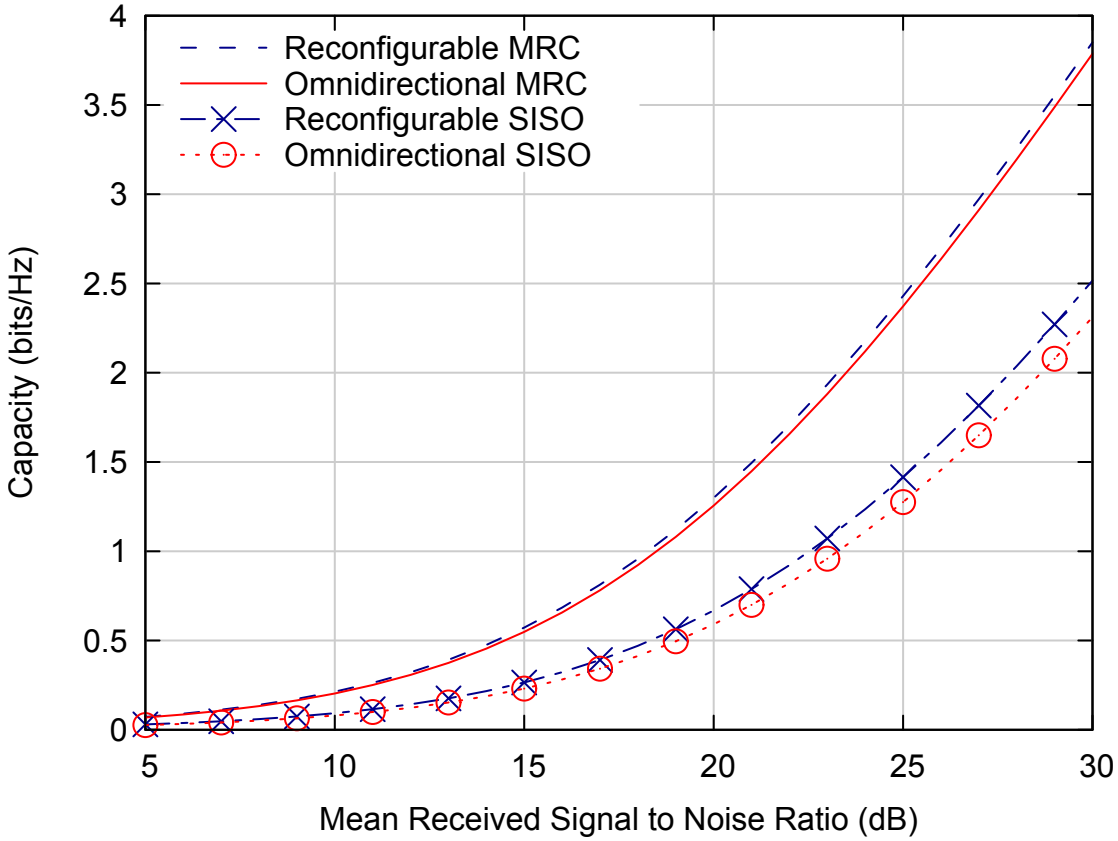

Figure 5.6: Coupled reverberation chambers. Observed system capacity for Receiver 1 across both physical layer schemes.

ening the recommendation to use a reconfigurable antenna in such scenarios. The reconfigurable antenna also has a small edge over the omnidirectional for all other cases, with improvements ranging from 0.9% to 11.9%.

5.4 Conclusions

The performance of a reconfigurable antenna was compared to a COTS omnidirectional antenna in the highly reverberant environment of coupled reverberation chambers. A series of experiments were conducted using a software defined, IEEE 802.11g OFDM test suite built with MATLAB and the WARP FPGA. Both SISO and MRC physical layer schemes were evaluated for a LOS and non-LOS receiver.

The reconfigurable antenna outperformed the omnidirectional antenna by 4.9 dB in PPSNR for

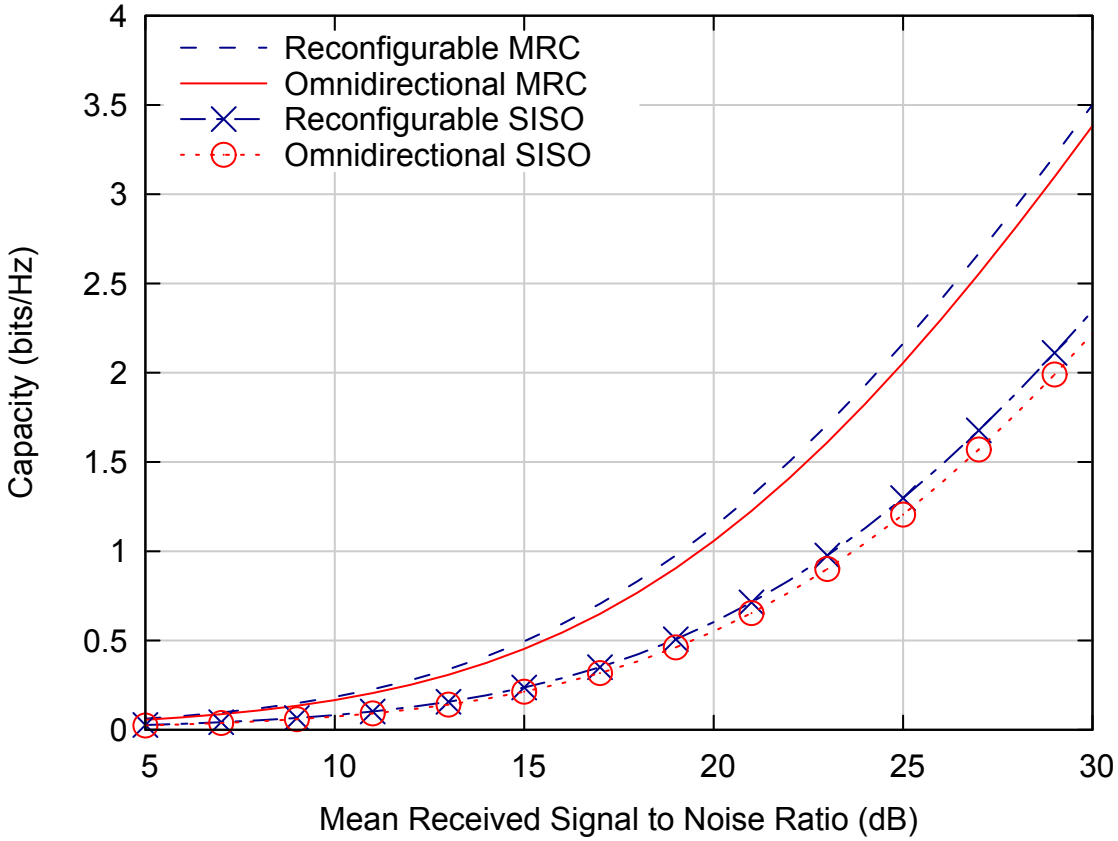

Figure 5.7: Coupled reverberation chambers. Observed system capacity for Receiver 2 across both physical layer schemes.

the LOS SISO receiver. The omnidirectional antenna performance was hampered by the effects of destructive multipath interference which the reconfigurable antenna was able to mitigate by dynamically altering the radiation pattern to minimize the destructive interference. The reconfigurable antenna also showed an improved capacity over the omnidirectional by 16.2%. As expected, the improvement was considerably more modest for MRC.

While the receiver diversity of MRC largely obviates the primary benefits of the reconfigurable antenna, these benefits may be realized solely by changing the antenna on the transmitter without any hardware modifications to the receiver. This feature is highly attractive for implementation in access points and network infrastructure. The ability of the reconfigurable antenna to dynamically alter its antenna patterns makes it particularly well suited for communicating with mobile receivers and sensors. Even if a receiver does incorporate additional diversity schemes (such as MRC), the

reconfigurable antenna still slightly outperforms the omnidirectional antenna. Performance never suffered as a result of using the reconfigurable antenna at the transmitter, and was much improved in some cases. Therefore, a reconfigurable antenna would be beneficial for use with access points and other stationary network infrastructure to facilitate the design and mobility of receivers.

Chapter 6: Conclusion

Interest in deploying Wireless LANs (WLANs) in highly reverberant environments, such as industrial facilities, naval vessels, aircraft, and spacecraft, is growing as a way to augment and, in some cases, fully replace existing, wired communications infrastructure. There are a plethora of benefits that can be realized by migrating to WLANs in these environments. Outside of the traditional benefits, WLANs also provide unique advantages because of the installation, maintenance, and redundancy factors compared to wired infrastructure. It has traditionally been thought that implementation of wireless networks in highly reverberant environments is challenging because of rich electromagnetic scattering that can result in multipath interference. The primary objective of this effort was to quantify the performance of wireless communications in reverberant spaces and assess the feasibility of Wireless Local Area Network (WLAN) deployment. It was also sought to correlate the performance of wireless communications to the electromagnetic properties of the environment. Work focused on experimental evaluation due to the complex physical geometries and signal propagation which are difficult and cumbersome to analyze through modeling and simulation.

The primary contributions of this work are:

1. An experimental methodology was developed for evaluating the performance of wireless communications including a measurement platform and testing protocol for Software Defined Radios (SDRs).

2. A measurement campaign was performed in the coupled reverberation chambers of the Naval Surface Warfare Center Dahlgren Division (NSWCDD) at the Naval Support Facility Dahlgren (NSFD) where the performance of wireless communications was assessed with respect to node and environmental parameters.

3. A measurement campaign was performed in the below-deck spaces of a naval vessel on the *Thomas S. Gates.* (CG 51) at the Naval Inactive Ship Maintenance Facility (NISMF) in

Philadelphia, PA, where the performance of wireless communications was assessed with respect to node and environmental parameters.

4. Empirical evaluation of a pre-existing Reconfigurable Leaky Wave Antenna (RLWA) was performed in the coupled reverberation chambers of the NSWCDD to evaluate its ability improve wireless communications performance in a highly reverberant environment.

It was necessary to characterize the electromagnetic properties of reverberant environments before assessing the performing wireless communications in them. A series of metrics that serve in this capacity were presented. The level of reverberance (loading) in below deck spaces, which was measured in previous studies, was used to configure the coupled reverberation chambers. The impulse response and the calculated electromagnetic properties for the configured states of the coupled reverberation chambers were provided.

A measurement platform was developed for the purpose of field testing both in coupled reverberation chambers and a naval vessel. Performing wireless communication experimentation in below decks spaces can be logistically difficult. Specialized equipment (e.g., signal generators and signal analyzers) tailored to collect comprehensive channel and link layer measurements is expensive and incompatible with the constraints of field work and mobile applications. A light-weight, mobile testing platform was needed that could provide the required measurement fidelity. As no current Software Defined Radio (SDR) solution satisfied these requirements in addition to being capable of interfacing with mechanical controls and reconfigurable antennas, a custom solution had to be developed. For this purpose, a new MATLAB-based, wireless measurement platform using an existing software-defined radio architecture was developed. It augments IEEE 802.11g Multiple Input Multiple Output (MIMO) Orthogonal Frequency-Division Multiplexing (OFDM) physical layer schemes with receiver diversity physical layer schemes such as Maximal Ratio Combining (MRC), Alamouti Space-Time Block Code (STBC), and Vertical Bell Laboratories Layered Space-Time (VBLAST) Spatial Multiplexing (SMUX). The platform provides a series of metrics, including system capacity, Error Vector Magnitude (EVM), Post Processing Signal-to-Noise-Ratio (PPSNR), and throughput to characterize link and network performance. The software implementation and test protocol of

the platform were presented.

Using the measurement platform, the effect of electromagnetic reverberance on the performance of wireless communications was assessed through two measurement campaigns. The first campaign was conducted in the coupled reverberation chambers of the NSWCDD. The reverberance of the chambers was configured to emulate the reverberance exhibited in the below-deck spaces of a naval vessel. The influence of several parameters was considered in relation to the level of reverberance: signal propagation (Line Of Sight (LOS) vs Non Line of Sight (NLOS)), receiver diversity (Single Input Single Output (SISO) vs MRC), and cavity coupling (small vs large effective aperture) between the chambers.

It was expected that communication quality degrades as the loading decreases due to increased multipath interference. In these experiments, this effect was observed in some cases, but there were several instances that defied this notion. The complexity of signal propagation in highly reverberant environments in combination with other environmental and node parameters led to several unintuitive and novel results. The performance of the LOS Receiver degraded for lower loading. Surprisingly, the reverse was true for the NLOS Receiver as it had improved performance for lower loading. Two physical layer transmission schemes were compared in which the receiver diversity scheme (MRC) produced substantial gains in PPSNR. The gains were increased for lower loading likely due to the decreased correlation of the received signals. Cavity coupling was also investigated where the effective aperture size between the two connected cavities was varied. The largest effective aperture proved to be the best for both receivers. The LOS Receiver benefited from reduced multipath while the NLOS benefited from the higher signal power.

The second campaign was performed in the below deck spaces of the *T*homas S. Gates (CG 51), a decommissioned Ticonderoga-class U.S. Navy cruiser. Several scenarios were tested including an engine room, a passageway, and a set of coupled compartments. It was shown that wireless communications were able to propagate between compartments even with the hatches closed. In some cases, closing the hatches improved performance. The quality of communications in regards to PPSNR, system capacity, and throughput benefited from advanced physical layer schemes implementing re-

ceiver diversity (MRC, Alamouti STBC) and MIMO (VBLAST-SMUX) schemes. An experimental approach proved useful, because these conclusions are not strictly intuitive. They would also not be simple to observe through modeling and simulation.

The results from both campaigns were compared to determine the feasibility of emulating the below deck spaces in the reverberation chambers. The trends in PPSNR and system capacity proved to be similar across the campaigns and indicate that emulation is possible.

Reconfigurable antennas were investigated as a method to mitigate the multipath interference. An electrically reconfigurable antenna was compared to a Commercial, Off-The-Shelf (COTS) omnidirectional antenna in the coupled reverberation chambers. The reconfigurable antenna was shown to outperform the omnidirectional antenna in both PPSNR and system capacity for LOS links and some other scenarios. This technology is particularly attractive, because unlike the advanced physical layer schemes, it does not place software or hardware constraints on mobile nodes in the network. Benefits can be realized by only installing on the stationary network infrastructure.

The implications of this work with respect to non-reverberant environments was presented. Trends for line-of-sight links would likely extend to non-reverberant environments, except at smaller scale. High multipath interference in reverberant environments degrades LOS link quality significantly. As the level of multipath is considerably less in typical environments, this effect is not nearly as pronounced. It is difficult to extrapolate the performance of NLOS links in reverberant environments to those in non-reverberant environments because of the link specific effects observed which are dependent on the complex signal propagation and physical geometry inherent in reverberant environments. Receiver diversity proved to be particularly well suited for reverberant environments due to the low correlation between receive streams. Receiver diversity also offers benefit in non-reverberant environments, though there is less to be gained than in reverberant environments where the interference in greater. The effect of coupling in reverberant environments does not apply well in non-reverberant environments. Non-reverberant environments exhibit high electromagnetic leakage, so propagation is not dependent on finding physical openings. It certainly does still help to higher coupling in non-reverberant environments, but the impact will be less than in reverberant

environments. LOS links in non-reverberant environments will not likely be affected by coupling as the level of multipath interference is significantly less.

There are several avenues through which a system designer could leverage this work to assist in implementation of a WLAN. While EVM, PPSNR, and system capacity can provide great insight on channel and link performance, it is more useful for a designer to consider throughput and error rate which are the primary requirements for the flows and applications on the network.

The achievable throughput that was presented serves as the minimum threshold for link performance and can be inform several choices in implementation. For example, consider a WLAN deployment in the engine room of a naval vessel that must support VoIP. The throughput requirement for a VoIP session is quite small, typically less than 100 kbps depending on the codec used [74]. VoIP sessions quickly degrade with high error rates, so the selected SER constraint is $1 \times 10^{-}5$. The lowest PPSNR measured in the engine room in this work was 10.4 dB, transmitting from the top deck to the bottom deck. Using this information, the achievable throughput is determined to be 6 Mbps. Hence, the network will be able to support sixty (60) concurrent VoIP sessions.

In a more general example, a WLAN is being deployed in the engine room of a naval vessel that has a throughput constraint. If a SER is selected, then the minimum PPSNR can be determined. The minimum PPSNR will then influence how far nodes are spaced from each other. Conversely, if the PPSNR is constrained (because of node placements), then the operational Symbol Error Rate (SER) can be determined. From the perspective of the designer, this is a trade-off between throughput, SER, and PPSNR. A constraint on any one of them will impact the entire network design.

The required empirical measure is the PPSNR, so the designer must have some way of determining the PPSNR for the links in their environment. Fortunately, the exact location of nodes when measuring is not important due to the dynamic nature of wireless channels. The important factors are the physical layout and the distance between the nodes. Hence, there is inherent flexibility in the application of these measurements, and it is not necessary to measure at each location permutation. For instance, the measurements recorded in this work on the *Thomas S. Gates* can be used to provide

operational ranges for ships from the same class. While not the exact same ship, ships from the same class will have similar layout and construction which are the main factors in determining the electromagnetic environment.

There are plethora of options available if the designer requires more from the network. In this effort, receiver diversity schemes and a reconfigurable antenna were explored as methods to increase the signal quality, and spatial multiplexing was shown to increase throughput. There are multitudes of other advanced techniques, and each have its own trade-offs in terms of hardware, software, cost, and complexity. There is no one-size-fits-all solution. The designer must weigh the constraints and options to determine the appropriate implementation for their network. The work presented in this document is a resource to do so.

In conclusion, it has been shown that scenarios exist in which increased multipath is favorable for wireless communications; receiver diversity is well suited for improving signal quality in in the presence of multipath interference; increased cavity coupling can benefit receivers even when they are in the same cavity as the transmitter; and reverberation chambers can be used to emulate actual highly reverberant environments. There are many benefits to using reverberation chambers as a substitute for highly reverberant environments. Reverberation chambers are controllable for systematic experimentation, and it is logistically easier to test in a reverberation chamber than in the field.

Through this effort, numerous benefits and trade-offs of implementing WLANs in highly reverberant environments have been demonstrated. Wireless communication is possible with simple point to point links, but there are many possibilities to incorporate advanced hardware and software schemes to improve link quality and network robustness. Ultimately, leveraging this work, system designers can tailor their implementation to the needs and constraints of their application.

Bibliography

[1] V. Gungor and G. Hancke, "Industrial wireless sensor networks: Challenges, design principles, and technical approaches," *IEEE Trans. Ind. Electron.*, vol. 56, no. 10, pp. 4258–4265, Oct 2009.

[2] P. Angskog, C. Karlsson, J. F. Coll, J. Chilo, and P. Stenumgaard, "Sources of disturbances on wireless communication in industrial and factory environments," in *Proc. Asia-Pacific Symp. on Electromagnetic Compatibility*, 2010.

[3] E. Balboni, J. Ford, R. Tingley, K. Toomey, and J. Vytal, "An empirical study of radio propagation aboard naval vessels," in *Proc. IEEE-APS Conf. on Antennas and Propagation for Wireless Commun.*, 2000, pp. 157–160.

[4] A. Mariscotti, "Experimental determination of the propagation of wireless signals on board a cruise ship," *Measurement*, vol. 44, no. 4, pp. 743–749, 2011.

[5] A. Sarkar, S. Majumdar, and P. P. Bhattacharya, "Path loss estimation for a wireless sensor network for application in ship," *Int. J. of Comput. Sci. and Mobile Computing*, vol. 2, no. 6, pp. 87–96, 2013.

[6] A. Daga, D. Borah, G. Lovelace, and P. DeLeon, "Physical layer effects on MAC layer performance of IEEE 802.11 a and b WLAN on the Martian surface," in *Proc. IEEE Aerospace Conf.*, 2006.

[7] E. L. Mokole, M. Parent, T. T. Street, and E. Tomas, "RF propagation on ex-*USS Shadwell*," in *Proc. IEEE-APS Conf. Antennas and Propagation for Wireless Commun.*, 2000, pp. 153–156.

[8] M. Chitre, S. Shahabudeen, and M. Stojanovic, "Underwater acoustic communications and networking: Recent advances and future challenges," *Marine Technology Soc. J.*, vol. 42, pp. 103–116, 2008.

[9] A. Willig, K. Matheus, and A. Wolisz, "Wireless technology in industrial networks," *Proceedings of the IEEE*, vol. 93, no. 6, pp. 1130–1151, June 2005.

[10] K.-S. Low, W. Win, and M. J. Er, "Wireless sensor networks for industrial environments," in *Computational Intelligence for Modelling, Control and Automation, 2005 and International Conference on Intelligent Agents, Web Technologies and Internet Commerce, International Conference on*, vol. 2, Nov 2005, pp. 271–276.

[11] *IEEE Standard for Ethernet*, IEEE Standard 802.3, 2013.

[12] *IEEE Standard for Wireless LANs*, IEEE Standard 802.11, 2013.

[13] G. Tait, M. Slocum, D. Hilton, C. Dilay, and D. Southworth, "Off-hull radio frequency emissions from below-deck spaces in ships," in *2010 IEEE International Symposium on Electromagnetic Compatibility*, Jul. 2010, pp. 875–880.

[14] A. Saleh and R. Valenzuela, "A statistical model for indoor multipath propagation," *IEEE J. Sel. Areas Commun.*, vol. 5, no. 2, pp. 128–137, February 1987.

[15] G. Hooghiemstra, L. Meester, and Sahid, "Analysis of a stochastic model for indoor multipath propagation," in *IEEE Int. Conference Personal Wireless Commun.*, 2000, pp. 298–302.

[16] T. Carter, S. Kim, and M. Johnson, "High throughput, power and spectrally efficient communications in dynamic multipath environments," in *IEEE Military Commun. Conference*, vol. 1, Oct 2003, pp. 61–66 Vol.1.

[17] T. Sarkar, Z. Ji, K. Kim, A. Medouri, and M. Salazar-Palma, "A survey of various propagation models for mobile communication," *IEEE Antennas Propagat. Mag.*, vol. 45, no. 3, pp. 51–82, June 2003.

[18] H. Fielitz, K. Remley, C. Holloway, Q. Zhang, Q. Wu, and D. Matolak, "Reverberation-chamber test environment for outdoor urban wireless propagation studies," *Antennas and Wireless Propagation Letters, IEEE*, vol. 9, pp. 52–56, 2010.

[19] G. B. Tait and M. B. Slocum, "Electromagnetic environment characterization of below-deck spaces in ships," in *Proc. IEEE Int. Symp. on Electromagnetic Compatibility*, Aug. 2008, pp. 1–6.

[20] J. Giuseppe, C. Hager, and G. Tait, "Wireless rf energy propagation in multiply-connected reverberant spaces," *IEEE Antennas Wireless Propag. Lett.*, vol. 10, pp. 1251–1254, 2011.

[21] G. Tait, R. Richardson, M. Slocum, M. Hatfield, and M. Rodriguez, "Reverberant microwave propagation in coupled complex cavities," *IEEE Trans. Electromagn. Compat.*, vol. 53, no. 1, pp. 229–232, Feb 2011.

[22] G. B. Tait and R. E. Richardson, "Wireless channel modeling of multiply-connected reverberant spaces: Application to electromagnetic compatibility assessment," *IEEE Trans. on Electromagn. Compat.*, vol. 55, pp. 1320–1327, 2013.

[23] G. Nastasia, M. Falzarano, A. Corucci, P. Usai, and A. Monorchio, "Channel characterization of wireless systems on board of ships by using an efficient ray-tracing," in *Proc. IEEE Antennas and Propagation Soc. Int. Symp.*, 2012, pp. 1–2.

[24] "Structure." [Online]. Available: structure.io

[25] "Atap project tango." [Online]. Available: https://www.google.com/atap/projecttango/#project

[26] "List of software-defined radios — Wikipedia, the free encyclopedia," 2015. [Online]. Available: http://en.wikipedia.org/wiki/List_of_software-defined_radios

[27] "Ettus research." [Online]. Available: http://www.ettus.com

[28] "Gnuradio." [Online]. Available: http://gnuradio.org

[29] "Warp project." [Online]. Available: http://warpproject.org

[30] R. Measel, D. J. Bucci, C. S. Lester, K. Wanuga, R. A. Primerano, K. Dandekar, and M. Kam, "A MATLAB platform for characterizing MIMO–OFDM communications with software-defined radios," in *International Communications Quality and Reliability Workshop*, May 2014. [Online]. Available: http://dflwww.ece.drexel.edu/archives/280/

[31] *Inform. Technology—Telecommun. and Inform. Exchange Between Syst.—Local and Metropolitan Area Networks—Specific Requirements—Part 11: Wireless LAN Medium Access Control (MAC) and Physical Layer (PHY) Specifications*, IEEE Std. 802.11-1997.

[32] A. Goldsmith, *Wireless Communications*. New York, NY, USA: Cambridge University Press, 2005.

[33] M. Jankiraman, *Space-time codes and MIMO systems*. Artech House, Inc., 2004.

[34] S. M. Alamouti, "A simple transmit diversity technique for wireless communications," *IEEE J. Sel. Areas Commun.*, vol. 16, no. 8, pp. 1451–1458, Oct. 1998.

[35] G. J. Foschini, "Layered space-time architecture for wireless communication in a fading environment when using multi-element antennas," *Bell Labs Tech. J.*, vol. 1, no. 2, pp. 41–59, 1996. [Online]. Available: http://dx.doi.org/10.1002/bltj.2015

[36] D. Piazza, M. D'Amico, and K. R. Dandekar, "Performance improvement of a wideband MIMO system by using two-port RLWA," *IEEE Antennas Wireless Propag. Lett.*, vol. 8, pp. 830–834, Jul. 2009.

[37] G. Tait and M. Slocum, "Electromagnetic environment characterization of below-deck spaces in ships," in *IEEE Int. Symp. Electromagn. Compat.*, Aug 2008, pp. 1–6.

[38] K. Wanuga, R. Measel, C. S. Lester, D. J. Bucci, D. Gonzalez, R. A. Primerano, M. Kam, and K. Dandekar, "Performance evaluation of MIMO–OFDM systems in on-ship below deck environments," *IEEE Antennas and Wireless Propagation Letters*, vol. 13, pp. 173–176, January 2014. [Online]. Available: http://dflwww.ece.drexel.edu/archives/278/

[39] C. S. Lester, R. Measel, D. J. Bucci, K. Wanuga, R. A. Primerano, M. Kam, and K. Dandekar, "Effects of reconfigurable antennas on wireless network performance within a ticonderoga-class engine room," in *American Society of Naval Engineers (ASNE) Electric Machines Technology Symposium (EMTS) 2014*, May 2014. [Online]. Available: http://dflwww.ece.drexel.edu/archives/286/

[40] R. Mehmood and J. W. Wallace, "Increased interference-limited MIMO capacity with parasitic reconfigurable aperture antennas," in *Proc. IEEE Antennas and Propagation Soc. Int. Symp.*, 2012, pp. 1–2.

[41] V. Vakilian, J.-F. Frigon, and S. Roy, "Performance evaluation of reconfigurable MIMO systems in spatially correlated frequency-selective fading channels," in *Proc. IEEE Veh. Technology Conf.*, 2012, pp. 1–5.

[42] J. Kountouriotis, D. Piazza, P. Mookiah, M. D'Amico, and K. R. Dandekar, "Reconfigurable antennas for MIMO ad-hoc networks," in *Proc. IEEE Radio and Wireless Symp.*, 2008, pp. 563–566.

[43] D. Piazza and K. R. Dandekar, "Reconfigurable antenna solution for MIMO-OFDM systems," *Electronics Lett.*, vol. 42, no. 8, pp. 446–447, Apr. 2006.

[44] C. Gomez-Calero, J. Mora-Cuevas, L. Cuellar, R. Martinez, and L. De-Haro, "Measurement of diversity gain and capacity on a MIMO-OFDM channel comparing different types of antennas," in *Proc. 3rd European Conf. on Antennas and Propagation*, 2009, pp. 1037–1041.

[45] R. Measel, C. S. Lester, D. J. Bucci, K. Wanuga, G. Tait, R. A. Primerano, K. Dandekar, and M. Kam, "Reconfigurable antennas in highly multipath environments," in *IEEE International Symposium on Antennas and Propagation*, July 2014. [Online]. Available: http://dflwww.ece.drexel.edu/archives/283/

[46] D. Piazza, M. D'Amico, and K. R. Dandekar, "Two port reconfigurable CRLH leaky wave antenna with improved impedance matching and beam tuning," *European Conference on Antenna and Propagation*, 2009.

[47] ——, "Performance improvement of a wideband MIMO system by using two-port RLWA," *Antennas and Wireless Propagation Letters*, 2009.

[48] H. Paaso, A. Mammela, D. Patron, and K. R. Dandekar, "Modified MUSIC algorithm for DoA estimation using CRLH leaky-wave antennas," in *Int. Conf. Cognitive Radio Oriented Wireless Networks*, July 2013, pp. 166–171.

[49] R. Measel, D. J. Bucci, C. S. Lester, K. Wanuga, G. Tait, R. A. Primerano, K. Dandekar, and M. Kam, "The effect of electromagnetic reverberance on wireless ofdm communications," *IEEE Transactions on Wireless Communications (submitted)*, vol. 13, January 2015.

[50] K. Remley, G. Koepke, C. Holloway, C. Grosvenor, D. Camell, J. Ladbury, R. Johnk, and W. Young, "Radio-wave propagation into large building structures, part 2: Characterization of multipath," *IEEE Trans. Ant. and Propag.*, vol. 58, no. 4, pp. 1290–1301, April 2010.

[51] A. Molisch, *Wireless Communications*. Wiley-IEEE Press, 2005.

[52] C.-T. Chen, *Linear System Design and Theory*. Oxford University Press, 2010.

[53] D. K. Cheng, *Field and Wave Electromagnetics*. Addison-Wesley, 1989.

[54] *DOD Interface Standard – Electromagnetic Enivornmental Effects Requirements for Systems*, DOD MIL-STD-464C, 2010.

[55] JPL, "Wireless channels – indoor propagation at 2.4ghz." [Online]. Available: http://mangocomm.com/802.11

[56] ——, "Wireless channels – multipath propagation." [Online]. Available: http://mangocomm.com/802.11

[57] "Mango communications 802.11 reference design." [Online]. Available: http://mangocomm.com/802.11

[58] Rice University, "Wireless Open-Access Research Platform." [Online]. Available: http://warp.rice.edu

[59] P. O. Murphy, "Design, implementation, and characterization of a cooperative communications system," Ph.D. dissertation, Rice University, Dec. 2010.

[60] R. Janaswamy, *Radiowave Propagation & Smart Antennas for Wireless Communications*. Kluwer Academic Publishers, 2000.

[61] S. M. Alamouti, "A simple transmit diversity technique for wireless communications," *IEEE J. Sel. Areas Commun.*, vol. 16, pp. 1451–1458, Oct. 1998.

[62] P. W. Wolniansky, G. J. Foschini, G. D. Golden, and R. Valenzuela, "V-BLAST: An architecture for realizing very high data rates over the rich-scattering wireless channel," in *Proc. URSI Int. Symp. on Signals, Syst., and Electronics*, 1998, pp. 295–300.

[63] S. Loyka and G. Levin, "On physically-based normalization of MIMO channel matrices," *IEEE Trans. Wireless Commun.*, vol. 8, no. 3, pp. 1107–1112, Mar. 2009.

[64] S. Sandhu and A. Paulraj, "Space-time block codes: a capacity perspective," *Communications Letters, IEEE*, vol. 4, no. 12, pp. 384–386, Dec 2000.

[65] Z. Shen, J. Andrews, and B. Evans, "Upper bounds on mimo channel capacity with channel frobenius norm constraints," in *Global Telecommunications Conference, 2005. GLOBECOM '05. IEEE*, vol. 3, Nov 2005, pp. 5 pp.–.

[66] R. A. Shafik, S. Rahman, R. Islam, and N. S. Ashraf, "On the error vector magnitude as a performance metric and comparative analysis," in *Int. Conf. Emerging Technologies*, Nov. 2006, pp. 27–31.

[67] F. Da Ros, R. Borkowski, D. Zibar, and C. Peucheret, "Impact of gain saturation on the parametric amplification of 16-QAM signals," in *Proc. Conf. on Optical Commun.*, 2012, pp. 1–3.

[68] D. Chizhik, G. Foschini, M. Gans, and R. Valenzuela, "Keyholes, correlations, and capacities of multielement transmit and receive antennas," *Wireless Communications, IEEE Transactions on*, vol. 1, no. 2, pp. 361–368, Apr 2002.

[69] D. Gesbert, H. Bolcskei, D. Gore, and A. Paulraj, "Mimo wireless channels: capacity and performance prediction," in *Global Telecommunications Conference, 2000. GLOBECOM '00. IEEE*, vol. 2, 2000, pp. 1083–1088 vol.2.

[70] P. Almers, F. Tufvesson, and A. Molisch, "Keyhole effect in mimo wireless channels: Measurements and theory," *Wireless Communications, IEEE Transactions on*, vol. 5, no. 12, pp. 3596–3604, December 2006.

[71] D. J. Love, R. W. Heath, V. K. N. Lau, D. Gesbert, B. D. Rao, and M. Andrews, "An overview of limited feedback in wireless communication systems," *IEEE J. Sel. Areas Commun.*, vol. 26, no. 8, pp. 1341–1365, Oct. 2008.

[72] C. S. Lester, R. Measel, , D. J. Bucci, K. Wanuga, R. A. Primerano, K. R. Dandekar, and M. Kam, "Performance of reconfigurable antennas in a below-decks environment," *IEEE Antennas and Wireless Propagation Letters*, 2015, accepted.

[73] A. Grau, H. Jafarkhani, and F. De Flaviis, "A reconfigurable multiple-input multiple-output communication system," *IEEE Trans. Wireless Commun.*, vol. 7, no. 5, pp. 1719–1733, 2008.

[74] Voip-Info.org, "Bandwidth consumption." [Online]. Available: http://www.voip-info.org/wiki/view/Bandwidth+consumption

Vita

Ryan Measel

Education

- Drexel University, Philadelphia, Pennsylvania USA
  - Ph.D., Electrical Engineering, January 2015
  - M.S., Electrical Engineering, June 2011
  - B.S., Computer Engineering, June 2011

Publications

- C. S. Lester, R. Measel, D. J. Bucci, K. Wanuga, R. Primerano, K. R. Dandekar, and M. Kam, " Performance of Reconfigurable Antennas in a Below-Decks Environment," *IEEE Antennas Wireless Propag. Lett.*, [accepted], 2015.
- R. Measel, C. S. Lester, D. J. Bucci, K. Wanuga, G. Tait, R. A. Primerano, K. Dandekar, and M. Kam, "Reconfigurable antennas in highly multipath environments," in *IEEE Int. Symp. on Antennas and Propagation* July 2014.
- C. S. Lester, R. Measel, D. J. Bucci, K. Wanuga, R. Primerano, M. Kam, and K. Dandekar, "Effects of reconfigurable antennas on wireless network performance within a Ticonderoga-class engine room," in *Proc. ASNE Electric Machines Technology Symp.*, (Villanova, PA), May 2014.
- R. Measel, D. J. Bucci, C. S. Lester, K. Wanuga, R. A. Primerano, K. Dandekar, and M. Kam, "A MATLAB platform for characterizing MIMO-OFDM communications with software-defined radios," in *IEEE Int. Comm. Quality and Rel. Workshop*, May 2014.
- R. Measel, C. S. Lester, Y. Xu, R. Primerano, and M. Kam, "Detection performance of spread spectrum signatures for passive, chipless RFID," in *Proc of IEEE RFID Conf.*, April 2014.
- . K. Wanuga, R. Measel, C. S. Lester, D. J. Bucci, D. Gonzalez, R. Primerano, M. Kam, and K. R. Dandekar, Performance evaluation of MIMOOFDM systems in on-ship below-deck environments," *IEEE Antennas Wireless Propag. Lett.*, vol. 13, pp. 173176, 2014.
- R. Measel, "IPv6 compression techniques and performance," Masters thesis, Drexel University, 2011.
- G. D. Sworo, R. Measel, M. Kam, and K. Dandekar, "Optimization of adaptive modulation and coding techniques for OFDM systems," in *Int. Conf. on Sig. Proc. and Comm. Sys.*, pp. 15, Dec 2011.
- J. Wildman, D. Hamel, R. Measel, D. Oakum, S. Weber, and M. Kam, "Performance and scaling of wireless ad hoc IPv6 stateless address autoconfiguration under mobile gateways," in *IEEE Military Comm. Conf.*, pp. 19, Oct 2007.

Professional Experience

- Data Fusion Laboratory – Financial Manager *August 2012 to December 2014*
- Forward Dynamics, Inc. – Research Consultant *April 2011 to September 2011*
- US Naval Research Laboratory – Research Intern *September 2007 to December 2007*
- Drexel Smart House – Co-Founder & Vice President *January 2005 to January 2007*